ELUCIDATION OF THE EFFECT OF LAURIC ACID ON HEPATIC STEATOSIS AND INSULIN RESISTANCE IN DIET-INDUCED OBESE MICE

WONG CHI HAU

MASTER OF SCIENCE IN BIOLOGICAL SCIENCE

FACULTY OF SCIENCE
UNIVERSITI TUNKU ABDUL RAHMAN
OCTOBER 2025

ELUCIDATION OF THE EFFECT OF LAURIC ACID ON HEPATIC STEATOSIS AND INSULIN RESISTANCE IN DIET-INDUCED OBESE MICE

By

WONG CHI HAU

A dissertation submitted to the Department of Allied Health Science,
Faculty of Science,
Universiti Tunku Abdul Rahman,
in partial fulfillment of the requirements for the degree of
Master of Science in Biological Science
October 2025

ABSTRACT

ELUCIDATION OF THE EFFECT OF LAURIC ACID ON HEPATIC STEATOSIS AND INSULIN RESISTANCE IN DIET-INDUCED OBESE MICE

Wong Chi Hau

Insulin resistance occurs when the peripheral tissues exhibit reduced sensitivity to insulin, leading to impaired glucose uptake. This metabolic defect promotes lipid accumulation in the liver, causing metabolic dysfunction-associated fatty liver disease (MAFLD) and increasing the risk of developing type 2 diabetes mellitus. This study aimed to investigate the effects of oral gavage of lauric acid on insulin resistance and lipid metabolism in high-fat diet (HFD)-induced obese male C57BL/6J mice. The mice were fed an HFD continuously for eight weeks to induce metabolic dysfunction, while the control group received a normal chow diet. Two treatment groups were administered lauric acid by oral gavage at doses of 12 mg/kg and 24 mg/kg, and a separate group received rosiglitazone (20 mg/kg) alongside HFD for eight weeks. Lauric acid supplementation has been shown to reduce body weight, calorie intake, serum triglyceride levels, fasting blood glucose levels, insulin levels and HOMA-IR values. Although total cholesterol levels increased, high-density lipoprotein (HDL) levels also increased. Moreover, lauric acid upregulated hepatic expression of *Apoa2*, *Pparg1* and *Srebf2*, and downregulated *Hmgcr* genes compared to the HFD control group. Lauric acid treatment exhibited a non-significant trend toward enhanced AMPK phosphorylation and reduced total hepatic SREBP-1 and

SREBP-2 protein levels. However, histological features of lauric acid-fed mice resembled those of HFD mice with no observable difference. Finally, the data suggest that lauric acid may improve insulin resistance and lipid metabolism in HFD-induced metabolic syndromes.

Keywords: MAFLD, insulin resistance, lauric acid, lipid metabolism, C57BL/6J mice, HOMA-IR

Subject Area: QD415-436 Biochemistry, QP501-801 Animal Biochemistry

ACKNOWLEDGEMENT

First and foremost, I would like to express my deepest gratitude to my main supervisor, Associate Professor Dr. Chew Choy Hoong, for her excellent teaching and enormous patience while guiding me through my Master of Science journey. The compilation of this project would be very much impossible without her experience and dedication. I am also thankful to the support given by my co-supervisor, Assistant Professor Dr. Choo Quok Cheong and Associate Professor Dr. Fong Lai Yen.

I appreciate Universiti Tunku Abdul Rahman (UTAR) for giving me such an opportunity to pursue my master's degree and providing the necessary facilities for the research project. This research was funded by a grant from the Ministry of Higher Education of Malaysia (FRGS/1/2021/SKK0/UTAR/02/3).

My sincere appreciation also goes to the laboratory staff and colleagues in the Faculty of Science for their technical assistance, cooperation, and for creating a stimulating research environment. I am so grateful to my seniors, Mr. Ho Wai Yew and Dr. Toh Wai Keat, for their time, support and knowledge on the experiment procedure and data analysis. I am also thankful to my lab-mates for their constructive comments and suggestions, which have helped me improve the quality of this study.

Lastly, I want to thank my family members for their unconditional love and endless support throughout my master's academic journey.

TABLE OF CONTENTS

LIST OF TABLES

LIST OF FIGURES

hepatic proteins

LIST OF ABBREVIATIONS

4-HNE	4-hydroxynonenal
5FU	5-fluorouracil
ABCA1	ATP-binding cassette transporter A1
ACAD	Acyl-CoA dehydrogenases
ACC	Acetyl-CoA Carboxylase
ACE-i	Angiotensin-converting enzyme inhibitor
ACLY	ATP citrate lyase
ACOX	Acyl-CoA oxidase
AICAR	5-aminoimidazole-4-carboxyamide ribonucleoside
AMPK	AMP-activated protein kinase
aP2	Adipocyte fatty acid binding protein
APOA1	Apolipoprotein A1
APOA2	Apolipoprotein A2
apoB100	Apolipoprotein B100
APS	Ammonium persulfate
AR	Aldose reductase
ATF6	Activating transcription factor 6
AUC	Area under the curve
AZIP	A-ZIP/F-1
BBB	Blood-brain barrier
BHB	β-hydroxybutyrate
BMI	Body mass index
BSA	Bovine serum albumin
CA 19-9	Carbohydrate antigen 19-9

CaMKKβ	Calcium/calmodulin-dependent protein kinase kinase-β
CAT	Catalase
CETP	Cholesterol ester transfer protein
ChREBP	Carbohydrate-responsive element-binding protein
CI	Confidence interval
Cidec	Cell death-inducing DFFA-like effector C
CPT1	Carnitine palmitoyl transferase I
CVAI	Chinese visceral adiposity index
Cyp4a	Cytochrome P450 family 4 subfamily a polypeptide
DAGs	Diacylglycerols
DALYs	Disability-adjusted life years
DAMPs	Damage-associated molecular patterns
ER	Endoplasmic reticulum
ERAD	ER-associated degradation
ETC	Electron transport chain
FA	Fatty acid
FASN	Fatty acid synthase
FFA	Free fatty acids
GGPP	Geranylgeranyl pyrophosphate
GLP-1	Glucagon-like peptide-1
GLP1-RA	Glucagon‐like peptide‐1 receptor agonist
GLUT	Glucose transporter
GML	Glycerol monolaurate
GPR-40	G Protein-Coupled Receptor 40
GSH	Glutathione

H&E	Haematoxylin and eosin
HCC	Hepatocellular carcinoma
HDL	High-density lipoprotein
HFD	High-fat diet
HFHC	High-fat, high-cholesterol and high fructose
HFHS	High fat, high sucrose
HMGCR	3-hydroxy-3-methylglutaryl-CoA reductase
HMGCS	3-hydroxy-3-methylglutaryl-CoA synthase
HOMA-IR	Homeostatic Model Assessment for Insulin Resistance
HSP90	Heat shock protein 90
HSV	Herpes simplex virus
ICAM-1	Intercellular adhesion molecule-1
IFN-γ	Interferon-gamma
IDL	Intermediate-density lipoprotein
IL	Interleukin
INHAND	International Harmonisation of Nomenclature and Diagnostic Criteria for Lesions in Rats and Mice
IRE	Inositol-requiring enzyme
IRS-1	Insulin receptor substrate-1
JNK	c-jun N-terminal kinase
KLF10	Krüppel-like factor 10
L-PBE	L-peroxisomal bifunctional enzyme
LCAT	Lecithin–cholesterol acyltransferase
LC-MASLD	Liver complications related to metabolic dysfunction-associated steatotic liver disease
LCFAs	Long-chain fatty acids

LDL	Low-density lipoprotein
LIPC	Hepatic lipase
LKB1	Liver-kinase-B1
LPL	Lipoprotein lipase
LPS	Lipopolysaccharides
LXR	Liver X receptor
MafA	MAF bZIP Transcription Factor A
MAFLD	Metabolic dysfunction-associated fatty liver disease
MBS	Metabolic and bariatric surgery
MCFA	Medium-chain fatty acid
MCTs	Medium-chain triglycerides
MDA	Malondialdehyde
MTP	Microsomal triglyceride transfer protein
MPO	Myeloperoxidase
NAFLD	Non-alcoholic fatty liver disease
NASH	Non-cirrhotic non-alcoholic steatohepatitis
NeoroD1	Neuronal differentiation 1
NF-κB	Nuclear factor kappa B
NNT	Nicotinamide nucleotide transhydrogenase
NPC1L1	Niemann-Pick C1-like 1
OGTT	Oral glucose tolerance test
OXPHOS	Oxidative phosphorylation
p38 MAPK	p38 mitogen-activated protein kinases
PAMPs	Pathogen-associated molecular patterns
PBS	Phosphate-buffered saline

PEPCK	Phosphoenolpyruvate carboxykinase
PERK	Protein Kinase R-like Endoplasmic Reticulum Kinase
PGC-1α	Peroxisome proliferator-activated receptor gamma coactivator 1-alpha
PKB	Protein kinase B
PLTP	Phospholipid transfer protein
PI3K	Phosphoinositide 3-kinase
PPAR-γ	Peroxisome proliferator-activated receptor gamma
PRDM16	Positive regulatory domain zinc finger region protein 16
PRRs	Pattern recognition receptors
PVDF	Polyvinylidene difluoride
PXR	Pregnane X receptor
ROS	Reactive oxygen species
RT-qPCR	Reverse transcription quantitative PCR
RYGP	Roux-en-Y gastric bypass
SCD1	Stearoyl-CoA desaturase 1
SDH	Sorbitol dehydrogenase
SDS-PAGE	Sodium Dodecyl Sulfate-PolyAcrylamide Gel Electrophoresis
SEM	Standard error of the mean
SGLT2‐i	Sodium‐glucose cotransporter‐2 inhibitor
SIRT1	Sirtuins
SOD	Superoxide dismutase
SREBP	Sterol regulatory element-binding protein
SSD	Sterol-sensing domain
T2DM	Type 2 diabetes mellitus

TEM	Transmission electron microscopy
TEMED	N,N,N′,N′ -Tetramethylethylenediamine
THR-β	Thyroid hormone receptor β
TLR	Toll-like receptor
TNF-α	Tumour necrosis factor-alpha
Ubxd8	Ubiquitin regulatory X domain-containing protein 8
UCP1	Uncoupling protein 1
UPR	Unfolded protein response
VCAM-1	Vascular cell adhesion molecule-1
VLDL	Very low-density lipoprotein
VSV	Vesicular stomatitis virus
VV	Visna virus
WDR6	WD40 repeat-containing protein 6

CHAPTER 1

INTRODUCTION

Metabolic dysfunction-associated fatty liver disease (MAFLD), formally termed non-alcoholic fatty liver disease (NAFLD), is the most widespread chronic liver condition worldwide that contributes to liver-related complications and death, with an estimated global prevalence of 30.2% (Eslam *et al*., 2020a; Amini Salehi *et al*., 2024). MAFLD contributes not only to liver-related morbidity and mortality but also increases risks of cardiovascular disease, chronic kidney disease, progression of liver failure and overall mortality (Eslam *et al*., 2020b; Boccatonda *et al*., 2023). The rising prevalence and clinical burden of MAFLD pose significant health risks, necessitating urgent attention and comprehensive management strategies. Obesity and insulin resistance are recognised as central drives of metabolic dysfunction, particularly MAFLD and type 2 diabetes mellitus. Insulin resistance impairs glucose and lipid homeostasis, resulting in hyperglycaemia, dyslipidaemia and hepatic steatosis. The two conditions are closely interlinked; type 2 diabetes mellitus elevates the prevalence and severity of MAFLD, while hepatic fat accumulation exacerbates systemic insulin resistance, creating a vicious cycle of metabolic dysfunction. Importantly, the coexistence of MAFLD and type 2 diabetes mellitus markedly elevates the risk of cardiovascular disease, which remains the primary cause of mortality in affected individuals (Sakurai *et al.*, 2021; Ding *et al.*, 2023). Understanding the molecular and nutritional modulators of insulin

resistance is therefore critical for identifying strategies to prevent or attenuate these interconnected disorders.

Rezdiffra (resmetirom) has been approved by the U.S. Food and Drug Administration for treating adult patients with non-cirrhotic non-alcoholic steatohepatitis (NASH) accompanied by moderate to advanced liver fibrosis, in combination with diet and exercise (U.S. Food and Drug Administration, 2024). In Malaysia, the Malaysian Society of Gastroenterology and Hepatology has issued a consensus recommending pioglitazone and vitamin E for MAFLD patients, along with glucose-lowering agents such as sodium–glucose cotransporter-2 inhibitor (SGLT2-i) and glucagon-like peptide-1 receptor agonist (GLP1-RA), as well as cardioprotective drugs such as statins and angiotensin-converting enzyme inhibitor (ACE-i) (Chan *et al*., 2022). While these pharmacological options represent important advances, they are associated with adverse effects and are generally used for advanced disease. Lifestyle modifications remain the cornerstone of treatment, yet the long-term adherence to these interventions is challenging, highlighting the need for complementary approaches (Le, Wang and Xue, 2022). In Malaysia, the burden of metabolic disease is substantial and rising. The National Health and Morbidity Survey 2023 reports that approximately 28.2% of adults are affected by MAFLD (Wan *et al*., 2024). This trend is concerning because obesity and insulin resistance, both highly prevalent in Malaysia, are major causes of MAFLD and type 2 diabetes mellitus. Given the scale of the problem and limitations of pharmacological treatments, nutraceutical strategies may offer

cost-effective, complementary approaches to manage and prevent metabolic diseases. The growing interest in nutritional strategies has highlighted the potential of dietary intervention, particularly on functional lipids, as an alternative approach to improve metabolic health. Various functional lipids, including medium-chain triglycerides, conjugated linoleic acids, diacylglycerides, omega-3 and omega-6 fatty acids, have been studied for their physiological benefits for reducing the risks of chronic diseases. (Omachi, Aryee and Onuh, 2024). Lauric acid is a saturated medium-chain fatty acid (MCFA) with a 12-carbon chain backbone that can be abundantly found in coconut oil and palm kernel oil. Coconut oil consists of 48-53% lauric acid, suggesting that its health-promoting benefits may be largely derived from lauric acid (Ströher *et al*., 2020; Ramya *et al*., 2022). Recent studies indicate that lauric acid exhibits antimicrobial, anti-inflammatory, antioxidant and anti-obesity properties, and has been shown to enhance energy expenditure and improve lipid profiles (Gao *et al*., 2022; Ameena *et al*., 2024). These properties support its potential as a functional lipid supplementation for reducing the risk of obesity-related disorders. Given the beneficial effects of lauric acid, it is hypothesised that oral supplementation with lauric acid could ameliorate dyslipidaemia, delay the progression of hepatic steatosis and improve insulin resistance in high-fat diet (HFD)- fed C57BL/6J mice. By utilising the diet-induced obesity model, this study aimed to elucidate the mechanisms through which lauric acid regulates glucose and lipid metabolism. Given that the diet-induced obesity model closely mimics the metabolic disturbances seen in human physical inactivity and calorie surplus, these findings may provide a critical mechanistic foundation for the use of lauric acid as a targeted

nutraceutical intervention. This research could offer a cost-effective strategy to improve metabolic health in sedentary populations at high risk for MAFLD and type 2 diabetes mellitus. To test this hypothesis, this study investigated the effects of lauric acid supplementation in HFD-fed C57BL/6J mice by assessing body weight, caloric intake, blood lipid profiles, hepatosteatosis-associated genes and proteins, fasting glucose, glucose tolerance, insulin levels, and insulin signalling pathways.

This project was aimed to achieve the following objectives:

i. To study the effect of lauric acid on the physiological parameters and blood lipid profiles of HFD-fed mice.

ii. To examine the effects of lauric acid on HFD-induced insulin resistance.

iii. To investigate the effect of lauric acid on hepatic steatosis in HFD-fed mice.

iv. To elucidate the effect of lauric acid on the insulin signalling pathway and lipid synthesis-associated gene expression in HFD-fed mice.

CHAPTER 2

LITERATURE REVIEW

2.1 Metabolic dysfunction-associated fatty liver disease (MAFLD)

2.1.1 Nomenclature and diagnostic criteria

An international consensus has recently introduced a revised nomenclature, recommending the term metabolic dysfunction-associated fatty liver disease (MAFLD) instead of non-alcoholic fatty liver disease (NAFLD). Alongside this new terminology, a set of positive diagnostic criteria was established to provide a clearer representation of liver disease associated with metabolic dysfunction (Eslam *et al*., 2020a). The diagnosis of MAFLD requires evidence of hepatic steatosis, confirmed by liver biopsy, imaging or non-invasive scoring, together with overweight or obesity, type 2 diabetes mellitus (T2DM), or at least two metabolic risk factors, such as increased waist circumference, elevated blood pressure, raised plasma triglycerides, reduced plasma high-density lipoprotein-cholesterol, prediabetes, insulin resistance (as indicated by an increased homeostasis model assessment of insulin resistance score), or elevated plasma high-sensitivity C-reactive protein (Eslam *et al*., 2020a). Unlike the exclusion-based criteria used for NAFLD, the MAFLD definition incorporates contributing factors such as alcohol consumption and viral infections. The change aims to reflect the underlying cause of the disease,

which is the metabolic problem, rather than focusing on what it is not. This change enhances understanding of disease pathogenesis, improves diagnostic accuracy, and supports the detection of comorbidities, therapeutic targets, and clinical outcomes (Gofton *et al*., 2022).

2.1.2 Epidemiology of MAFLD

The worldwide prevalence of MAFLD has increased significantly over time and is projected to rise at an alarming rate. The systematic review and meta-analysis by Amini-Salehi *et al*. (2024) estimated a global prevalence of MAFLD to be 30.2% (95% CI: 28.7–31.7%), Riazi *et al*. (2022) estimated the overall prevalence of MAFLD worldwide to be 32.4% (95% CI 29·9%-34·9%), Amin *et al*. (2023) reported a prevalence of 30.05% (95% CI: 27.88%–32.32%), while Chan *et al*. (2022) reported a prevalence of 38.77% (95% CI 32.94%-44.95%), in which 5.37% (95% CI 4.36% to 6.59%) and 29.78% (95% CI 26.06% to 33.79%) are lean and nonobese MAFLD individuals respectively. Moreover, Liu *et al*. (2022) estimated, through systematic review and meta-analysis, that about half of overweight or obese adults (50.7%; 95% CI 46.9-54.4) worldwide are affected by MAFLD, independent of diagnostic techniques, while Quek *et al*. (2023) reported that MAFLD in overweight population has a prevalence of 69·99% (95% CI 65·40–74·21).

The prevalence of MAFLD has demonstrated a progressive increase over the past decades, corresponding with global shifts in lifestyle, dietary habits, and the rising incidence of metabolic risk factors such as obesity and T2DM. According to Liu *et al*. (2022), the prevalence of MAFLD rose notably from 27.94% (95% CI 26.23–29.69) in years 2000-2010 to 31.63% (95% CI 30.23–33.04) in years 2011-2021. Between 1990 and 2021, a significant upward trend was observed in the incidence, prevalence, mortality, and disability-adjusted life years (DALYs) associated with hepatic complications related to metabolic dysfunction-associated steatotic liver disease (LC-MASLD). Specifically, incidence and prevalence increased at an average annual rate of 0.73%, while mortality and DALYs rose by 0.19% and 0.16% per year, respectively (Lu *et al*., 2024).

The increasing incidence of MAFLD with age is well-documented and reflects the cumulative impact of metabolic risk factors over time. For instance, Liu *et al*. (2022), in a systematic review and meta-analysis, reported a global MAFLD prevalence of 29.38%, with the highest prevalence observed in individuals aged 40 to 60 years. Furthermore, Chan *et al*. (2022) reported that the mean age of MAFLD patients in their study was 51.99 years, reinforcing the association between advancing age and MAFLD prevalence. The ageing process is linked to physiological alterations, including diminished insulin sensitivity, elevated visceral fat formation, and a reduction in mitochondrial function, all of which facilitate hepatic fat deposition (Alqahtani and Schattenberg, 2021; Chen *et al*., 2023; Guo *et al*., 2025). Furthermore, prolonged exposure to obesogenic environments, sedentary lifestyles, and

comorbidities such as T2DM and hypertension significantly increases the chance of developing MAFLD in elderly people. Consequently, age is regarded as an independent risk factor, with the prevalence of MAFLD typically reaching its highest level in middle-aged and older demographics.

In Malaysia, the prevalence of MAFLD is estimated at 28.2%. Males have a higher prevalence (31.6%) than females (24.5%), consistent with previous reports. The highest-risk age group is individuals aged 50–59 years, with a prevalence of 34.1%, followed by those aged 30–39 years at 31.5%. Compared to the global average, Malaysian patients with MAFLD are typically 10 years younger and present with a greater prevalence of comorbidities, such as diabetes and hypertension. Additionally, Malaysian patients tend to have less favourable metabolic profiles, including higher mean waist circumference, body mass index (BMI), and adverse lipid parameters such as lower HDL cholesterol and higher LDL cholesterol levels (Wan *et al*., 2024). As of recent national health surveys, the prevalence of metabolic syndrome in Malaysia is estimated at approximately 35.9 %, while T2DM affects about 15.6 % of the adult population (Institute for Public Health, 2023; Wan *et al*., 2024).

2.1.3 MAFLD and diabetes mellitus

MAFLD is highly related to T2DM and obesity, as these conditions share key pathophysiological features, including insulin resistance, metabolic syndrome, and chronic inflammation (Gutiérrez-Cuevas, Santos and

Armendariz-Borunda, 2021; Sakurai *et al.*, 2021). The relationship between MAFLD and T2DM is bidirectional. A recent systematic review and meta-analysis by Cao *et al*. (2024) has reported that approximately 26–28% of people with MAFLD also have T2DM. In support of this, a population-based study in Korea found that MAFLD was associated with a 6.1-fold increased risk of diabetes in young adults, primarily due to metabolic dysfunction (Ha *et al*., 2024). Evidence further indicates that the coexistence of MAFLD and T2DM worsens disease severity. T2DM has been shown to accelerate the progression of MAFLD to more severe liver disease, whereas advanced MAFLD increases the risk of developing T2DM (Jeeyavudeen *et al.*, 2023). Independent of obesity and other prevalent metabolic risk factors, MAFLD confers nearly a twofold higher risk for the development of T2DM (Ballestri *et al*., 2016). A study from Indonesia (Sekarsari *et al*., 2023) found that approximately 60 % of T2DM patients also have MAFLD. The coexistence of MAFLD and T2DM has been shown to increase serum triglyceride levels and the presence of diabetes complications. Duan *et al*. (2025) reported that patients with T2DM and MAFLD exhibited significantly higher insulin resistance and adiposity scores compared to those without MAFLD. Among the indices evaluated, the Chinese visceral adiposity index (CVAI) scores showed the strongest predictive value for the presence of MAFLD and liver fibrosis, emphasising the contribution of visceral adiposity and insulin resistance to disease progression. The patients with both T2DM and MAFLD also showed a greater prevalence of comorbidities such as hypertension, coronary heart disease, stroke and peripheral arterial disease. These findings reinforce the concept that insulin resistance underlies the close relationship between MAFLD and T2DM.

Conversely, improvements in hepatic steatosis or resolution of MAFLD are related to a reduced risk of T2DM, supporting the potential of liver-targeted interventions in diabetes prevention. Obesity, particularly visceral obesity, plays a critical role in the development and progression of both MAFLD and T2DM, largely through the induction of insulin resistance. Notably, in non-obese individuals with T2DM, elevated BMI and the presence of metabolic abnormalities are independently associated with the risk of MAFLD (Dang *et al*., 2023).

2.1.4 Pathogenesis of MAFLD

MAFLD develops through a complex interplay of metabolic, inflammatory, and immune mechanisms. A "multi-hit" hypothesis has been suggested, encompassing various mechanisms, including insulin resistance, lipotoxicity, immune and cytokine dysregulation, innate immunity activation, and modifications in gut microbiota (Fang *et al.*, 2018). **Figure 2.1** shows a brief explanation of the pathophysiology of MAFLD.

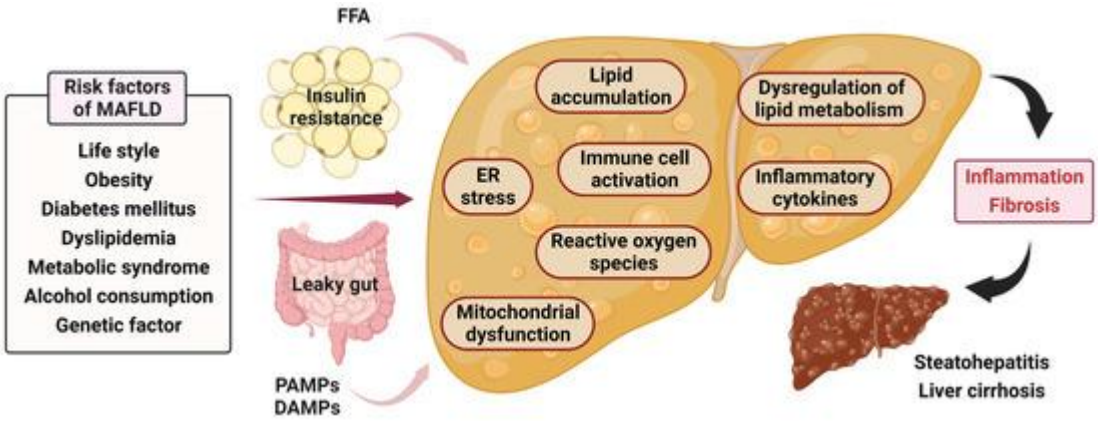

Figure 2.1: **Pathophysiology of metabolic dysfunction-associated fatty liver disease (MAFLD).** Multiple risk factors contribute to the progression of MAFLD, especially insulin resistance. The figure is adapted from Yang and Song (2023).

Insulin resistance is a central driver in the onset and advancement of MAFLD. Insulin resistance is associated with lifestyle factors, including physical inactivity and a sedentary lifestyle, and consumption of a Western-style diet, which is typically high in saturated fat and refined sugars. This would lead to excessive calorie intake, resulting in weight gain and visceral adiposity, which sequentially contribute to the development of insulin resistance (Samuel and Shulman, 2016). When the body's tissues exhibit less responsiveness to insulin, excessive nutrient consumption and modified gut microbiota lead to hepatic fat buildup, exacerbating insulin resistance and creating a vicious cycle (Vesković *et al.*, 2023). Under physiological conditions, insulin plays a key regulatory role in modulating hepatic glucose and lipid metabolism by suppressing gluconeogenesis and promoting de novo lipogenesis (Rahman *et al.*, 2021).

Hepatic de novo lipogenesis is stimulated by the activation of key transcription factors, including sterol regulatory element-binding protein 1 (SREBP-1), carbohydrate-responsive element-binding protein (ChREBP), and peroxisome proliferator-activated receptor gamma (PPAR-γ) (Khan *et al*., 2019). Insulin resistance promotes increased lipolysis in adipose tissue, leading to elevated circulating free fatty acids (FFA), which are transported into the liver and esterified into triglycerides. The combination of FFA influx and upregulated de novo lipogenesis accelerates hepatic triglyceride accumulation and worsens the progression of hepatic steatosis. Notably, a phenomenon termed 'selective hepatic insulin resistance' has been observed in MAFLD patients in which insulin fails to suppress gluconeogenesis but promotes de novo lipogenesis. Clinical study found that the influence of hepatic de novo lipogenesis on intrahepatic triglyceride accumulation was negatively correlated with both hepatic and whole-body insulin sensitivity, indicating that increased lipogenesis is associated with reduced insulin action. Moreover, hepatic de novo lipogenesis is positively associated with integrated 24-hour plasma glucose and insulin levels, suggesting that chronic hyperglycaemia and hyperinsulinemia may drive lipogenic activity in the liver, further promoting fat accumulation and worsening metabolic dysfunction (Smith *et al.*, 2020). Another mouse study reported that the WD40 repeat-containing protein 6 (WDR6) promotes hepatic de novo lipogenesis during insulin resistance by upregulating fatty acid (FA) synthase (FASN) expression (Yao *et al.*, 2023).

In MAFLD patients, the hepatic triglyceride composition was derived 59 % from non-esterified fatty acid, 26 % from de novo lipogenesis and 15 % from dietary sources. This indicates that de novo lipogenesis is elevated during the fasting state of MAFLD, while non-esterified fatty acids serve as the primary contributor to the hepatic triglyceride formation (Donnelly *et al.*, 2005). In hepatocytes, the influx of FFA is catalysed by acyl-CoA synthases to form fatty acyl-CoAs, which are directed either towards esterification or β-oxidation pathways (Buzzetti, Pinzani and Tsochatzis, 2016). In the early stage of MAFLD, hepatocellular mitochondria can adapt to lipid overload by enhancing β-oxidation activity. However, the excessive influx of fatty acid substrates overwhelms the mitochondrial electron transport chain (ETC), leading to elevated production of reactive oxygen species (ROS). Over time, ROS accumulation impairs ETC function, and the persistence of high β-oxidation rates leads to the buildup of incomplete oxidation byproducts. Together, these by-products and elevated ROS levels contribute to the development of insulin resistance (Gusdon, Song and Qu, 2014).

Another mechanism related to hepatic lipid homeostasis is the export of hepatic lipids. Very low-density lipoprotein (VLDL) is composed of apolipoprotein B100 (apoB100) and lipid components (mainly triglycerides and cholesterol esters); it is assembled in the liver with the assistance of microsomal triglyceride transfer protein (MTP) (Nassir, 2022). VLDL serves to transport the lipids to the peripheral organs, such as adipose tissue and muscles. While moderate exposure to fatty acids can increase the apoB100 secretion, chronic lipid overload induces endoplasmic reticulum (ER) stress. This results in the

degradation of apoB100 and decreased apoB100 secretion, which impairs VLDL secretion. This dysfunction in lipid export further contributes to lipid retention and MAFLD progression (Ota, Gayet and Ginsberg, 2008).

Lipotoxicity, characterised by the harmful accumulation of lipid species that disrupt organelle function, dysregulate intracellular signalling pathways, and promote chronic inflammation and cell death, is a key feature in the pathogenesis of MAFLD. The accumulation of certain lipid intermediates, such as diacylglycerols (DAGs), ceramides, lysophosphatidylcholine, free cholesterol, and acylcarnitines, can disrupt intracellular signalling pathways, promote oxidative stress, and induce ER stress (Petersen and Shulman, 2017; Enooku *et al.*, 2019). Lipotoxicity initiates cellular stress responses, activates specific pathways of programmed cell death, and induces inflammation, all of which contribute to the development of fibrosis and may ultimately lead to carcinogenesis (Iturbe-Rey *et al.*, 2025).

Endoplasmic reticulum (ER) stress is a key contributor to the pathogenesis of MAFLD, particularly in response to lipid overload and lipotoxicity. ER is an organelle that regulates protein synthesis, lipid homeostasis and calcium storage within the cell. The buildup of excessive misfolded and unfolded proteins in the ER triggers ER stress and subsequently initiates the unfolded protein response (UPR). The UPR halts general protein translation, enhancing the degradation of misfolded protein, and stimulating the synthesis of chaperones involved in protein folding regulation. The ER stress is

sensed through three transmembrane proteins, inositol-requiring enzyme (IRE1), Protein Kinase R-like Endoplasmic Reticulum Kinase (PERK), and activating transcription factor 6 (ATF6) (Liu and Green, 2019). According to Sharma *et al*. (2015), UPR activation through the ATF6 pathway was shown to stimulate β-cell proliferation, suggesting a role in cellular adaptation. The UPR also facilitates the clearance of misfolded proteins through ER-associated degradation (ERAD) and autophagy, maintaining ER and cellular homeostasis (Lee and Lee, 2022). However, when ER stress is chronic and prolonged, it contributes to the progression of MAFLD through impaired VLDL secretion, increased lipid synthesis, and hepatic insulin resistance, primarily via activation of the IRE1α pathway. Moreover, UPR-induced activation of c-jun N-terminal kinase (JNK) and nuclear factor kappa B (NF-κB) triggers an inflammatory response and activates hepatic stellate cells, promoting fibrosis and increasing risk of cirrhosis (Zhou *et al.*, 2022).

Oxidative stress represents an important mechanism in the progression of MAFLD. The excessive hepatic accumulation of FFA, mitochondrial dysfunction and ER stress increase the production of ROS, which causes cell damage and induces inflammation. ROS such as superoxide, hydroxyl radicals, and hydrogen peroxide are key contributors to oxidative stress and are primarily generated at low physiological levels in the mitochondria and peroxisomes (Hurrle and Hsu, 2017). A clinical study involving healthy male subjects found that oxidative stress in adipose tissue led to extensive protein oxidation and carbonylation, including modification of glucose transporter (GLUT) 4 near its glucose transport site. This oxidative damage impaired GLUT4 function,

reducing glucose uptake and contributing to the development of insulin resistance (Boden *et al.*, 2015). Another study by Tirosh *et al*. (1999) demonstrated that oxidative stress impairs insulin-stimulated GLUT4 translocation by disrupting the intracellular trafficking of insulin receptor substrate-1 (IRS-1) and phosphoinositide 3-kinase (PI3K), along with inhibiting the activation of protein kinase B isoforms PKBα and PKBγ. These disruptions interfere with the insulin signalling cascade, thereby promoting the onset of insulin resistance. In addition to its direct effects on insulin signalling, oxidative stress promotes insulin resistance indirectly by elevating ROS levels, which activate stress-related pathways such as NF-κB, JNK, and p38 mitogen-activated protein kinases (p38 MAPK). This activation triggers mitochondrial stress responses and inflammatory processes that further impair cellular signalling and exacerbate insulin resistance (Tsai *et al.*, 2011; Al-Lahham, Deford and Papaconstantinou, 2015).

Oxidative stress acts as an upstream trigger of inflammation by activating monocytes and macrophages, thereby promoting inflammatory responses that contribute to the development of insulin resistance and diabetes mellitus. Exposure to inflammatory stimuli such as interferon-gamma (IFN-γ), toll-like receptor (TLR) ligands, and proinflammatory cytokines promotes the polarisation of liver macrophages from the anti-inflammatory M2 phenotype to the proinflammatory M1 phenotype, leading to increased production of tumour necrosis factor-alpha (TNF-α) and various chemokines (Vesković *et al.*, 2023). Immune cells engage pattern recognition receptors (PRRs) to detect damage-associated molecular patterns (DAMPs) and pathogen-associated molecular

patterns (PAMPs), thereby initiating downstream signalling cascades that activate proinflammatory pathways and contribute to the innate immune response (Arrese *et al.*, 2016). Beyond immune cell activation by endogenous stress signals, inflammation in MAFLD is also driven by signals originating from the gut. Gut dysbiosis, commonly observed in MAFLD, is characterised by a reduction in beneficial bacteria such as *Akkermansia* and *Prevotella*, along with an overgrowth of potentially pathogenic species. Such microbial imbalance increases intestinal permeability, enabling the translocation of microbial components, particularly lipopolysaccharides (LPS), into the portal circulation. After reaching the liver, LPS interacts with toll-like receptor 4 (TLR4) on Kupffer cells and hepatocytes, initiating proinflammatory signalling cascades that further amplify hepatic inflammation and injury (Yang and Song, 2023; Buchynskyi *et al.*, 2025).

2.1.5 Treatment for MAFLD

MAFLD will become the leading indication of liver transplantation driven by the growing global burden of obesity and diabetes, and the lack of diagnostic tools for early-stage diagnosis (Eslam *et al*., 2020b). In many Western countries, MAFLD-related cirrhosis and hepatocellular carcinoma (HCC) have emerged as the leading indications for liver transplantation, reflecting their growing burden in both end-stage liver disease and liver cancer (Battistella *et al.*, 2022). Metabolic and bariatric surgery (MBS), especially procedures like Roux-en-Y gastric bypass (RYGB) and sleeve gastrectomy, has

been shown to improve MAFLD significantly and steatohepatitis by reducing hepatic steatosis, inflammation, fibrosis, and liver-related cancer risk. Based on these findings, bariatric surgery can be considered for patients with a BMI ≥ 35 kg/m² who do not respond to lifestyle interventions, with RYGB demonstrating more pronounced histological benefits (Liu *et al.*, 2025).

The U.S. Food and Drug Administration approved Rezdiffra (resmetirom) in March 2024 for adult patients with noncirrhotic non-alcoholic steatohepatitis (NASH) accompanied by moderate to advanced liver fibrosis. The medication is intended to be used in combination with dietary and lifestyle modifications (Office of the Commissioner, 2024). Resmetirom, a thyroid hormone receptor β (THR-β) agonist, effectively reduces hepatic fat, lowers liver enzymes, decreases liver stiffness, improves non-invasive fibrosis markers, and enhances cardiovascular health by lowering serum lipids such as LDL cholesterol (Karim and Bansal, 2023). Pioglitazone, at a dosage of 30–45 mg/day, has been shown in clinical trials to improve serum aminotransferase levels and liver histology in patients with biopsy-confirmed non-alcoholic steatohepatitis, particularly among non-diabetic individuals. Vitamin E, administered at 800 IU/day, has demonstrated similar benefits in non-diabetic, biopsy-proven NASH patients, with consistent improvement in hepatic steatosis and liver enzyme levels, although its effect on the overall NAFLD activity score remains variable (Sanyal *et al.*, 2010). Large-scale cohort studies indicated that higher dietary consumption of vitamin E is linked to lower risks of all-cause and cardiovascular mortality, highlighting the potential protective role of vitamin E-rich diets in supporting heart health and reducing mortality (Zeng *et al.*, 2024).

Despite its therapeutic benefits, pioglitazone has been associated with weight gain as a notable adverse effect in clinical trials (Belfort *et al.*, 2006; Sanyal *et al.*, 2010). Additionally, some observational studies have raised concerns about a potential increased risk of bladder cancer with long-term use, particularly at higher cumulative doses, although the evidence remains inconclusive (Davidson and Pan, 2017; Tang *et al.*, 2018). According to the 6th Edition of the Clinical Practice Guidelines on the Management of Type 2 Diabetes Mellitus, statins are recommended for patients with dyslipidaemia to lower the cardiovascular disease risk, which is commonly associated with MAFLD. Although metformin has not demonstrated efficacy in improving steatohepatitis, it may be beneficial in enhancing metabolic parameters and is commonly prescribed for glycaemic control in patients with coexisting diabetes mellitus and MAFLD (Ministry of Health Malaysia, 2020; Chan *et al.*, 2022).

2.1.6 Animal models of diet-induced obesity and metabolic syndrome

Diet-induced obesity (DIO) in rodents has become a cornerstone for modelling the complex phenotype of human metabolic syndrome, encompassing obesity, insulin resistance, dyslipidaemia, MAFLD, and cardiovascular dysfunction (Buettner, Schölmerich and Bollheimer, 2007). Among murine models, the C57BL/6 background, particularly the C57BL/6J substrain, is widely used owing to its high susceptibility to DIO and related metabolic derangements (Gallou-Kabani *et al.*, 2007). The HFD-induced C57BL/6J mouse model is widely used to study obesity and metabolic disorders

due to its susceptibility to diet-induced metabolic alterations (Siersbæk *et al.*, 2020). When fed an HFD, these mice reliably develop a phenotypic profile that closely parallels human metabolic syndrome, including truncal obesity, hyperinsulinemia, hyperglycaemia, and hepatic steatosis. These metabolic changes make the model particularly useful for investigating mechanisms underlying impaired glucose and lipid metabolism and for evaluating potential therapeutic interventions (Della Vedova *et al.*, 2016). Unlike genetic models (such as *ob/ob* or *db/db* mice), which rely on monogenic mutations in the leptin pathway, the HFD-fed C57BL/6J model represents a polygenic and environmental approach. This is more relevant to human sedentary populations, where disease progression is typically driven by chronic caloric surplus and dietary composition rather than a single genetic defect (Haluzik *et al.*, 2004; Boivin *et al*, 2014; Burke *et al.*, 2017). Based on the previous finding, Gargiulo *et al*. (2024) used a Western diet (38.1% kcal from fat, 47% carbohydrate, 33% sucrose, 0.2% cholesterol) in C57BL/6J mice from Charles River and observed a progressive, moderate obesity phenotype that more closely recapitulates gradual weight gain in humans. Fraulob *et al*. (2010) used a more extreme HFD (60% kcal from fat; 26% carbohydrate) in C57BL/6 mice, producing a robust metabolic syndrome phenotype within 16 weeks, including significant weight gain, impaired glucose clearance and enlarged pancreatic islets.

However, despite these similarities, certain physiological and metabolic differences between mice and humans persist, such as variation in lipid metabolism and disease progression. A notable feature of the "6J" substrain is a spontaneous mutation in the nicotinamide nucleotide transhydrogenase (NNT)

gene, which may exacerbate glucose intolerance and oxidative stress compared to other substrains (Siersbæk *et al*., 2020). Although the core biochemical activity of NNT is conserved, studies comparing human mutations and mouse models suggest that the physiological consequences of NNT deficiency differ between species, partly due to tissue-specific expression patterns and experimental context, which complicates direct translational interpretation (Gan *et al*., 2024). Furthermore, while the C57BL/6J mouse model effectively reproduces early features of metabolic liver disease, including hepatic steatosis and insulin resistance, progression to advanced fibrosis or steatohepatitis typically requires prolonged feeding or additional dietary stressors such as high fructose or cholesterol (Zhang *et al*., 2023). Previous studies have reported that fibrosis may develop only after prolonged feeding periods approaching 50 weeks (Ito *et al.*, 2007). Another study has shown that high-fat diet feeding alone often induces only mild hepatic steatosis in mice, whereas the addition of dietary cholesterol markedly exacerbates liver pathology, promoting steatosis, inflammation, and fibrosis (Kim *et al.*, 2016). Despite these limitations, the C57BL/6J mouse remains a robust and highly reproducible system for elucidating the mechanistic pathways of nutraceuticals such as lauric acid in the regulation of lipid and glucose metabolism. Therefore, while the HFD-induced C57BL/6J mouse model provides valuable insights into metabolic dysfunction, caution is necessary when translating findings from animal studies to human conditions.

2.2 Lauric acid

2.2.1 Source of lauric acid

Lauric acid, chemically known as dodecanoic acid, belongs to the group of saturated medium-chain fatty acid (MCFA) containing 12-carbon atoms. The main sources of lauric acid are coconut oil and palm kernel oil, which contain approximately 45–53% (Dayrit, 2014; Silalahi *et al.*, 2018) and 47–49% lauric acid, respectively (Mancini *et al.*, 2015; Silalahi *et al*., 2018). In addition to plant-based sources, lauric acid is also naturally present in animal-derived products, accounting for approximately 6.2% of the total fatty acids in human breast milk, 3.1% in goat milk, and 2.9% in cow milk (Sandhya, Talukdar and Bhaishya, 2016).

2.2.2 Metabolism of lauric acid

Dietary triglycerides undergo enzymatic hydrolysis by pancreatic lipase into free fatty acids and 2-monoglycerides. Among the resulting fatty acids, short-chain and medium-chain fatty acids (MCFAs), including lauric acid (C12:0), are more readily absorbed by the intestinal epithelial cells. Unlike long-chain fatty acids, MCFAs do not require micelle formation or incorporation into chylomicrons. Instead, they are directly transported to the liver via the portal vein, where they are rapidly metabolised for energy production rather than being re-esterified and stored in adipose tissue as fat

(Cassiday, 2016; Wallace, 2018). This unique absorption pathway makes lauric acid less likely to be stored as fat, contributing to its potential metabolic benefits. In the liver, MCFAs diffuse directly into mitochondria and are quickly metabolised, unlike long-chain fatty acids (LCFAs), which require carnitine-dependent transport. As a result, MCFAs serve as a faster and more efficient energy source than LCFAs (Huang, Gao and Chen, 2021). The lauric acid is rapidly metabolised to produce acetyl-CoA through the β-oxidation pathway, which can either enter the citric acid cycle to produce energy or be metabolised into ketone bodies (acetoacetate, β-hydroxybutyrate, and acetone) for alternative energy use in tissues such as the muscle, brain and heart. The secondary pathway, ω-oxidation, normally contributes about 10–20% of total liver fatty acid breakdown. It generates hydroxylated fatty acids that are further converted into dicarboxylic acids and may help reduce excess fatty acid load on the mitochondrial respiratory chain (Cassiday, 2016).

2.2.3 Antimicrobial effect of lauric acid

Both lauric acid and glycerol monolaurate (GML), its monoglyceride form, display strong antimicrobial properties, mostly against Gram-positive bacteria, especially *S. aureus*, fungi such as *C. Albicans*, and viruses, including vesicular stomatitis virus (VSV), herpes simplex virus (HSV), and visna virus (VV) (Nitbani *et al.*, 2022; M *et al*., 2024). As a natural antibacterial agent, lauric acid functions by inhibiting MurA, an enzyme necessary for bacterial cell wall synthesis (Herdiyati *et al.*, 2020). A study from Yang *et al*. (2018) showed

that lauric acid inhibits the growth of *C. difficile* in vitro and reduces *C. difficile* infection symptoms and proinflammatory cytokine production. The antimicrobial effect of lauric acid might contribute to the production of ROS and cell membrane damage in bacteria (Yang *et al.*, 2018). A study by Nakatsuji *et al.* (2009) demonstrated that lauric acid exhibits strong antibacterial activity against *Propionibacterium acnes* without causing cytotoxicity to human sebocytes. In vivo, lauric acid also significantly reduced *P. acnes*-induced ear swelling and granulomatous inflammation in mice, indicating its therapeutic potential for inflammatory acne.

2.2.4 Anti-inflammatory effect of lauric acid

In an animal model of lipopolysaccharide (LPS)-induced liver inflammation, lauric acid was found to lower the levels of pro-inflammatory cytokines, reduce hepatic inflammation, and suppress the expression of TLR4/NF-κB pathway-related proteins in liver tissue (Khan *et al.*, 2020). Lauric acid has also demonstrated an anti-inflammatory effect against *P. acnes* by inhibiting NF-κB activation and suppressing the phosphorylation of MAP kinases in vitro (Huang *et al.*, 2013). In the swimming crab model, lauric acid demonstrated dose-dependent effects. At moderate levels, it enhanced antioxidant activity, improved gut microbiota composition, and increased peritrophic membrane thickness. Additionally, lauric acid repressed the pro-inflammatory gene expressions, suggesting a protective role in maintaining intestinal immune balance (Zhan *et al.*, 2024). Lauric acid was shown to

downregulate genes associated with oxidative stress and inflammatory responses, indicating its potent antioxidant and anti-inflammatory properties. These effects contributed to the suppression of neuroinflammation and enhanced cellular protection. Additionally, lauric acid exhibited a protective effect on normal cell lines, such as fibroblasts (L929), further supporting its safety and therapeutic potential (Ramya *et al.*, 2022). In a hyperglycaemia-aggravated mouse model of ischemic stroke, lauric acid showed neuroprotective properties by decreasing infarct volume and cerebral oedema. It enhanced the expression of antioxidant proteins and lowered levels of lipid peroxidation marker 4-hydroxynonenal (4-HNE) within microvascular structures, thereby preserving blood-brain barrier (BBB) integrity. These protective effects were further supported by improvements in neurological function and behavioural performance (Shaheryar *et al*., 2023).

2.2.5 Anti-cancer properties of lauric acid

Lauric acid has shown its potential for anti-tumour and muscle-protecting effects. Two studies have explored the anti-cancer potential of lauric acid on colorectal cancer cell lines HT29 and CT26. The first study reported that lauric acid inhibited cancer cell proliferation by inducing mitochondrial oxidative stress via increased reactive oxygen species (ROS), suppressing oxidative phosphorylation (OXPHOS), and triggering apoptosis. These antitumor effects were also linked to enhanced ROS production and stimulation of effector T cell energy metabolism (Mori *et al.*, 2025). The second study

demonstrated that lauric acid treatment shifted cancer cells toward OXPHOS, reduced stemness characteristics, elevated ROS levels, and induced cell death, effectively reversing resistance to 5-fluorouracil (5FU). This suggests that alterations in metabolic pathways and stem-like properties contribute to 5FU resistance in colorectal cancer, which lauric acid may help counteract (Fujiwara-Tani *et al.*, 2025). Lauric acid has demonstrated anticancer properties against breast and endometrial cancer cells by stimulating the generation of reactive oxygen species (ROS) and activating key signalling pathways, including the upregulation of $p21^{Cip1/WAF1}$, independent of p53. This mechanism contributes to its antiproliferative and pro-apoptotic effects, supporting its potential in cancer therapy (Lappano *et al.*, 2017).

2.2.6 Metabolic and physiological effects of lauric acid

Beyond its well-established antimicrobial and anti-inflammatory properties, accumulating evidence suggests that lauric acid may exert significant metabolic and physiological benefits. These include favourable effects on lipid metabolism, energy homeostasis, insulin sensitivity, and oxidative stress regulation. Our group has shown that lauric acid restored the mitochondrial biogenesis in insulin-resistant macrophages by enhancing ATP production, increasing oxygen consumption, and upregulating the expression of the mitochondrial biogenesis regulator gene (Tham *et al.*, 2020). Lauric acid has also demonstrated prophylactic effects against atherosclerosis by reducing plaque instability through the regulation of key genes, such as metalloprotease

enzymes (Ong *et al*., 2019). It also suppresses the expression of intercellular adhesion molecule-1 (ICAM-1) and vascular cell adhesion molecule-1 (VCAM-1) in THP-1 macrophages in a dose-dependent manner (Lim *et al*., 2015). In a mouse model, coconut milk supplementation enhanced cholesterol elimination via faecal bile excretion but did not significantly alter the serum cholesterol levels in C57BL/6 mice (Wong, Choo and Chew, 2020). Together, these findings highlight the multifaceted benefits of lauric acid and coconut-derived components, underscoring their potential in modulating metabolic health and offering protective effects against cardiovascular and mitochondrial dysfunction.

Virgin coconut oil was found to improve HDL cholesterol levels and significantly reduce triglyceride concentrations in both the liver and serum. It also significantly elevated hepatic glutathione (GSH) levels, enhanced antioxidant enzyme activities, and lowered lipid peroxidation. These improvements were consistent with decreased liver enzyme activity and restoration of normal hepatic morphology (Narayanankutty *et al.*, 2018). Focus on lauric acid, it enhances endurance and muscle strength by promoting fat mobilisation, altering tissue lipid profiles, and stimulating hepatic fatty acid oxidation via the AMP-activated protein kinase- Acetyl-CoA Carboxylase (AMPK-ACC) pathway in sedentary mice, suggesting that lauric acid could be a potential nutritional supplement to improve aerobic exercise in sedentary people (Guo *et al.*, 2023). Lauric acid has demonstrated protective effects against chronic diabetic complications, including retinopathy and nephropathy, by inhibiting the activities of aldose reductase (AR) and sorbitol dehydrogenase (SDH) in Wistar rats, and by dose-dependently suppressing AR activity in HRT-

15 cells (Sheela *et al*., 2017). Anuar *et al*. (2023) reported that lauric acid alleviated insulin resistance in streptozotocin-induced diabetic rats by normalising blood glucose levels, improving insulin and testosterone concentrations, and restoring the oxidant–antioxidant balance. The improvement in the hormonal profile and glucose homeostasis contributes to tissue regeneration and enhanced sperm quality in diabetic rats. A recent study by Maznan *et al*. (2025) further underscores the nephroprotective potential of lauric acid, showing that it enhances antioxidant defence by increasing superoxide dismutase (SOD) and catalase (CAT) activities, improves kidney function, and helps regulate glucose and insulin levels in streptozotocin-induced diabetic nephropathy in rats.

The anti-glycaemic properties of lauric acid, along with its modulatory effects on lipid metabolism, underscore its potential therapeutic strategy in managing diabetes mellitus and MAFLD. Lauric acid exhibited potent antidiabetic effects by lowering fasting blood glucose levels and enhancing pancreatic β-cell regeneration in high-fat diet and streptozotocin-induced type 2 diabetic rat models (Alex *et al.*, 2020). Lauric acid has been shown to enhance cholesterol metabolism by inhibiting HMG-CoA reductase activity and increasing lipoprotein lipase activity in rat models. These effects were associated with improvements in serum lipid profiles, including reduced triglyceride and low-density lipoprotein (LDL) cholesterol levels, and elevated high-density lipoprotein (HDL) cholesterol levels (Sheela *et al*., 2016). Sedik *et al.* (2024) evaluated the therapeutic potential of lauric acid in a high-fat diet (HFD)-induced MAFLD model using adult male Sprague Dawley rats, and

significantly improved metabolic parameters, including serum triglycerides, total cholesterol, liver enzymes (ALT, AST), glucose, and insulin levels. Antioxidant enzyme activities (SOD, GSH, catalase) and anti-inflammatory cytokine IL-10 were increased, while oxidative stress and inflammatory markers (malondialdehyde (MDA), ROS, myeloperoxidase (MPO), 4-HNE, IL-1β, TNF-α) were reduced. Gene expression analysis revealed upregulation of IRS1, AMPK, PI3K, and sirtuins (SIRT1), along with a decrease in apoptotic marker annexin V. Histological examination supported these findings, showing improved liver architecture. These results suggest that lauric acid may offer protective effects against MAFLD through modulation of metabolic, oxidative, inflammatory, and apoptotic pathways. A recent postprandial intervention study in healthy adults demonstrated that coconut oil, rich in lauric acid, elicited metabolic responses comparable to those of medium-chain triglycerides (MCTs). Coconut oil intake resulted in significantly lower very-low-density lipoprotein cholesterol (VLDL-C) and intermediate-density lipoprotein cholesterol (IDL-C) responses compared to LCTs. These findings suggest that lauric acid-rich CO may be beneficial for the prevention of dyslipidaemia and reduce cardiovascular risk (Furuta *et al.*, 2023). Another study highlighted the potential synergistic effect of lauric acid and tryptophan in regulating blood glucose homeostasis. Intraduodenal administration of the combination in healthy men results in a modest drop in fasting plasma glucose levels, accompanied by increased insulin secretion, possibly mediated through both insulin and glucagon-like peptide-1 (GLP-1) pathways (McVeay *et al.*, 2019).

2.3 Genes involved in MAFLD and insulin resistance

2.3.1 Apolipoprotein A2 (APOA2)

APOA2 constitutes the second most plentiful protein in high-density lipoprotein (HDL), accounting for approximately 20% of its total protein content. APOA2 plays important physiological roles in regulating lipid metabolism and influencing cardiovascular health and disease risk. It contributes to the structural stability of HDL particles and reduces their susceptibility to remodelling (Lund-Katz and Phillips, 2010). HDL is central to the process of reverse cholesterol transport, which helps to remove excess cholesterol from peripheral tissues and direct it to the liver for excretion (Sucharski and Koenig, 2022). In this process, apolipoprotein A1 (APOA1) primarily functions as the cholesterol acceptor within HDL, facilitating cholesterol efflux. Sarkar *et al.* (2024) reported that lapidated HDL particles containing both APOA1 and APOA2 enhance cholesterol efflux through the ATP-binding cassette transporter A1 (ABCA1). Their findings also revealed that APOA2 induces conformational changes in the N- and C-terminal helices of APOA1, thereby facilitating ABCA1-dependent cholesterol efflux. While its role in cardiovascular disease is still debated, APOA2 is known to regulate key enzymes involved in lipoprotein metabolism. It inhibits cholesterol ester transfer protein (CETP), responsible for the exchanging cholesteryl esters and triglycerides between lipoproteins; stimulates lecithin–cholesterol acyltransferase (LCAT), which converts the free cholesterol into cholesteryl esters; and increases phospholipid transfer protein (PLTP) activity, facilitating

the transfer of phospholipids from triglyceride-rich lipoproteins to HDL. Additionally, APOA2 influences hepatic lipase (LIPC) activity, which is involved in the hydrolysis of triglycerides (Boughanem *et al.*, 2020).

A well-characterised polymorphism in the APOA2 gene, -265T>C (rs5082), has been demonstrated to affect APOA2 expression levels and is related to metabolic conditions, including obesity and insulin resistance. This genetic variant has been linked to increased visceral fat accumulation in postmenopausal women, along with higher body mass index (BMI), greater food intake, and an altered postprandial response to saturated fat consumption in healthy men (Lara-Castro *et al.*, 2005; Corella *et al.*, 2007). A study by Jafari Azad *et al*. (2021) highlights that the APOA2-265 T>C polymorphism may exacerbate oxidative stress and inflammation in T2DM patients, particularly in carriers of the CC genotype, and underscores the value of genotype-based dietary guidance, such as the inclusion of antioxidant-rich foods, for managing cardiovascular risk in this population. Furthermore, APOA2 could be used as a biomarker to predict the risk of diseases. Higher serum APOA2 levels are linked to a reduced risk of major adverse cardiovascular events in patients undergoing coronary interventions, making it a strong independent predictor of prognosis (Akiyama *et al.*, 2024). The APOA2 isoform (APOA2-i) index, when combined with carbohydrate antigen 19-9 (CA 19-9), enhances the diagnostic accuracy for early-stage pancreatic cancer, underscoring its potential utility as a clinical biomarker (Shionoya *et al.*, 2025).

To date, no study has directly examined the role of APOA2 in the development and progression of MAFLD. MAFLD shared common risk factors with cardiovascular disease, including obesity, metabolic syndrome and hepatic inflammation. Hepatic steatosis and progression to hepatic fibrosis are pathophysiological features of MAFLD, which has been shown to worsen cardiac function and subsequently lead to heart failure. Moreover, the cardiovascular disease incidence is also higher in the MAFLD patients, supporting that MAFLD independently contributed to the progression of cardiovascular disease (Yang and Song, 2023). In the context of MAFLD, apolipoproteins are often discussed with reference to altered lipid profiles, such as a low apolipoprotein B to apolipoprotein A1 ratio, reduced HDL level and increased LDL and VLDL (Cazac *et al*., 2022). However, the specific role of ApoA2 in MAFLD has not been directly mentioned in the literature. Instead, evidence comes from studies linking APOA2 genetic variations to metabolic traits. A study by Lai *et al.* (2018) suggests that the genetic variation in the APOA2 regulatory region, which is the APOA2-265 T>C polymorphism, interacts with saturated fat intake to influence obesity risk. Carriers of the CC genotype consuming a high saturated fat diet showed reduced APOA2 expression, and metabolomic profiling revealed perturbations in branched-chain amino acid and tryptophan pathways (Lai *et al*., 2018). This APOA2 gene-diet interaction highlights how APOA2 may influence obesity risk, thereby indirectly contributing to the risk of MAFLD.

2.3.2 Peroxisome proliferator-activated receptor gamma (PPARγ)

PPARγ functions as a nuclear receptor crucial for controlling the transcription of genes involved in lipid and glucose metabolism, adipocyte differentiation, and insulin sensitivity. Its expression is predominantly found in adipose tissue and immune cells. Among its isoforms, PPARγ1 is broadly expressed across various tissues, including white and brown adipose tissue, cardiac muscle, liver and immune cells, such as monocytes/macrophages, dendritic cells, and T lymphocytes. In contrast, PPARγ2 expression is largely restricted to adipose tissue. PPARγ regulates the transcription of a broad array of genes implicated in energy balance, carbohydrate metabolism, and lipid homeostasis. Apart from regulating metabolism, PPARγ also participates in regulating inflammatory responses and cell proliferation, which is linked to tumorigenesis. It is widely recognised as a master regulator of adipogenesis and for the development of mature adipocytes (Kroker and Bruning, 2015).

PPARγ contributes significantly to maintaining glucose homeostasis and enhancing insulin sensitivity through multiple mechanisms, including the regulation of adipocyte differentiation and function, modulation of brown adipose tissue activity, suppression of inflammation, and enhancement of insulin signalling pathways (**Figure 2.2**). PPARγ promotes adipogenesis by inducing several specific adipocyte markers expression, such as adipocyte fatty acid binding protein (aP2), phosphoenolpyruvate carboxykinase (PEPCK), and lipoprotein lipase (LPL) (Imai *et al*., 2004; Leonardini *et al*., 2009). Remarkably,

the ectopic expression of PPARγ can induce adipogenic conversion in non-adipogenic cells such as NIH-3T3 cells (Wu *et al.*, 1995). Additionally, the PPARγ promotes the apoptosis of mature adipocytes, leading to the replacement with smaller, more insulin-sensitive adipocytes (Okuno *et al*., 1998). PPARγ activation also facilitates the absorption and deposition of free fatty acids (FFAs) within adipose tissue by upregulating genes involved in lipid transport and metabolism. For instance, CD36 and fatty acid transport protein facilitate FFA uptake, while PEPCK contributes to the generation of the glycerol backbone for triglyceride synthesis. This process promotes triglyceride storage in subcutaneous fat depots, reducing circulating FFAs and alleviating lipotoxicity in insulin-sensitive tissues such as muscle and the liver. In brown adipose tissues, PPARγ plays a central role in thermogenic programming through the interaction with transcriptional regulatory factors such as positive regulatory domain zinc finger region protein 16 (PRDM16), Peroxisome proliferator-activated receptor gamma coactivator 1-alpha (PGC-1α), and uncoupling protein 1 (UCP1), promoting the transcription of brown adipose tissue-specific genes and mitochondrial function (Koppen and Kalkhoven, 2010). Moreover, PPARγ regulates the production and secretion of adipokines within adipose tissue. It downregulates pro-inflammatory adipokines such as tumour necrosis factor-alpha (TNF-α), interleukin-6 (IL-6), and resistin, all of which contribute to the development of insulin resistance in peripheral tissues. In contrast, PPARγ activation stimulates the secretion of adiponectin, an insulin-sensitising adipokine that promotes fatty acid oxidation, enhances glucose uptake in skeletal muscle, and reduces hepatic gluconeogenesis. (Choi, Park and Choi, 2014). Furthermore, PPARγ appears to upregulate glucose transporters GLUT1

and GLUT4 expression and their translocation to the membrane, facilitating glucose uptake in the liver and skeletal muscle cells and ultimately reducing the blood glucose levels (Staels and Fruchart, 2005).

PPARγ is involved in lipid metabolism, adipogenesis, and the activation of hepatic stellate cells and macrophages, exerting its protective effects against the progression of MAFLD. Activation of PPARγ has been shown to improve insulin resistance and increase adiponectin secretion, thereby improving glucose and lipid metabolism and ameliorating hepatic steatosis. Notably, hepatic expression of PPARγ was significantly increased in MAFLD patients, and the clinical trial showed that treatment with PPARγ agonist, thiazolidinediones, markedly reduced the hepatic steatosis. Thus, PPARγ remains an important therapeutic target, with partial activation of PPARγ offering its beneficial effects while avoiding the unwanted effects, such as adipogenesis (Skat-Rørdam *et al.*, 2018).

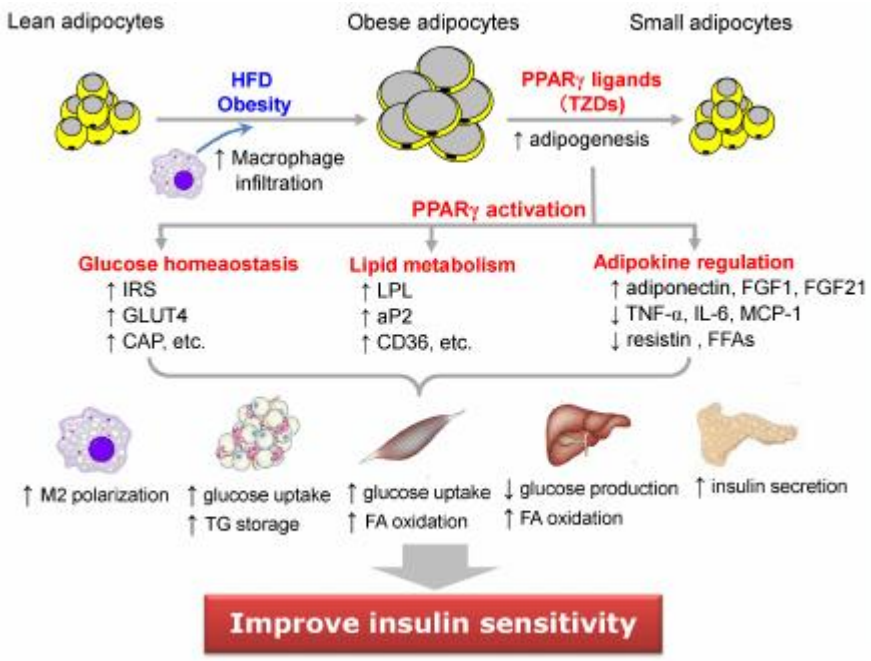

Figure 2.2: **PPARγ roles in metabolism to improve insulin resistance**. Activation of PPARγ stimulates glucose uptake, reduces circulating free fatty acids and promotes insulin secretion. The figure is adapted from Choi, Park and Choi (2014).

2.3.3 Sterol regulatory element-binding proteins (SREBP)

SREBPs are transcriptional factors that are key regulators of lipid metabolism, controlling the synthesis of triglycerides and cholesterol, as well as the function of multiple organs. SREBPs are crucial for regulating lipid homeostasis, and their disruption has been linked to various pathological conditions, including diabetes mellitus, ER stress, atherosclerosis and MAFLD. The SREBP family consists of three isoforms: SREBP-1a and SREBP-1c, both encoded by the *SREBF1* gene, and SREBP-2, encoded by the *SREBF2* gene. SREBP-1c is predominantly expressed in the liver, white adipose tissue, adrenal glands, skeletal muscle, and brain, whereas SREBP-1a is expressed at lower

levels, mainly in cell lines, spleen, and intestinal tissues (Moslehi and Hamidi-Zad, 2018). SREBP activity is regulated at multiple levels, including mRNA synthesis, proteolytic activation, and transcriptional control. High sterol levels inhibit SREBP activation, while low levels promote it. Lipid-derived molecules such as cholesterol, oxysterols, and unsaturated fatty acids modulate the SREBP pathway by binding to specific regulatory proteins: cholesterol binds to Scap, oxysterols to Insigs, and unsaturated fatty acids to Ubiquitin regulatory X (UBX) domain-containing protein 8 (Ubxd8). These interactions influence the ER-to-Golgi transport of Scap–SREBP complexes, thereby controlling the proteolytic activation of SREBPs. However, oxysterols also promote the activation of SREBP-1c by activating the liver X receptor (LXR). LXR binds to the SREBF1 promoter, thus increasing the SREBP-1c expression (Repa *et al*., 2000).

SREBPs contribute to the pathophysiology of metabolic diseases, such as obesity, diabetes, dyslipidaemia and MAFLD. **Figure 2.3** shows the relationship of SREBP1 and SREBP2 with MAFLD. SREBP-1c plays an important role in the biogenesis of lipids. Insulin stimulates SREBP-1c expression via the PI3K/Akt/mTORC1 signalling pathway, resulting in the upregulation of lipogenic genes such as FASN, ACC, and Stearoyl-CoA desaturase 1 (SCD1). Under physiological conditions, this ensures adequate lipid supply; however, chronic overactivation of SREBP-1c, such as in states of hyperinsulinemia, drives excessive fatty acid and triglyceride synthesis. Higuchi *et al*. (2008) reported that hepatic *LXRα* mRNA levels are markedly elevated in MAFLD and show a strong positive association with *SREBP-1c* expression, which in turn drives the upregulation of downstream lipogenic

genes such as *ACC1* and *FAS*. Latorre *et al.* (2017) provide compelling evidence that MAFLD is associated with distinct changes in hepatic microRNAs, which correlate with a metabolic shift toward increased lipogenesis and reduced fatty acid utilisation and glucose metabolism. These molecular patterns are consistent with excessive SREBP-1c-driven lipogenic activity, a hallmark of insulin resistance and metabolic liver disease. Nagaya *et al.* (2010) demonstrate that SREBP-1c expression and activity decline sharply in advanced, fibrotic stages of NASH, while inflammatory signalling such as TNF-α rises. This pattern supports a metabolic transition from lipogenesis to inflammatory/fibrotic processes as disease progresses. Chronic overexpression of SREBP-1c in mouse liver leads to notable hepatic lipid accumulation and systemic insulin resistance, even under normal calorie intake. Thus, extended SREBP-1c activation is a direct driver of metabolic dysfunction (Knebel *et al.*, 2012). SREBPs and their chaperone SCAP serve as central regulators of hepatic lipid metabolism. Yellaturu *et al*. (2009) demonstrated that insulin increases the post-transcriptional activation of SREBP-1c through suppression of INSIG-2a, promoting lipogenic transcription and triglyceride accumulation in liver cells. While this pathway drives steatosis, Kawamura *et al.* (2022) found that complete inhibition of SCAP/SREBP signalling paradoxically worsened liver injury, fibrosis, and carcinogenesis in mouse models of NASH, due to disrupted phospholipid homeostasis and ER stress; these effects were reversed by restoring SREBP activity. Together, these findings underscore that targeting insulin-driven SREBP-1c activity may offer therapeutic benefit. In addition to triglyceride lipogenesis, the cholesterol overload is also involved in the progression of MAFLD. Caballero *et al*. (2009) demonstrated that in human

NAFLD, hepatic expression of cholesterol-regulatory genes is selectively upregulated: SREBP-2 mRNA levels were elevated in both simple steatosis and steatohepatitis, accompanied by parallel increases in HMG-CoA reductase, whereas SREBP-1c and FAS expression remained unchanged. Collectively, SREBPs function as metabolic integrators linking nutrient and hormonal signals to lipid metabolism. Their dysregulation is a central mechanism in the pathogenesis of insulin resistance, obesity, T2DM, and MAFLD.

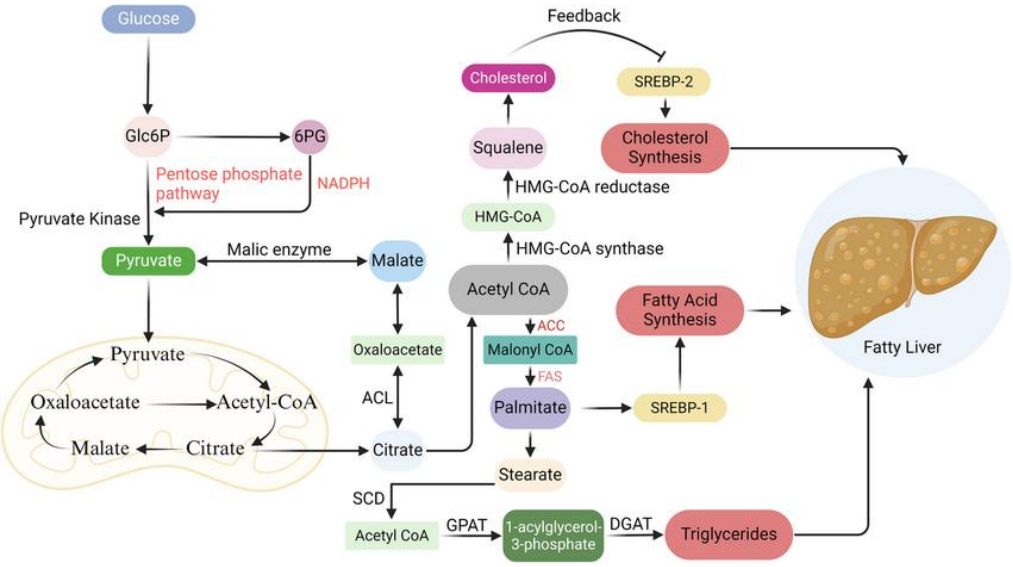

Figure 2.3: **The link between SREBP1 and SREBP2 with MAFLD**. SREBP1 regulates lipogenesis while SREBP2 modulates cholesterol synthesis. The dysregulation of SREBPs leads to the progression of MAFLD. The figure is adapted from Barbhuiya, Yoshitomi and Pathak (2025)

2.3.4 HMGCR (3-hydroxy-3-methylglutaryl-CoA reductase)

HMGCR acts as the rate-limiting enzyme in cholesterol biosynthesis, catalysing the conversion of HMG-CoA to mevalonate. Cholesterol is synthesised via the mevalonate pathway or acquired from extracellular low-density lipoproteins (LDL), functioning as a critical component of cellular membranes, lipoproteins, and acting as a precursor to steroid hormones, vitamin D, and bile acids. Along with sterols, the mevalonate pathway generates non-sterol isoprenoids, such as geranylgeranyl pyrophosphate (GGPP), that are essential for cellular viability (Faulkner and Jo, 2022). The flux through this pathway is tightly regulated, balancing the need for non-sterol isoprenoids while preventing excessive sterol accumulation. Transcriptional regulation of HMGCR is primarily coordinated by the SREBP–Scap pathway: under low sterol conditions, SREBPs are activated and translocated to the nucleus to enhance HMGCR transcription. Elevated sterols inhibit this cleavage via Insig-mediated retention in the ER. Post-translational regulation is triggered by intracellular sterol accumulation, which promotes HMGCR ubiquitination and facilitates proteasome-mediated ER-associated degradation (ERAD). Key to this process is the Insig protein, which binds a sterol-sensing domain (SSD) within HMGCR's N-terminal transmembrane region, enabling ubiquitination and ERAD (Chen *et al.*, 2022).

Excessive hepatic HMGCR activity increases endogenous cholesterol synthesis, raising circulating LDL, an established driver of atherosclerosis via cholesterol deposition in arterial walls and inflammation (Chakraborty *et al.*, 2023). Statins, the principal pharmacological inhibitors of HMGCR, significantly reduce LDL and lower cardiovascular morbidity and mortality (Huang *et al*., 2023). Meta-analyses have shown that statin therapy is generally safe in patients with MAFLD and is associated with improvements in hepatic steatosis, inflammation, and fibrosis, together with a reduced hepatocellular carcinoma risk (Swerdlow *et al*., 2014). In addition, MAFLD are characterised by dysregulated cholesterol metabolism with increased expression and activity of HMGCR, often driven by elevated SREBP2 signalling and reduced phosphorylation-mediated inhibition. Studies in human liver samples have demonstrated that HMGCR expression correlates strongly with intracellular free cholesterol, downregulation of LDL receptor, histologic severity, and decreased HMGCR phosphorylation. This indicates that the deregulation of hepatic cholesterol synthesis contributes to the progression of MAFLD, as shown in **Figure 2.4** (Min *et al*., 2012).

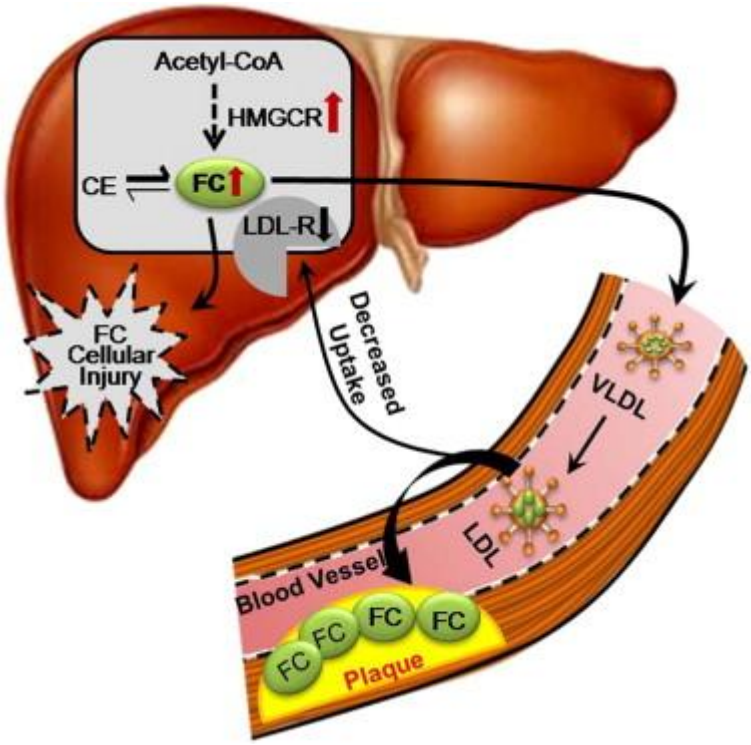

Figure 2.4: **Cholesterol synthesis by HMGCR**. Dysregulation of cholesterol metabolism contributes to fatty liver disease and increases the risk of cardiovascular disease. The figure is adapted from Min *et al* (2012).

2.3.5 AMP-activated protein kinase (AMPK)

AMPK is a crucial cellular energy sensor that acts to maintain the metabolic energy balance. It is a heterotrimeric serine/threonine kinase with α, β and γ subunits (Steinberg and Hardie, 2022). AMPK activity is regulated by both nucleotide-dependent and nucleotide-independent mechanisms. In a classical nucleotide-dependent manner, an increased AMP/ATP or ADP/ATP ratio promotes AMPK activation by phosphorylation at Thr172 by upstream kinases such as liver-kinase-B1 (LKB1), and protects AMPK from dephosphorylation, sustaining its activation under energy stress. Alternatively, AMPK can be activated in a nucleotide-independent manner by

calcium/calmodulin-dependent protein kinase kinase β (CaMKKβ) in response to intracellular calcium elevation, independent of AMP or ADP levels (Garcia and Shaw, 2017).

AMPK is activated when the AMP/ATP or ADP/ATP ratio rises, commonly occurring during metabolic stress conditions such as hypoxia, glucose deprivation, or exercise (Herzig and Shaw, 2017). Once activated, AMPK restores energy balance by inhibiting anabolic pathways that consume ATP, including fatty acid synthesis, cholesterol synthesis, and protein synthesis, while simultaneously promoting catabolic pathways such as fatty acid oxidation and autophagy, as shown in **Figure 2.5** (Garcia and Shaw, 2017; Steinberg and Hardie, 2022). AMPK is central to lipid metabolism, directly controlling key enzymes and transcription factors responsible for lipogenesis and cholesterol synthesis. One of its primary targets is acetyl-CoA carboxylase 1 (ACC1), which catalyses the conversion of acetyl-CoA to malonyl-CoA, a rate-limiting step in fatty acid biosynthesis. AMPK phosphorylates and inactivates ACC1, thereby reducing malonyl-CoA levels and promoting mitochondrial fatty acid oxidation (Fullerton *et al*., 2013). In addition, AMPK negatively regulates HMGCR, the rate-limiting enzyme in the mevalonate pathway of cholesterol synthesis, through direct phosphorylation, leading to decreased hepatic cholesterol production (Loh *et al.*, 2018). Beyond enzymatic control, AMPK also suppresses the transcription of SREBP-1c, a master transcription factor driving de novo lipogenesis. AMPK inhibits SREBP-1c at both transcriptional and post-translational levels, thereby downregulating the lipogenic gene expression, such as FASN and ACC1, contributing to reduced lipid

accumulation in hepatocytes (Li *et al*., 2011; Fang *et al*., 2022). Boudaba *et al*. (2018) demonstrated that hepatic AMPK deletion alone does not cause steatosis or cholesterol accumulation, suggesting that decreased AMPK activity might result from fatty liver rather than lead to it. However, pharmacological activation of AMPK suppressed de novo lipogenesis and reduced cholesterol synthesis in an AMPK-dependent, transcription-independent manner. Through these mechanisms, AMPK acts as a metabolic brake on lipogenesis and cholesterol biosynthesis, promoting lipid catabolism and improving lipid homeostasis.

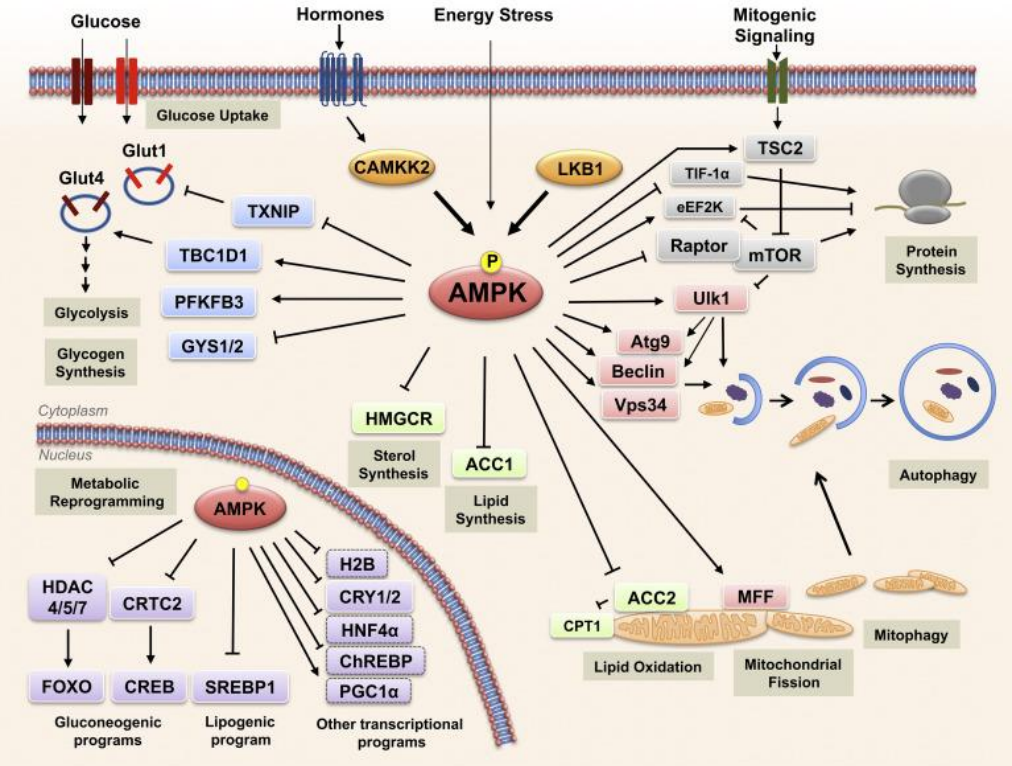

Figure 2.5: **The regulation of AMPK on multiple metabolic processes in cells**. Activation of AMPK suppresses SREBP-1 and HMGCR, which reduces lipogenesis and cholesterol synthesis. The figure is adapted from Garcia and Shaw (2017).

CHAPTER 3

MATERIAL AND METHODS

3.1 Animals and experimental design

This study received ethical approval from the UTAR Scientific and Ethical Review Committee (SERC) (U/SERC/241/2021) for the experimental study and the handling of mice. Five-week-old male C57BL/6J mice were purchased from USM (Kubang Kerian) and underwent a one-week adaptation period to acclimate to the new environment before the experiments began. The mice were housed in the animal cabin at UTAR Kampar under a 12-hour light/dark cycle at a temperature of 25 ºC in polypropylene cages (Tecniplast, Italy) with wood bedding, which was replaced every two weeks. The mice were randomly assigned to five groups, with six in each group. Group 1 mice were fed with normal chow diet (Gold Coin, Malaysia; 20% protein, 50% carbohydrate, 5% fat by energy, 3.25 kcal/g), while group 2 to 5 were fed with high fat diet (HFD) (Altromin, Germany; 60% of fat, 16% of protein, and 24% of carbohydrates (5.23 kcal/g)). The mice had *ad libitum* access to the food pellet and distilled water. Co-treatment began after eight weeks, with mice in groups 3 and 4 receiving 12 mg/kg and 24 mg/kg of lauric acid (Sigma Aldrich, USA) once daily for eight weeks, respectively. Group 5 mice were co-fed with 20 mg/kg rosiglitazone (TCI, Japan) as a positive control until the end of the experiment. Lauric acid and rosiglitazone were prepared and administered using

5% (v/v) undenatured ethanol (Chemiz, Malaysia) as the vehicle. Mice in groups 1 and 2 did not receive any co-treatment and served as control groups. To ensure reproducibility and statistical power, the experiment was conducted in two independent cohorts under the same conditions. The resulting data sets were pooled and analysed collectively, with findings presented as the combined mean of both replicates. All experimental procedures followed the guidelines under the Code of Practice for the Care and Use of Animals for Scientific Purposes of UTAR (POL-IPSR-R&D-006).

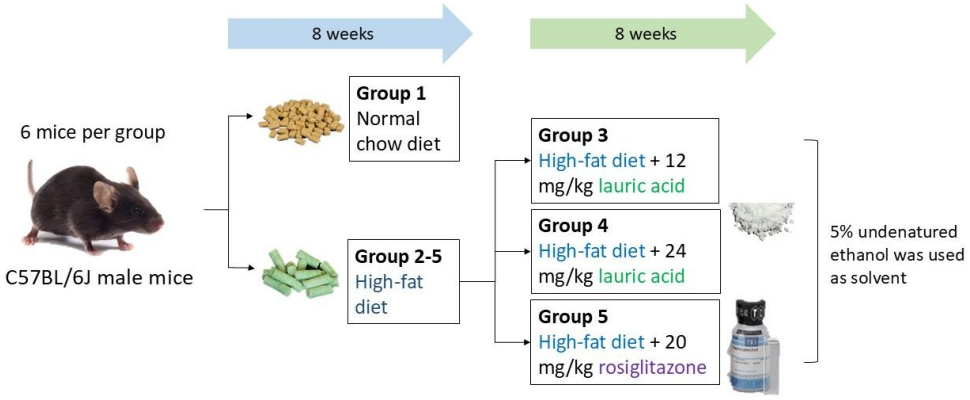

Figure 3.1: **Experimental design of the study.** Mice were divided into five groups: normal chow diet, high-fat diet (HFD), HFD treated with 12 mg/kg and 24 mg/kg lauric acid, and HFD treated with 20 mg/kg rosiglitazone.

3.2 Oral gavage procedure

The mice were maintained and cared for until 14 weeks of age before the gavage experiment began. To familiarise the mice with oral gavage feeding, they were gavaged with 0.2 mL of distilled water per day prior to the actual experiment. The gavage familiarisation was carried out for one week. Fresh working stocks of lauric acid and rosiglitazone were prepared daily in 5% (v/v) undenatured ethanol. To achieve homogeneous preparation, the samples were

sonicated in a 40 °C water bath for 20 minutes. Using a 1 mL syringe (Terumo, Japan) and a gavage needle (PetSurgical, USA), lauric acid (12 or 24 mg/kg of mouse body weight) or rosiglitazone (20 mg/kg) was administered to the mice by gavage. The general condition of the mice was monitored following gavage for any abnormal or distressed behaviours. The oral gavage was performed daily for 8 weeks.

3.3 Measurement of physical parameters

3.3.1 Mice body weight monitoring

The body weight of the mice was measured weekly, starting on the first day of each week. Firstly, the beaker was weighed, and the scale was tared. The mouse was then placed in the beaker, and its body weight was recorded (Jackson Laboratory, 2014; Ballard and Cazarin, 2022). Each measurement was repeated three times to obtain an average reading. The body weight gain of the mice was calculated based on the formula (Kao *et al*., 2018):

$$\text{weight gain (\%)} = \frac{\text{final weight} - \text{initial weight}}{\text{initial weight}} \times 100\%$$

3.3.2 Food and calorie intake

The average food intake of mice was measured on the first three days of every week. A total of 30-40 g of food pellets was measured and provided to the mice. The remaining food pellets were measured after 2 days. The individual food intake was calculated using the equation below (Ballard and Cazarin, 2022):

$$\text{Individual food intake} = \frac{(\text{initial food mass} - \text{final food mass}) \div 3 \text{ days}}{\text{amount of mice in the cage}}$$

The calorie intake of mice was calculated by using the formula (Grobe, 2017):

$$\text{Calorie consumed(kcal)} = \text{food consumed(g)} \times \text{calorie density } \left(\frac{\text{kcal}}{\text{g}}\right).$$

The overall calorie density of the chow diet was 3.250 kcal/g, while that of the HFD was 5.228 kcal/g. The caloric density of the chow diet was estimated from its macronutrient composition: 20% protein, 5% fat, and 50% carbohydrates. Fibre content was excluded as it does not contribute to caloric density. The following standard physiological fuel values were applied to calculate the energy contribution per 100g of diet: Protein: 4 × 20 = kcal/100g; Fat: 9 ×5 = 45 kcal/100g; Carbohydrates: 4 × 50 = 200 kcal/100g. By summing these values, the total energy content was determined to be 325 kcal/100g, resulting in a final caloric density of 3.250 kcal/g. In contrast, the exact caloric density of the HFD was utilised as specified by the manufacturer (Altromin, Germany), ensuring precise energy intake monitoring across both dietary groups.

3.4 Assessment of blood glucose level

3.4.1 Fasting blood glucose level and oral glucose tolerance test

Fasting blood glucose levels were measured triweekly, starting at 8 weeks of age. The mice were fasted for 6 hours before measurement. Blood was collected via the tail vein sampling, and the fasting blood glucose levels were measured using the One Touch Select Simple Glucose Meter (LifeScan, USA).

3.4.2 Oral glucose tolerance test （OGTT）

The oral glucose tolerance test (OGTT) was performed when the mice reached 21 weeks of age. The mice were fasted for 6 hours before the experiment. The fasting blood glucose levels (0 hour) were measured. Next, the mice were gavage-fed with 2 g/kg body weight of a 0.25 g/mL D-(+)-Glucose (Himedia, India) solution. Blood glucose levels were measured at 1 hour and 2 hours after glucose administration (Al Rijjal and Wheeler, 2022).

3.5 Euthanasia, tissue harvesting and sample collection

The mice were sacrificed after 8 weeks of oral gavage using the cervical dislocation method (UQ Biological Resources, 2020) and carefully dissected. The blood was drawn from the aorta of the mice using a 1 mL syringe with needle (Terumo, Japan) and stored in the sterile 1.5 mL microcentrifuge tube (Kirgen, China). The microcentrifuge tube was left uninterrupted at room temperature for 30 minutes to allow blood clotting, then centrifuged at 2000 x

g for 10 minutes to separate the serum. The serum was transferred to a new 1.5 mL microcentrifuge tube and stored at -20 ºC for further analysis. The livers were harvested and rinsed with phosphate-buffered saline (PBS) (Oxoid, USA) to remove the excess blood. The absolute liver weight was measured, and the relative liver weight was calculated by normalising to the final body weight of the mice. The liver was divided into two portions: one half was preserved in 10% (v/v) neutral-buffered formalin (Surgipath, Germany) at room temperature for histological examination, while the other half was snap-frozen in liquid nitrogen and stored at -20 °C for molecular studies.

3.6 Histological examination of liver sample

The mice liver samples were outsourced to the Universiti Putra Malaysia (UPM) veterinary laboratory service unit for professional processing and examination. The liver tissues were stained with haematoxylin and eosin (H&E) to evaluate the histological architecture. The histological assessment was performed by UPM veterinary anatomic pathologist, Dr Kok Mun Keong, to assess the key features such as hepatocyte morphology, inflammatory infiltration, lipid accumulation and other pathological changes. The International Harmonisation of Nomenclature and Diagnostic Criteria for Lesions in Rats and Mice (INHAND) guideline was taken as a reference for classifying microscopic lesions and steatosis observed in the hepatobiliary system of laboratory rats and mice (Thoolan *et al.*, 2010). Stained slides were examined under the light microscope, and the images were captured using Leica Application Suite Version 3.4.0 (Leica Microsystems, Switzerland).

3.7 Biochemical analysis of blood serum for lipids and insulin

The serum biochemical analyses of triglycerides, total cholesterol and high-density lipoprotein (HDL) were performed using the metabolism assay kit from Elabscience. At the same time, the insulin levels were measured using the ELISA kit (Elabscience, USA). All assays were conducted according to the manufacturer's protocols. The absorbance readings were obtained using the microplate reader (FLUOstar Omega, Germany) at the specified wavelength. The concentrations of the serum lipid profile (total cholesterol, HDL, and triglycerides) were calculated using the formulas provided in the metabolism assay kit protocols. In contrast, insulin concentration was determined based on the standard curve. The results of triglycerides, total cholesterol and HDL were expressed in mmol/L, while insulin was expressed in pg/mL. The low-density lipoprotein (LDL) levels were calculated using the Friedewald equation (Matthews *et al.,* 1985; Cacho *et al*.,2008):

$$LDL\ (mmol/L) = total\ cholesterol - HDL - (\frac{triglyceride}{2.2}),$$

where triglyceride/2.2 is the estimation of very low-density lipoprotein level.

3.8 Calculation of insulin resistance (HOMA-IR)

Homeostatic Model Assessment for Insulin Resistance (HOMA-IR) is an index used to measure the severity of insulin resistance. HOMA-IR was calculated using the following formula:

HOMA-IR = [insulin(mU/L) × glucose(mmol/L)] / 22.5.

A HOMA-IR value greater than or equal to 2.0 is considered indicative of insulin resistance (Salgado *et al.*, 2010).

3.9 RNA and protein analysis

3.9.1 RNA and protein extraction

RNA and protein from the liver samples were extracted using TRIzol reagent (Invitrogen, USA) according to the manufacturer's protocol. The aqueous phase was transferred to a sterile 1.5 mL microcentrifuge tube after the phase separation. RNA isolation was then continued following the TRIzol protocol. For protein extraction, minor modifications to the standard protocol were made based on the method described by Simões *et al*. (2013). After the aqueous phase, the protein was precipitated from the remaining interphase and organic phase. The protein pellet was washed 3 times with 0.3M guanidine hydrochloride (Calbiochem, Germany) in 95% (v/v) ethanol (Chemsol, USA) and 1 time with absolute ethanol (Merck, Germany). The pellet was then resuspended in 200 µL of 1:1 solution of 1% (w/v) SDS (1st BASE. Singapore)

and 8 M urea (Chemiz, Malaysia) in Tris–HCl (Fisher Scientific, USA) 1 M, pH 8.0, by pipetting up and down, and incubated in 50 ºC water bath for 1 hour to resuspend the protein completely into the solution. This was followed by centrifugation for 10 minutes at 10,000 × g at 4 °C to remove any insoluble material. The protein samples, which were the supernatant, were transferred to new 1.5 mL microcentrifuge tubes and stored at -20 ºC for further analysis.

3.9.2 RNA quantification and quality assessment

The concentration and purity of the extracted RNA were determined using a Nanodrop spectrophotometer (NanoDrop™ 2000/2000c Spectrophotometer, Thermo Fisher Scientific, USA). RNA integrity was further assessed by electrophoresis on a 1% (w/v) denaturing formaldehyde (Agors, Belgium) agarose gel according to protocol (Wendel Lab, 2003; Brown, Mackey, and Du, 2004). The 1% agarose gel (Invitrogen, USA) containing formaldehyde was prepared in 10× MOPS buffer (US Biological, US) and pre-stained with EtB 'Out' Nucleic Acid Staining Solution 2.0 (Yeastern Biotech, Taiwan). Electrophoresis was performed at 90V for 50 minutes, and the gel was visualised using the gel imager (Gel Doc XR+ Gel Documentation system, Bio-Rad, USA).

3.9.3 Protein quantification

The concentration of protein samples was quantified using the Bio-Rad DC Protein Assay (Bio-Rad, USA), based on the Lowry method. The assay was carried out following the microplate assay procedure described in the manufacturer's protocol.

Briefly, a series of bovine serum albumin (BSA) solutions was prepared by dissolving BSA (Life Science Production, UK) in the same buffer used for protein samples (1:1 solution of 1% SDS and 8 M urea in 1M Tris–HCl (pH 8.0)) to generate the standard curve. For each sample and standard, 5 µL of protein solution was mixed with 25 µL of reagent A (alkaline copper tartrate solution) and 200 µL of reagent B (diluted Folin Reagent) in a sterile 96-well plate (Biologix, USA). The mixture was incubated for 15 minutes at room temperature, and the absorbances were measured at 750 nm using a microplate reader (FLUOstar Omega, Germany). Protein concentrations were measured based on the standard curve.

3.9.4 Primer sequences for quantitative PCR

The target genes analysed in this study included *Srebf2*, *Hmgcr*, *Pparg1*, and *ApoA2*, with *Actb* used as the housekeeping gene for normalisation. The primer sequences were adapted from Wong, Choo and Chew (2020). The primer sequences of the targeted genes and housekeeping genes were listed in **Table 3.1**.

Table 3.1: List of primers used in the qPCR experiment.

Gene	Forward (5'-3')	Reverse (5'-3')	Size (bp)	Citation
Actb	TCATGAAGTGTGACGTTGACATCCGT	CCTAGAAGCATTTGCGGTGCACGATG	285	Wong, Choo and Chew, 2020
Srebf2	CCCTTGACTTCCTTGCTGCA	GCGTGAGTGTGGGCGAATC	222	
Hmgcr	GATTCTGGCAGTCAGTGGGAA	GTTGTAGCCGCCTATGCTCC	214	
Pparg1	CATTTGTATGACTCATACATAAAGT	CGGATGGCCACCTCTTTGCTCTG	191	Son *et al.*, 2007
ApoA2	GCCCTGTTCACTCAATACTTTCAG	CAGACTAGTTCCTGCTGACC	155	Wang *et al.*, 2011

3.9.5 Reverse transcription quantitative PCR (RT-qPCR)

Gene expression analysis was performed using a one-step real-time PCR protocol in this study. RT-qPCR was performed using the CFX96 Touch Real-Time PCR Detection System (Bio-Rad, USA) and Luna® Universal One-Step RT-qPCR Kit (New England Biolabs, USA). The RT-qPCR reaction was prepared according to **Table 3.2,** which was adapted from the Luna® Universal One-Step RT-qPCR Kit protocol.

Table 3.2: The concentration and volume of the RT-qPCR component.

Components	20 µL reaction	Final concentration
Luna One-Step Reaction Mix	10 µL	1×
Luna WarmStart RT Enzyme Mix	1 µL	1×
Forward primer (10 µM)	0.8 µL	0.4 µM
Reverse primer (10 µM)	0.8 µL	0.4 µM
Template RNA	Variable	100 ng
Distilled water	To 20 µL	

The reaction mixture was pipetted into the PCR strip tubes and briefly spun down to remove bubbles and ensure all the fluid was collected at the bottom of the tubes. The real-time PCR instrument was programmed according to the manufacturer's indicated thermocycling protocol, as detailed in **Table 3.3**. The SYBR® or SYBR/FAM scan mode setting was selected for detection on the real-time instrument.

The RT-qPCR results were processed and analysed using the CFX Manager Software version 3.0 (Bio-Rad, USA). The software was used to determine the Ct value, analyse the melt curve and calculate relative gene expression using the double delta Ct method ($2^{-\Delta\Delta Ct}$ method).

Table 3.3: Stages and conditions of RT-qPCR.

Cycle step	Temperature	Time	Cycles
Reverse transcription	55 ºC	10 minutes	1
Initial denaturation	95 ºC	1 minutes	1
Denaturation	95 ºC	10 seconds	40
Extension	60 ºC	30 seconds (+ plate read)	
Melt curve	60-95 ºC	Increment for 0.5 ºC for 5 seconds	1

3.9.6 Western blot

Western blot analysis was performed to evaluate the effects of lauric acid on the protein expression level in mouse liver samples. This study examined the expression levels of total AMPK, phosphorylated AMPK (phospho-AMPK), SREBP1, and SREBP2. β-actin served as a housekeeping protein for loading control and normalisation.

Mini-PROTEAN Tetra Vertical Electrophoresis System (Bio-Rad, USA) was used for the SDS gel electrophoresis (SDS-PAGE). The gels with a thickness of 1 mm were prepared using the 1 mm spacer from the electrophoresis system. The 12% (w/v) resolving gel and 4% (w/v) stacking gel were hand-cast based on the Nacalai Tesque protocol with modification. The composition of the acrylamide gel used for SDS-PAGE is summarised in **Table 3.4.**

Table 3.4: Recipes for stacking and resolving gel.

	Stacking gel	Resolving gel
	4%	12%
40% (v/v) Acrylamide/Bis	630 µL	3.0 mL
0.5 M Tris-HCl, pH 6.8	1 mL	-
1.5 M Tris-HCl, pH 8.8	-	2.5 mL
10% (w/v) SDS	40 µL	100 µL
ddH_2O	2.3 mL	4.4 mL
10% (w/v) APS	70 µL	100 µL
TEMED	8 µL	10 µL

The 10% (w/v) ammonium persulfate (APS) (Amresco, USA) solution was prepared fresh before casting the acrylamide gel. After adding the APS and N,N,N′,N′ -Tetramethylethylenediamine (TEMED) (Bio Basic Inc, Canada) into the resolving solution, the mixture was immediately poured into the gel mould. A thin layer of butanol (Emsurem, India) was added on top of the

resolving solution to ensure a flat surface. The resolving gels were allowed to polymerise for 30 minutes. Once polymerisation was completed, the butanol was removed, and the stacking gel solution was added. The combs were inserted into the stacking gel to create wells and left undisturbed until fully polymerised. The combs were removed slowly and gently to avoid damaging the wells. **Table 3.5** lists the ingredients and concentrations used for buffer preparation in electrophoresis and transfer steps.

Table 3.5: Buffer preparation for electrophoresis and transfer steps.

Buffers	Materials
Loading buffer: 2x Laemmli buffer	4% (w/v) SDS, 10% (v/v) 2-mercaptoethanol (Merck, Germany), 20% (v/v) glycerol (Chemiz, Malaysia), 0.004% (w/v) bromophenol blue (Chemiz, Malaysia), 0.125 M Tris-HCl
1× Running buffer	25 mM Tris (Fisher Scientific, USA), 190 mM glycine (USB Corporation, USA), 0.1% (w/v) SDS
1× Wet transfer buffer	25 mM Tris, 190 mM glycine, 20% (v/v) methanol (Emsure, India)
Tris-buffered saline with Tween 20 (TBST) buffer	20 mM Tris, pH 7.5, 150 mM NaCl (Merck, Germany), 0.1% (v/v) Tween 20 (Amresco, USA)
Blocking buffer	3% (w/v) bovine serum albumin (BSA) in TBST
Mild stripping buffer	15 g glycine, 1 g SDS, 10 mL Tween 20, pH 2.2, add distilled water to 1 L

A total of 20 μg of protein sample was used for the SDS-PAGE. An equal volume of 2× Laemmli buffer was mixed with the protein sample, boiled at 95 ºC for 5 minutes, and briefly centrifuged to collect the solution. The acrylamide gels were assembled into the electrophoresis tank, and the protein samples were

loaded into the wells. The 1× SDS running buffer was added to the indicated mark. The electrophoresis was initially run at 50 V for 20 minutes to allow the protein to migrate through the stacking gel. Once the samples had reached the resolving gel, the voltage was increased to 150 V and run for 1 hour.

After the SDS PAGE, the protein was transferred onto the Immobilon polyvinylidene difluoride (PVDF) membrane (0.45 μM, Merck, Germany) using the Mini Trans-Blot® Cell (Bio-Rad, USA) for wet transfer. The PVDF membranes were cut into a 6 × 6 cm square, pre-activated by soaking in methanol for 30 seconds, and rinsed with distilled water. The PVDF membranes, acrylamide gels and blotting filter papers (Merck, Germany) were soaked in ice-cold 1× wet transfer buffer for 10 minutes before assembling the transfer sandwich. The transfer sandwich was assembled with the blot positioned towards the cathode and the gel towards the anode, ensuring no air bubbles were trapped within the layers, as these could affect the transfer process. The transfer tank was placed in the ice box filled with ice, and wet transfer was performed at 100 V for 1 hour and 30 minutes.

Following the transfer process, the PVDF membrane was immediately incubated in the blocking buffer to prevent non-specific binding. The PVDF membrane was blocked for 1 hour at room temperature with agitation. The membrane was incubated overnight at 4 ºC with primary antibodies diluted 1:1000 in blocking buffer. The primary antibodies used were AMPK alpha 1/2 polyclonal antibody, Phospho-AMPK alpha1/2 (Thr183/172) polyclonal antibody, SREBP2 polyclonal antibody, β-actin polyclonal antibody

(Elabscience, USA) and SREBP1 polyclonal antibody (Novus Biologicals, USA). The membrane was washed with washing buffer three times, 10 minutes each with agitation. The horseradish peroxidase-conjugated goat anti-rabbit IgG secondary antibody (GeneTex, USA) was diluted 1:5000 with blocking buffer and incubated on the membrane for 1 hour at room temperature with agitation. The membrane was washed three times with washing buffer at room temperature with agitation. The Immobilon Western Chemiluminescent HRP substrate (Merck, Germany) was used for the chemiluminescent detection of antibodies in this study. Equal amounts of luminol and peroxide solutions were mixed 10 minutes before imaging. The membrane was placed on the transparent container and the HRP substrate was poured onto the membrane. The blot image was captured using the gel imager system and the band intensity was measured using ImageJ software (National Institutes of Health, USA).

3.10 Statistical analysis

Quantitative data were expressed as mean ± standard error of the mean (SEM). Statistical analysis was performed using one-way ANOVA in GraphPad Prism software (USA), followed by Tukey's post hoc test to compare differences between groups. A p-value of < 0.05 was considered statistically significant.

CHAPTER 4

RESULTS

4.1 Effect of HFD and treatment on body weight change

The body weight trends illustrated the effects of HFD and dietary interventions on weight gain over 16 weeks. The average body weight of mice increased over time, as shown in **Figure 4.1.1**. A two-way ANOVA revealed significant main effects for treatment group ($F(15, 896) = 41.27$, $p < 0.001$), time ($F(4, 896) = 43.59$, $p < 0.001$) and a significant treatment group × time interaction ($F(60, 896) = 1.619$, $p = 0.0026$). Tukey's post hoc test was used for pairwise comparisons. The HFD-fed groups exhibited a similar pattern of weight gain with no significant difference ($p > 0.05$) up to week 14. Following the oral gavage of lauric acid and rosiglitazone at week 14, the divergence of body weight gain was observed in these HFD groups. The mice with HFD alone exerted the highest average body weight among all treatment groups and showed a steep increase in body weight, starting from 21.530 g at week 6 and reaching the highest body weight, which was 37.374 g at week 21. Tukey's test indicated that the HFD control group had a significantly higher body weight compared to the chow diet group from week 14 onwards ($p < 0.05$). In contrast, the mice fed with the chow diet showed the lowest average body weight, starting at 21.664 g and reaching 26.618 g at week 21. Lauric acid treatment attenuated weight gain relative to the HFD group. The average body weight of the lauric acid-treated group was reduced compared to the HFD group from week 15. The

HFD-fed mice treated with 12 mg/kg lauric acid reached 30.390 g by week 21, while HFD-fed mice treated with 24 mg/kg lauric acid reached 31.356 g. Similarly, the HFD-fed mice treated with 20 mg/kg rosiglitazone also demonstrated a reduction in weight gain after the treatment compared to HFD group, with the final average body weight of 32.539 g at week 21. Tukey's post hoc test revealed that both lauric acid- and rosiglitazone-treated groups exhibited significantly lower body weights compared to the HFD control group during the final three weeks of the study (weeks 19 to 21; $p < 0.05$). Notably, the group receiving 12 mg/kg lauric acid demonstrated a more pronounced reduction in body weight, with greater statistical significance relative to the HFD control. For example, at week 21, the group treated with 12 mg/kg lauric acid showed a highly significant drop in body weight compared to the HFD control group ($p < 0.001$). The group with 12 mg/kg lauric acid also showed no significant difference in body weight compared to the chow diet group from week 18 to week 21 ($p > 0.05$). Notably, the rosiglitazone group has a slightly higher body weight than both lauric acid treatment group starting from week 15, but with no significant difference ($p > 0.05$).

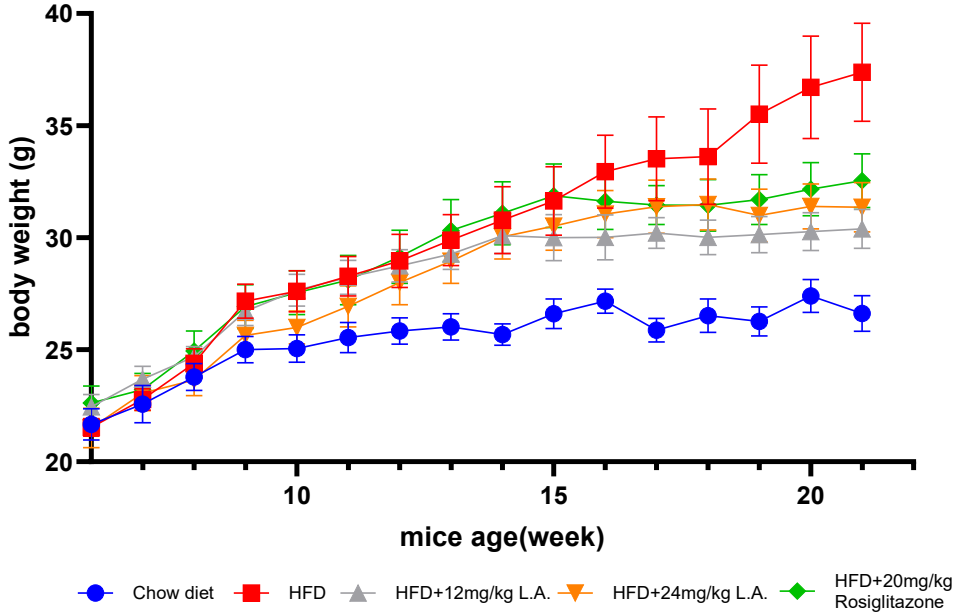

Figure 4.1.1: Body weight progression of mice throughout the experimental period. Body weight was measured weekly and plotted against the age of the mice (weeks), starting from week 6 of age. Mice were fed either a chow diet or HFD, with HFD groups receiving lauric acid (12 or 24 mg/kg), or 20 mg/kg rosiglitazone during the treatment phase. The average body weight of mice was presented as a line graph, expressed as the mean ± standard error of the mean (SEM) (n=12 per group, HFD control n=13).

The percentage body weight gain of mice was calculated (**Section 3.3.1**) and presented in **Figure 4.1.2**. The statistical analysis was performed using a one-way ANOVA test, followed by Tukey's post hoc test revealed a significant difference among the groups ($F(4, 56) = 155.5$, $p < 0.001$). The post hoc comparison revealed that the chow diet group was significantly different to all HFD-fed groups, while the HFD control group was significantly different from all treatment groups ($p < 0.001$). Among the groups, the chow diet group exhibited the lowest body weight gain (22.866 ± 1.057%), whereas the HFD control group exhibited the highest body weight gain (73.592 ± 2.226%) over the experimental period. Within the HFD-fed

group, treatment with 12 mg/kg lauric acid showed the lowest weight gain (35.368 ± 1.030%), followed by treatment with 20 mg/kg rosiglitazone (43.814 ± 1.422%), and treatment with 24 mg/kg lauric acid (45.751 ± 1.406%). Notably, the weight gain in the 24 mg/kg lauric acid treatment group was not statistically significant compared to the rosiglitazone treatment group ($p > 0.05$).

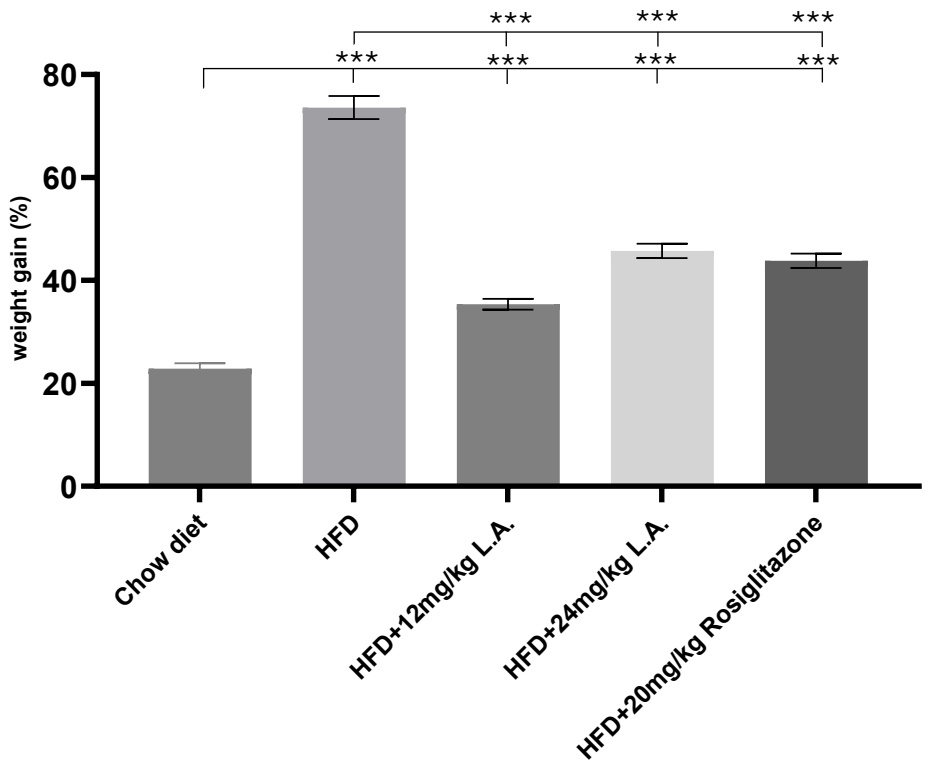

Figure 4.1.2: The percentage body weight gain of mice over the experimental period. Each bar represents the mean ± SEM profile (n=12 per group, HFD control n=13), and one-way ANOVA was performed to assess significance (***$p \leqslant 0.001$).

4.2 All treatments reduced the food and calorie intake of HFD-fed mice

Figure 4.2.1 illustrates the average daily food intake (g) of the mice across five different experimental groups from week 6 to week 21 of age. Lauric acid and rosiglitazone treatments commenced at week 14. The results were analysed using two-way ANOVA with treatment group and time as factors. The analysis revealed a significant main effect of treatment group ($F(4, 273) = 78.84$, $p < 0.001$) and a significant main effect of time ($F(15, 273) = 4.449$, $p < 0.001$). However, the treatment group × time interaction was not significant ($F(60, 273) = 0.5859$, $p = 0.9929$), suggesting that the effect of treatment on food intake was consistent across the experiment period. Tukey's post hoc test was used to examine the significant main effect of treatment group by comparing overall food intake averaged across all time points. Overall, the chow diet produced significantly higher food intake compared to all HFD groups ($p < 0.001$), and the HFD control group showed significantly higher food intake than the 12 mg/kg lauric acid treatment group ($p = 0.0353$). There was no significant difference in the average food intake of the HFD control group with 24 mg/kg lauric acid and 20 mg/kg rosiglitazone treatment group. The chow diet group exhibited the highest food intake among all groups throughout the study, starting from 4.577 g at week 6. Although some fluctuations were observed, the food intake of the chow diet group decreased to 3.336 g at week 13, slightly increased to 3.682 g at week 18 and reached 3.706 g at week 21. In contrast, the mice with HFD consistently consumed less food as compared to the chow diet group. The HFD-fed mice showed similar food intake from week 6 to week 11, ranging from 2.375 to 3.059 g. Following the initiation of treatment, HFD-fed mice with

lauric acid or rosiglitazone treatment demonstrated a further reduction in food intake compared to the untreated HFD control group. The HFD control group showed variable but generally higher food intake compared to the lauric acid or rosiglitazone treatment groups, starting from week 12. The food intake of the HFD group ranged from 2.300 to 3.027 g, with a noticeable peak at 3.027 g at week 18. In contrast, the HFD-fed mice with 12 mg/kg lauric acid treatment displayed a consistent reduction in food intake, averaging between 2.044 and 2.230 g from week 15 onwards, and reached 2.230 g at week 21. Similarly, the HFD-fed mice with 24 mg/kg lauric acid treatment also showed a reduced food intake as compared to the HFD control group after week 14, with food intake ranging from 2.066 to 2.310 g, and reaching 2.310 g at week 21. The HFD-fed mice with 20 mg/kg rosiglitazone treatment showed a generally lower average food intake relative to the HFD control group, with values fluctuating between 2.098 and 2.540 g, with a transient peak at week 15 and a final value of 2.325 g at week 21. Throughout the post-treatment period (from week 14 onwards), all treatment groups (lauric acid and rosiglitazone) have exhibited a lower average food intake compared to the untreated HFD group.

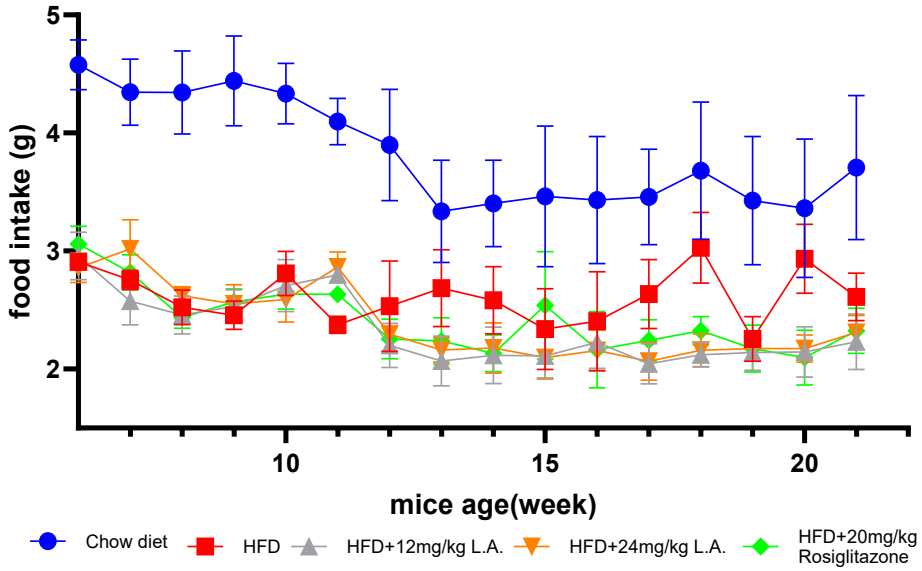

Figure 4.2.1: The average food intake of mice throughout the study period. Weekly food intake was measured and plotted against the age of the mice(weeks). Data were presented in a line graph expressed as mean±SEM (n=12 per group, HFD control n=13).

Figure 4.2.2 illustrates the average calorie intake (kcal) of the mice across five experimental groups from week 6 to week 21 of age. Treatments of lauric acid and rosiglitazone started at week 14. The calorie intake was analysed using two-way ANOVA with treatment group and time as factors. The analysis showed a significant main effect of treatment group ($F(4, 273) = 3.648$, $p = 0.0065$) and a significant main effect of time ($F(15, 273) = 4.659$, $p < 0.001$). However, the calorie intake showed similar results as food intake; there was no significant treatment group × time interaction ($F(60, 273) = 0.5961$, $p = 0.5961$), suggesting that the pattern of calorie intake over time was similar across all treatment groups. Tukey's post hoc test showed that the chow diet group has significantly lower calorie intake compared to HFD control group ($p = 0.0397$), and HFD control group has significantly higher calorie intake compared to

HFD-fed mice with 12 mg/kg lauric acid treatment group (p = 0.0.082) and HFD-fed mice with 24 mg/kg lauric acid treatment group (p = 0.0418). The chow diet group showed no significant difference in calorie intake compared to either the lauric acid or rosiglitazone treatment groups ($p > 0.05$). Mice fed a chow diet initially showed calorie intake of 14.875 kcal at week 6, gradually reduced to 14.085 kcal by week 10, followed by a more pronounced reduction to 10.840 kcal by week 13. The chow diet group maintained a stable calorie intake ranging from 10.930 to 12.044 kcal for the subsequent weeks and ending at 12.044 kcal by week 21. During the first five weeks of the pre-treatment period (week 6 to week 11), all HFD-fed mice showed comparable calorie consumption levels. At some points, the calorie intake of the HFD-fed mice showed a slightly higher calorie intake compared to the chow diet group. For example, at week 10, the HFD control group consumed 14.695 kcal, while the chow diet group consumed 14.085 kcal. A decline in calorie intake was observed in all groups except the HFD control group at week 12. Following the commencement of the treatment at week 14, a distinct pattern of calorie intake was observed across the HFD-fed groups. The HFD control group consistently exhibited higher calorie intake compared to the other experimental groups, peaking at 15.826 kcal in week 18, and ending at 13.649 kcal by week 21. In contrast, the HFD-fed mice with 12 mg/kg lauric acid treatment demonstrated a generally lower and more stable calorie intake post-treatment. From week 15 onwards, the calorie intake ranged from 10.685 to 11.658 kcal, ending at 11.658 kcal by week 21. The HFD-fed mice with 24 mg/kg lauric acid treatment also showed marked attenuation in calorie intake compared to the HFD control group after week 14, with values ranging from 10.801 to 12.075 kcal, and a final

intake of 12.075 kcal. Similarly, HFD-fed mice with 20 mg/kg rosiglitazone treatment exhibited lower calorie intake as compared to the HFD control group during the treatment period, with calorie intake between 10.967 and 13.279 kcal, and reached 12.155 kcal at week 21. Overall, the calorie intake of the three treatment groups (both lauric acid and rosiglitazone) from week 15 onwards showed comparable results to the chow diet group, and consistently lower than the HFD control group.

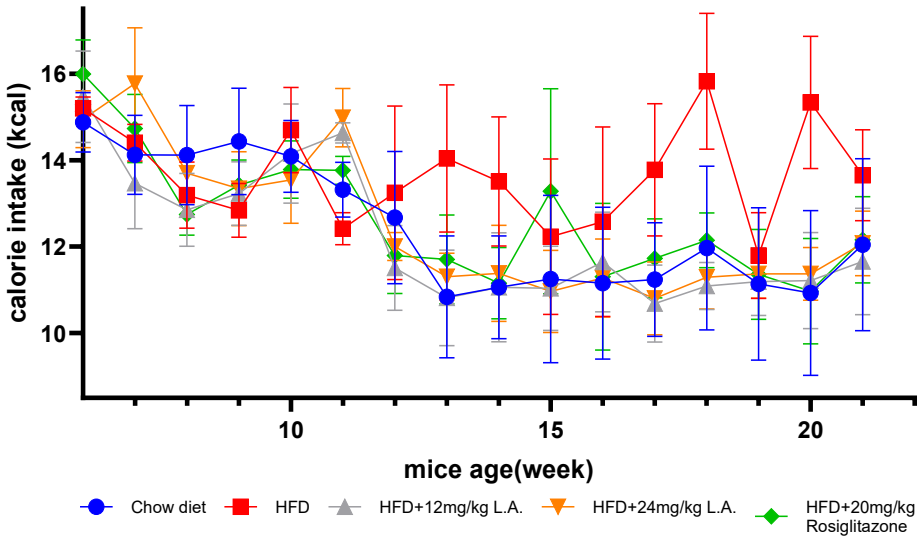

Figure 4.2.2: Average calorie intake of mice across the experimental period. Calorie intake was calculated weekly and plotted according to the age of the mice(weeks). Data were tabulated in a line graph, expressed as mean±SEM (n=12 per group, HFD control n=13).

The food intake (g) and calorie intake (kcal) serve as key indicators of the dietary behaviour of the mice across different experimental groups. Despite differences in the calorie density of the diet, where the HFD has a higher calorie density than the chow diet, the mice with HFD showed similar or even higher calorie intake than the chow diet group at certain time points, even though the chow diet group consistently consumed more food by weight than HFD-fed

mice. Following treatment initiation, both lauric acid and rosiglitazone-treated groups showed a reduction in both food intake and calorie intake. These reductions suggest that these interventions may influence the feeding behaviour or energy regulation. Notably, the calorie intake of the treatment groups approached the intake of the chow diet from week 15 onwards, demonstrating the ability of lauric acid to mitigate hypercaloric intake, particularly in HFD feeding.

4.3 Lauric acid co-treatment reduced the fasting blood glucose levels of HFD-fed mice

Figure 4.3 illustrates the fasting blood glucose levels (mmol/L) of the mice from five experimental groups from week 8 to week 21 of age (refer to **Section 3.4.1**). A two-way ANOVA was performed with treatment and time (mouse age) as factors, revealing a significant main effect of treatment group ($F(4, 172) = 6.896$, $p < 0.001$), indicating that different treatment groups exhibited different fasting blood glucose levels overall. However, there was no significant main effect of time ($F(4, 172) = 2.270$, $p = 0.0636$), suggesting that the overall fasting blood glucose level did not change significantly over the study period. Furthermore, there was no significant treatment group × time interaction ($F(16, 172) = 0.5465$, $p = 0.9186$), indicating that the pattern of blood glucose change over time was similar across all groups. Despite the significant main effect of treatment group, the Tukey's post hoc test was used to examine the overall changes in fasting blood glucose levels across different treatment groups. The

analysis showed that the HFD control group had significantly higher average fasting blood glucose levels (11.035 ± 0.140 mmol/L) compared to the chow diet group (9.186 ± 0.172 mmol/L, $p < 0.001$) and the HFD with 20 mg/kg rosiglitazone treatment group (10.061 ± 0.241 mmol/L, $p = 0.0378$). Interestingly, the chow diet group showed significantly lower average fasting blood glucose levels (9.186 ± 0.172 mmol/L) compared to the HFD with 12 mg/kg lauric acid treatment group (10.355 ± 0.323 mmol/L, $p = 0.0154$). No significant differences were observed among the lauric acid-treated groups and the rosiglitazone group (all $p > 0.05$). As shown in **Figure 4.3**, the chow diet group consistently exhibited the lowest fasting blood glucose levels among all treatment groups, ranging from 8.850 to 9.843 mmol/L, whereas the HFD control group exhibited the highest fasting blood glucose levels, ranging from 10.700 to 11.550 mmol/L. During the pre-treatment period (week 6 to week 14), all groups showed an increasing trend in blood glucose level. After treatment initiation at week 14, the HFD groups with lauric acid or rosiglitazone treatment showed a notable reduction in fasting blood glucose levels. The fasting blood glucose levels of the mice treated with 12 mg/kg lauric acid dropped from 10.950 mmol/L at week 14 to 9.567 mmol/L at week 21, while the fasting blood glucose levels of the 24 mg/kg lauric acid-treated group dropped from 10.229 mmol/L to 9.320 mmol/L at week 21. Similarly, the HFD-fed mice treated with 20 mg/kg rosiglitazone showed lower fasting blood glucose levels compared to the HFD control group during the treatment period, with a fasting blood glucose level dropping from 10.878 mmol/L at week 14 to 9.533 mmol/L at week 21.

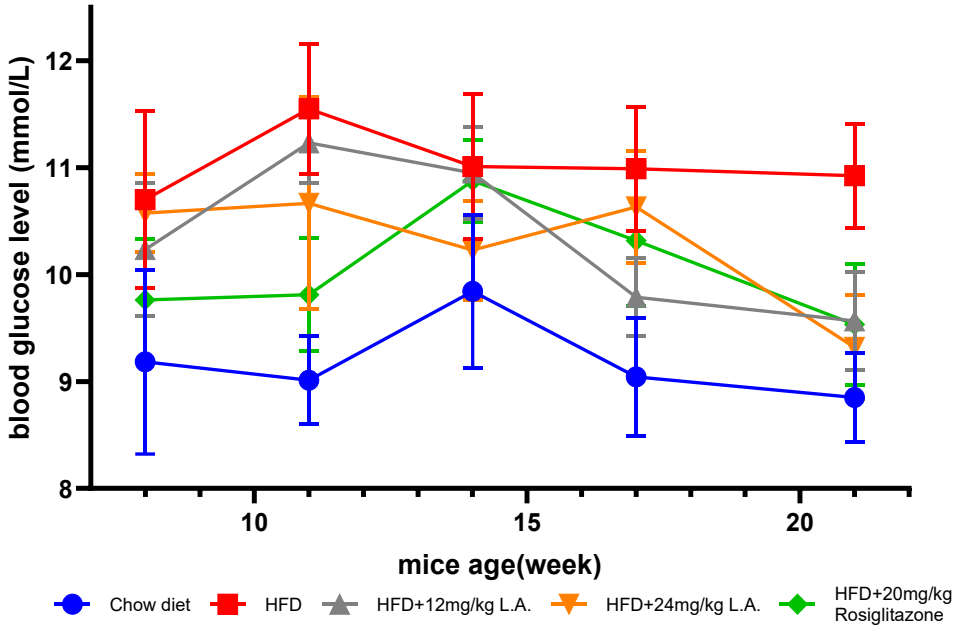

Figure 4.3: **Fasting blood glucose levels of five experimental groups over the mice's age (weeks) from week 8.** The results were tabulated in a line graph, expressed as mean ±SEM. The number of animals analysed at each time point varied slightly due to occasional unsuccessful blood sampling or insufficient blood volume (n = 6-12 per group).

4.4 Lauric acid improved oral glucose tolerance test (OGTT)

To assess glucose homeostasis, an OGTT was performed, and blood glucose levels were measured at 0, 60, and 120 minutes after oral glucose administration (refer to **Section 3.4.2**), as shown in **Figure 4.4**. At baseline (0 minutes), the fasting blood glucose of the HFD control group (10.925 mmol/L) was significantly higher than that of the chow diet group (8.850 mmol/L, p = 0.0367). In contrast, the HFD-fed mice treated with lauric acid and rosiglitazone showed fasting blood glucose levels not significantly different to the chow diet ($p > 0.05$). The OGTT was analysed using two-way ANOVA with treatment

group and time as factors. The test revealed a significant main effect of treatment group ($F(4, 126) = 6.357$, $p = 0.001$), suggesting overall differences in glucose response between groups. There was also a significant main effect of time ($F(2, 126) = 10.83$, $p < 0.001$), suggesting that the blood glucose levels changed significantly across the experimental period. However, the treatment group × time interaction showed no significant difference ($F(8, 126) = 0.09869$, $p = 0.9992$), suggesting that the pattern of blood glucose change over time was similar between the treatment groups. Following the significant main effect of treatment group, Tukey's post hoc test was performed to compare the overall mean of the blood glucose levels between different groups across the OGTT period. The post hoc test revealed that the HFD control group exhibited significantly higher overall blood glucose level (11.472 ± 0.466 mmol/L) as compared to the chow diet group (9.550 ± 0.513 mmol/L, $p < 0.001$) and HFD-fed mice treated with 24 mg/kg lauric acid (9.640 ± 0.336 mmol/L, $p < 0.001$). There was no significant difference between the HFD control group and the HFD-fed mice treated with 12 mg/kg lauric acid (10.300 ± 0.496 mmol/L) and the HFD-fed mice treated with 20 mg/kg rosiglitazone (10.315 ± 0.542 mmol/L) ($p > 0.05$). Notably, all treated HFD mice (both lauric acid and rosiglitazone) showed no significant difference in overall fasting blood glucose levels compared to the chow diet group ($p > 0.05$). The total glycaemic response during the OGTT was assessed by measuring the area under the curve (AUC) for the blood glucose levels from 0 to 120 minutes. A one-way ANOVA was performed on the AUC values, which showed no significant difference among the treatment groups ($F(4, 5) = 0.8388$, $p = 0.5551$). Although some groups demonstrated generally higher or lower blood glucose levels during the test, the

total glucose exposure over the 2-hour period did not differ significantly. In summary, the OGTT demonstrated that the HFD control group exhibited generally higher blood glucose levels compared to the chow-fed and treated HFD groups, suggesting impaired glucose regulation. However, the absence of significant interaction effects and AUC differences suggested that the pattern and extent of glucose clearance over time were comparable across groups. Nevertheless, the AUC result remains a valuable indicator of insulin sensitivity, as elevated AUC values are generally associated with reduced glucose tolerance and potential insulin resistance.

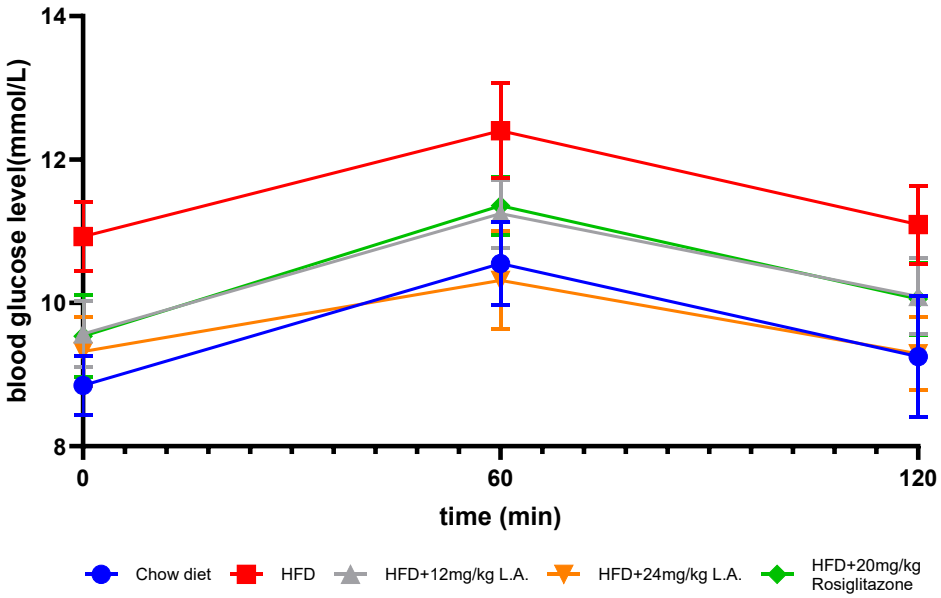

Figure 4.4: **OGTT results of different treatment groups over 2 hours**. Blood glucose levels were measured at the indicated time points following glucose administration. The results were tabulated in a line graph, expressed as mean ±SEM (n = 8–12 per group).

4.5 High-dose lauric acid improved insulin sensitivity

Figure 4.5.1 illustrates the fasting insulin levels (pg/mL) across different experimental groups. The statistical analysis was performed using a one-way ANOVA test, followed by Tukey's post hoc test. The ANOVA test revealed a significant difference among the groups ($F(4, 10) = 87.62$, $p < 0.001$). The post hoc comparison revealed that the HFD control group had significantly higher insulin levels (204.152 ± 4.986 pg/mL) compared to the chow diet group (99.301 ± 4.799 pg/mL, $p < 0.001$), suggesting hyperinsulinemia in the HFD-fed mice. Treatment with lauric acid resulted in a significant reduction in fasting insulin levels compared to the HFD control: 180.445 ± 6.062 pg/mL ($p < 0.05$) for the 12 mg/kg group, and 164.525 ± 3.536 pg/mL ($p < 0.01$) for the 24 mg/kg group. The rosiglitazone-treated group showed a more pronounced reduction in the insulin levels (102.216 ± 5.492 pg/mL, $p < 0.001$ vs HFD control). Compared to the chow diet group, both lauric acid-treated groups demonstrated significantly higher insulin levels ($p < 0.001$). However, the insulin levels in the rosiglitazone-treated group were not significantly different from those in the chow diet group ($p > 0.05$), indicating a near complete normalisation. In summary, the HFD led to hyperinsulinemia. While the lauric acid administration reduced the fasting insulin levels as compared to the HFD control, the effect was only partial. The rosiglitazone, on the other hand, showed an effective reduction in the insulin levels, comparable to those in the chow diet group, reflecting a strong insulin-sensitising effect.

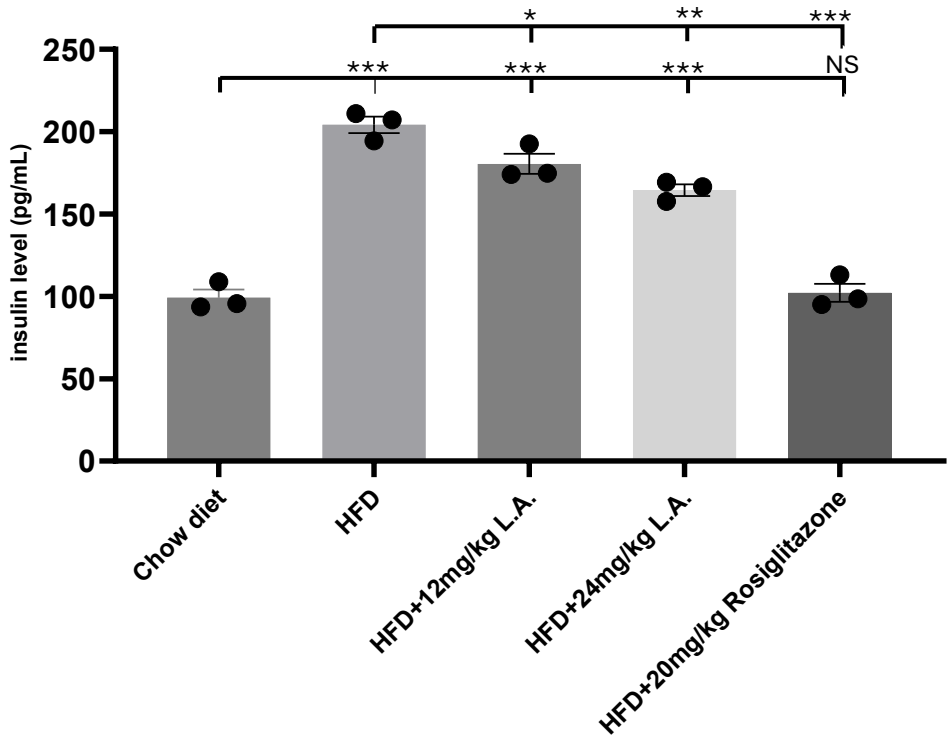

Figure 4.5.1: **The insulin levels of different experimental groups**. Each bar represents the mean ± SEM profile (n=3 per group), and one-way ANOVA was performed to assess significance (NS, no significance; *$p \leqslant 0.05$; **$p \leqslant 0.01$; ***$p \leqslant 0.001$).

Figure 4.5.2 illustrates the HOMA-IR values across different experimental groups. A one-way ANOVA test was performed, followed by Tukey's post hoc test. The statistical analysis showed a significant difference in HOMA-IR values among different experimental groups ($F(4, 10) = 10.97$, $p = 0.0011$). As observed in **Figure 4.5.2**, the chow diet group exhibited the lowest HOMA-IR value (1.153 ± 0.144), reflecting normal insulin sensitivity. In contrast, the HFD control group showed a substantially elevated HOMA-IR value (2.706 ± 0.150), which was significantly higher compared to the chow diet group ($p = 0.0017$), indicating insulin resistance induced by HFD. The HFD-fed mice with 12 mg/kg lauric acid administered group showed

significantly higher HOMA-IR value (2.224 ± 0.282) compared to the chow diet group ($p = 0.0212$), while the 24 mg/kg lauric acid treated group (1.964 ± 0.155) showed no significant difference compared to the chow diet group ($p = 0.0899$). However, neither lauric acid treatment significantly reduced the HOMA-IR value as compared to the HFD control ($p > 0.05$). However, the HFD-fed mice treated with 20 mg/kg rosiglitazone showed a significantly lower HOMA-IR value (1.272 ± 0.218) compared to the HFD control ($p = 0.0031$) and showed no significant difference from that of the chow diet group ($p > 0.05$), suggesting a restoration in insulin sensitivity. In summary, the HFD induced a significant insulin resistance, as reflected by increased HOMA-IR values. Although the lauric acid treatment improved insulin sensitivity, it did not significantly reverse the HOMA-IR elevation in HFD-fed mice. The rosiglitazone effectively restored HOMA-IR to levels comparable to the chow diet group, demonstrating a strong insulin-sensitising effect.

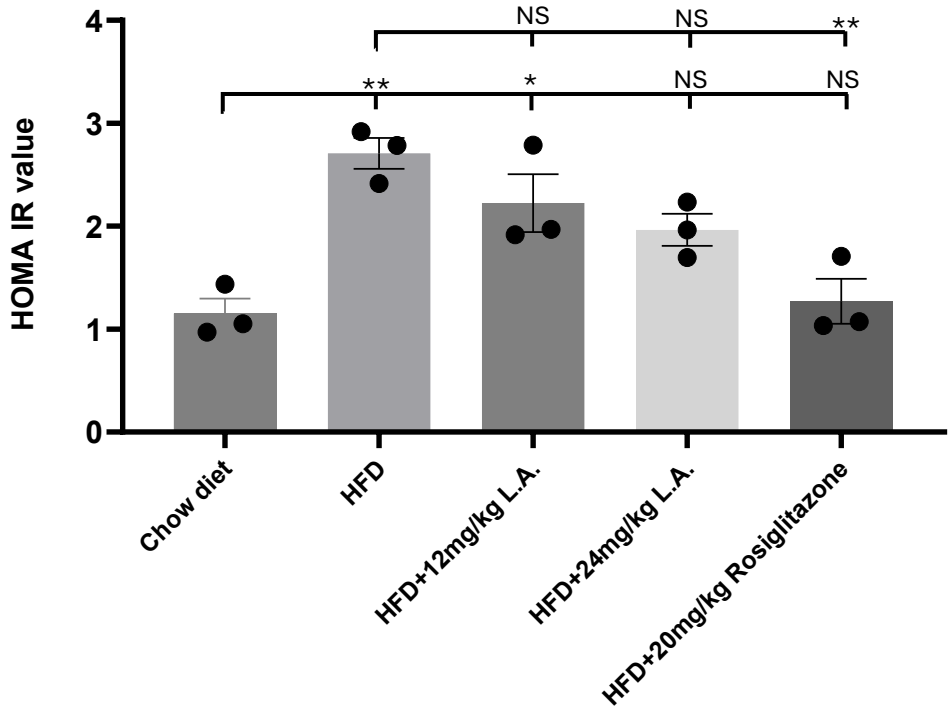

Figure 4.5.2: **HOMA-IR values of different experimental groups**. Each bar represents the mean ± SEM profile (n=3 per group), and one-way ANOVA was performed to assess significance (NS, no significance; *$p \leqslant 0.05$; **$p \leqslant 0.01$)

4.6 High-dose lauric acid improved mice's lipid profile, especially LDL levels

The effects of different dietary interventions and treatments on serum lipid profiles, including triglyceride, total cholesterol, high-density lipoprotein and low-density lipoprotein, were assessed and the results were tabulated in **Figure 4.6**. Each parameter was analysed using a one-way ANOVA followed by Tukey's post hoc test.

The one-way ANOVA analysis revealed a significant difference in serum triglyceride levels among the groups ($F(4, 35) = 31.46$, $p < 0.001$). The post hoc test indicated that all HFD groups had significantly higher triglyceride levels compared to the chow diet group (0.867 ± 0.032 mmol/L, all $p < 0.001$). The 12 mg/kg lauric acid-treated group (1.436 ± 0.060 mmol/L) did not differ significantly from the HFD control group (1.536 ± 0.051 mmol/L, $p = 0.541$). However, the 24 mg/kg lauric acid-treated group (1.323 ± 0.052 mmol/L, $p = 0.0177$) and 20 mg/kg rosiglitazone-treated group (1.294 ± 0.021 mmol/L, $p = 0.0054$) showed significantly lower triglyceride levels compared to the HFD control.

For total cholesterol, a significant difference was observed among the groups ($F(4, 35) = 3.646$, $p = 0.0139$). The HFD control group (3.736 ± 0.281 mmol/L) showed a significantly higher total cholesterol level compared to the chow diet group (2.392 ± 0.185 mmol/L, $p = 0.0170$). All treatment groups showed lower total cholesterol levels compared to the HFD control groups, with a more notable reduction in the 12 mg/kg lauric acid-treated group (3.223 ± 0.201 mmol/L). The 24 mg/kg lauric acid-treated group (3.365 ± 0.511 mmol/L) showed a higher total cholesterol level compared to the 12 mg/kg lauric acid-treated group. Notably, the 20 mg/kg rosiglitazone-treated group exhibited the lowest total cholesterol level (2.642 ± 0.068 mmol/L) among the HFD-fed groups. However, none of the treatment groups showed statistically significant differences compared to the HFD control group and chow diet ($p > 0.05$), and no significant differences were observed among the treatment groups themselves.

No significant difference was observed in the HDL levels among the groups ($F(4, 35) = 1.033$, $p = 0.4041$). The HFD control group (1.635 ± 0.096 mmol/L) has a similar HDL level compared to the 12 mg/kg lauric acid-treated group (1.702 ± 0.095 mmol/L) and the chow diet group (1.687 ± 0.167 mmol/L). The 24 mg/kg lauric acid-treated group (2.053 ± 0.314 mmol/L) and 20 mg/kg rosiglitazone-treated group (1.913 ± 0.090 mmol/L) showed a slightly higher trend in HDL levels compared to other groups, but these differences were not statistically significant.

For the LDL levels, a significant difference was found among the groups ($F(4, 35) = 8.630$, $p < 0.001$). The HFD control group (1.403 ± 0.239 mmol/L) exhibited a marked elevation in LDL level as compared to the chow diet group (0.311 ± 0.071 mmol/L, $p < 0.001$). All treatment groups showed no significant difference in the LDL levels compared to the chow diet group ($p > 0.05$). The 12 mg/kg lauric acid-treated group (0.869 ± 0.142 mmol/L) did not significantly differ from the HFD control group ($p > 0.1908$). In contrast, the 24 mg/kg lauric acid-treated group (0.711 ± 0.242 mmol/L) showed significantly lower LDL levels as compared to the HFD control group ($p = 0.0478$). The 20 mg/kg rosiglitazone-treated group exhibited significantly lower LDL levels (0.140 ± 0.043 mmol/L) than the HFD control group ($p < 0.001$) and the 12 mg/kg lauric acid-treated group ($p = 0.0334$).

In summary, HFD significantly altered blood lipid profiles, as evidenced by elevated triglycerides and total cholesterol levels. The lauric acid treatment demonstrated a partial lipid-lowering effect, with the 24 mg/kg lauric acid and rosiglitazone showing a strong reduction in triglyceride levels. HDL levels remained relatively unchanged across all groups, although a slight elevation was seen with the 24 mg/kg lauric acid group. LDL values were estimated using the Friedewald equation and should therefore be interpreted with caution, as this method was originally developed for human lipid measurements.

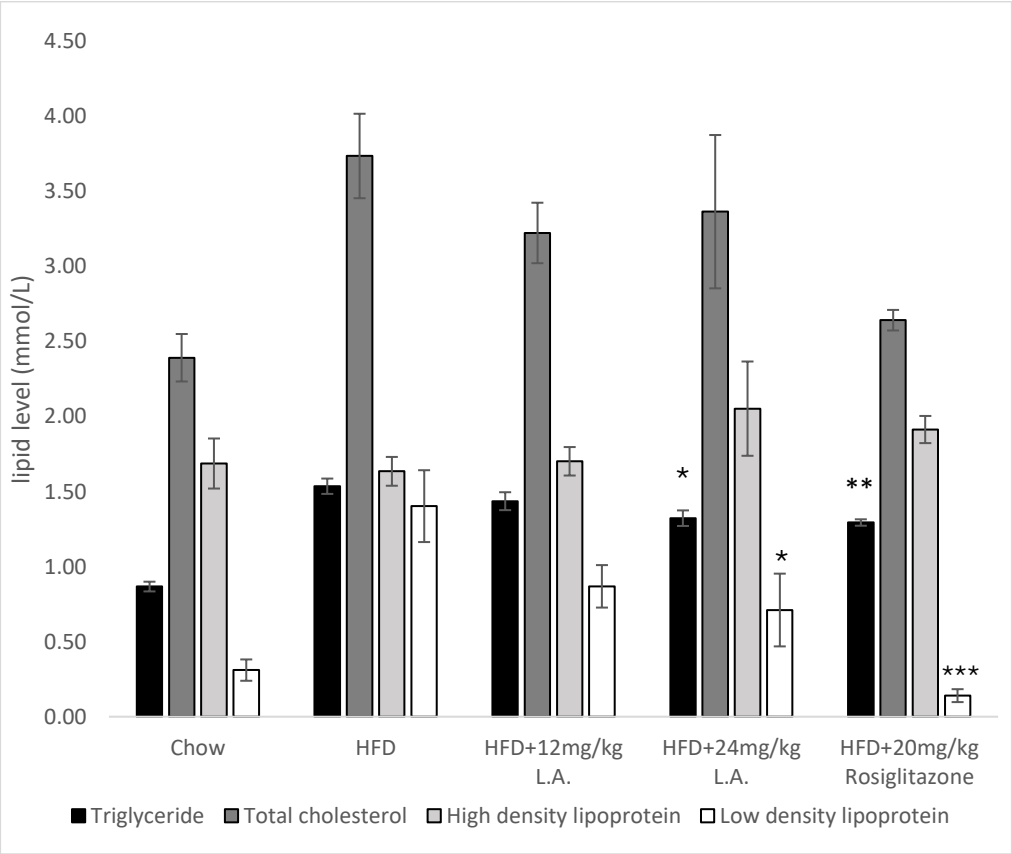

Figure 4.6: The blood lipid profiles of different experimental groups. Each bar represents the mean ± SEM profile (n=8), and one-way ANOVA was performed to assess significance. The pairwise comparisons shown in the figure represent the post hoc test results relative to the HFD control group. The non-significant results were not included in the graph (*$p \leqslant 0.05$; **$p \leqslant 0.01$; ***$p \leq 0.001$).

4.7 Treatment of lauric acid did not alter the relative liver weight for HFD-fed mice

Figure 4.7(A) illustrates the absolute liver weight (g) for all experimental groups at the end of the study. One-way ANOVA was conducted for statistical analysis, followed by Tukey's post hoc test to evaluate group differences. A significant difference in absolute liver weight was observed among the groups ($F(4, 25) = 3.789$, $p = 0.0153$). The post hoc test revealed that the HFD control group (1.547 ± 0.085 g) showed significantly higher absolute liver weight compared to the chow diet group ($p = 0.0113$), suggesting that the HFD-induced liver weight gain. The effects of different treatments on restoring HFD-induced liver weight gain were examined. Neither the 12 mg/kg lauric acid treatment (1.358 ± 0.066 g) nor the 24 mg/kg lauric acid treatment (1.502 ± 0.080 g) showed significant differences in absolute liver weight compared to the HFD control group ($p > 0.05$ for both comparisons). Similarly, the HFD-fed mice treated with 20 mg/kg rosiglitazone (1.443 ± 0.108 g) also did not differ significantly from the HFD control group ($p > 0.05$). Compared to the healthy chow diet group, the absolute liver weights of the 12 mg/kg lauric acid and 20 mg/kg rosiglitazone-treated groups showed no significant difference ($p > 0.05$ for both). However, the absolute liver weight of the 24 mg/kg lauric acid-treated group showed a significantly higher value compared to the chow diet group ($p = 0.0500$).

To determine whether the changes in the absolute liver weight were proportional to the changes in total body weight, relative liver weights were calculated as the percentage of final body weight, presented in **Figure 4.7(B)**. A one-way ANOVA test revealed no significant difference in the relative liver weight among the experimental groups ($F(4, 25) = 0.8805$, $p = 0.4897$). Although slight variations were observed, the post hoc comparisons confirmed no significant pairwise comparisons, with $p > 0.05$ for all comparisons. The chow diet group showed a mean relative liver weight of 4.355 ± 0.299 %, while the HFD control group showed a mean of 4.136 ± 0.213 %. Among the treatment groups, the 24 mg/kg lauric acid-treated group showed a slightly higher level of relative liver weight (4.714 ± 0.220 %) as compared to the 12 mg/kg lauric acid-treated group (4.077 ± 0.250 %) and 20 mg/kg rosiglitazone-treated group (4.109 ± 0.338 %), though these differences were not statistically significant.

These results suggest that the significant increase in absolute liver weight in the HFD group was proportional to the overall body weight, as reflected by the unchanged relative liver weight. The treatment of lauric acid or rosiglitazone did not significantly reduce the HFD-induced liver weight gain, and the changes in the liver weight were related to the changes in total body weight.

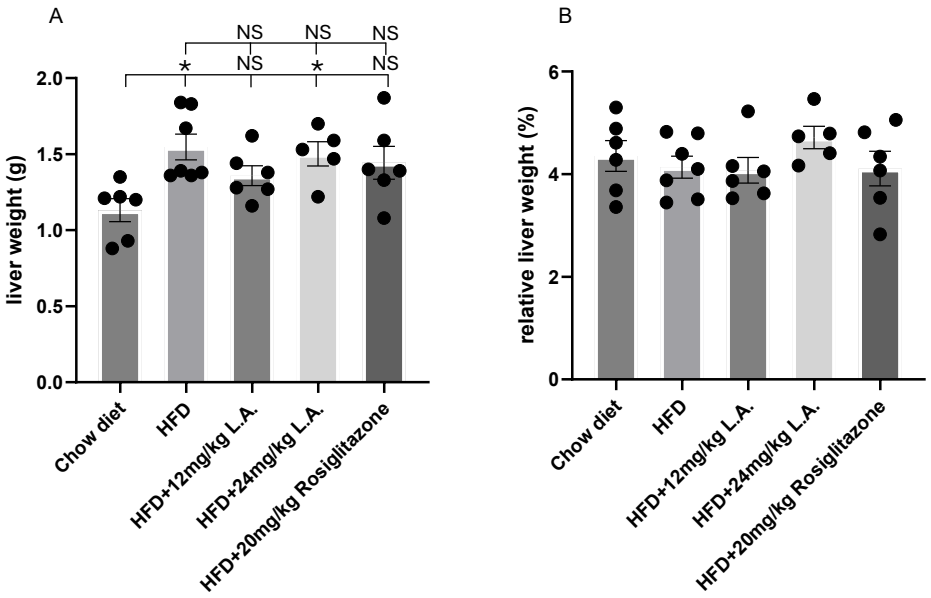

Figure 4.7: The liver weight of different treatment groups. (A) absolute liver weight and (B) relative liver weight. Each bar represents the mean ± SEM profile (n = 6, n = 7 for HFD control), and one-way ANOVA was performed to assess significance. The pairwise comparisons shown in the figure represent the post hoc test results. Since no significant differences were found in relative liver weight, the pairwise comparisons were not indicated in graph (B) (NS, not significant; *$p \leqslant 0.05$).

4.8 All treatments did not reverse the steatosis of HFD-fed mice

Liver sections from all experimental groups were stained with haematoxylin and eosin (H&E) to assess the effect of dietary interventions and treatments on liver morphology and lipid accumulation, as illustrated in **Figure 4.8**. The observed morphological changes were classified with reference to the INHAND guideline as discussed in **Section 3.6**. The liver histology of the chow diet group (Figure **4.8(A)**) displayed the normal nomenclature consistent with the healthy liver. The hepatocytes extended outward from the central vein towards the portal veins, and displayed abundant granular, eosinophilic cytoplasm with centrally positioned, prominent nuclei. There was no evidence

of lipid accumulation, fibrosis, inflammation or necrosis. In contrast, the liver from the HFD control group (**Figure 4.8(B)**) exhibited morphology alteration. Liver histology showed hepatocyte ballooning, as cells lost their characteristic polygonal shape and became rounded. The hepatocytes demonstrated diffuse hepatocellular vacuolisation consistent with microvesicular steatosis, where the hepatocytes were infiltrated with numerous small lipid vacuoles. The nucleus was not displaced by the lipid vacuoles to the periphery, distinguishing the condition from macrovesicular steatosis. Despite these lipid changes, there were no signs of inflammation, fibrosis or necrosis detected. The liver section from HFD-fed mice receiving treatments (**Figure 4.8 (C)-(E)**) did not show substantial histological improvements compared to the HFD control group. The microvesicular steatosis and hepatocyte ballooning persisted across the HFD groups, suggesting that the treatments were insufficient to reverse the HFD-induced lipid accumulation.

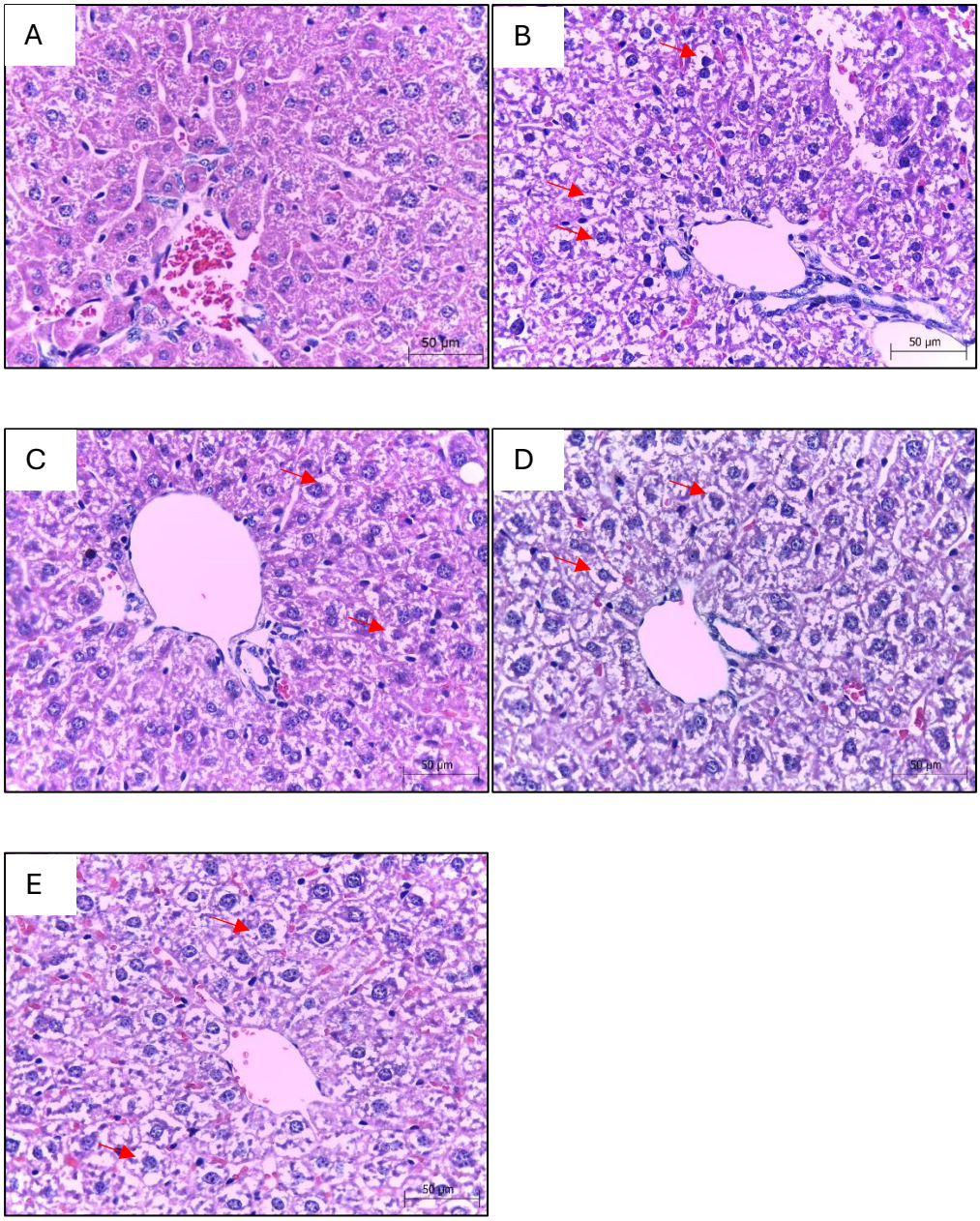

Figure 4.8: **Histological analysis of liver tissues**. H&E staining of liver sections for (A) chow diet; (B) HFD control; (C) HFD + 12 mg/kg lauric acid; (D) HFD + 24 mg/kg lauric acid; (E) HFD + 20 mg/kg rosiglitazone. Arrows indicated steatosis site. Magnification: 40×, scale bar: 50 µm.

4.9 HFD caused dysregulation of genes in lipid metabolism, where lauric acid co-treatment reversed them

To investigate the molecular mechanisms underlying the observed metabolic changes, the hepatic expression of key genes involved in lipid and cholesterol metabolism was assessed using RT-qPCR. The RNA samples were extracted from the liver tissues of the experimental groups, and gene expression levels were normalised to the housekeeping gene, beta-actin (*Actb*). Data were presented as fold changes relative to the chow diet group. Statistical significances were determined using a two-tailed, unpaired Student's t-test based on normalised gene expression value, as performed in Bio-Rad CFX Manager software.

Apolipoprotein A2 (*Apoa2*) is the gene that encodes for the component of HDL. The *Apoa2* showed a high expression level in the chow diet group. The HFD group exhibited a drastic and significant downregulation of *Apoa2* levels, with a 15.34-fold decrease relative to the chow diet group ($p < 0.001$). Although neither lauric acid nor rosiglitazone treatment was able to restore the expression to chow level, lauric acid showed a dose-dependent trend, with the 24 mg/kg of lauric acid showing relatively higher expression than 12 mg/kg lauric acid, suggesting partial modulation of HDL synthesis pathways.

Two key genes in the cholesterol biosynthesis pathway were assessed. The sterol regulatory binding factor 2 (*Srebf2*) is the transcription factor that regulates the expression of the cholesterol biosynthesis genes, whereas hepatic 3-hydroxy-3-methylglutaryl-CoA reductase (*Hmgcr*) is the rate-limiting enzyme in cholesterol synthesis. The HFD control group showed significant downregulation of both *Hmgcr* (1.51-fold, $p < 0.001$) and *Srebf2* (2.78-fold, $p < 0.001$) as compared to the chow diet group. This suggests the suppression of cholesterol synthesis in response to dietary fat intake. Interestingly, the lauric acid treatment showed dose-dependent modulation, whereby 24 mg/kg of lauric acid caused further reduction of *Hmgcr* (1.88-fold downregulation, $p < 0.001$) but a lesser downregulation of *Srebf2* (2.38-fold, $p \leq 0.001$). Notably, the rosiglitazone-treated group consistently showed the most pronounced reduction of the *Hmgcr* (3.03-fold, $p < 0.001$) and *Srebf2* (3.92-fold, $p = 0.002$) genes as compared to the chow diet. As compared to the HFD control group, only the rosiglitazone-treated group showed significant downregulation of the *Hmgcr* (2.01-fold, $p = 0.004$) and *Srebf2* (1.41-fold, $p = 0.035$) genes. These findings suggest a strong inhibitory effect of rosiglitazone on hepatic cholesterol synthesis.

Peroxisome proliferator-activated receptor gamma 1 (*Pparg1*) is involved in adipogenesis and fatty acid metabolism. The HFD led to a significant downregulation of *Pparg1* expression, with an 11.26-fold decrease compared to the chow diet group ($p < 0.001$). The treatment with 12 mg/kg lauric acid (1.03-fold, $p = 0.864$) and rosiglitazone (1.54-fold, $p = 0.04$) showed smaller changes in gene expression compared to the HFD control group,

suggesting a minimal effect on reversing downregulation. The 24 mg/kg lauric acid treatment appeared to be the most effective, with expression of 2.50-fold ($p = 0.0015$) increased relative to the HFD control group.

In summary, the HFD induced a dysregulation of genes involved in lipid metabolism, characterised by downregulation of the *Apoa2* and *Pparg1* expression and altered cholesterol synthesis via *Hmgcr* and *Srebf2*. The treatment of 24 mg/kg lauric acid reversed the downregulation of these genes, and rosiglitazone treatment exhibited strong inhibitory effects on genes involved in cholesterol biosynthesis. These molecular alterations provide insights into the therapeutic effects of reversing the HFD-induced hepatic lipid changes.

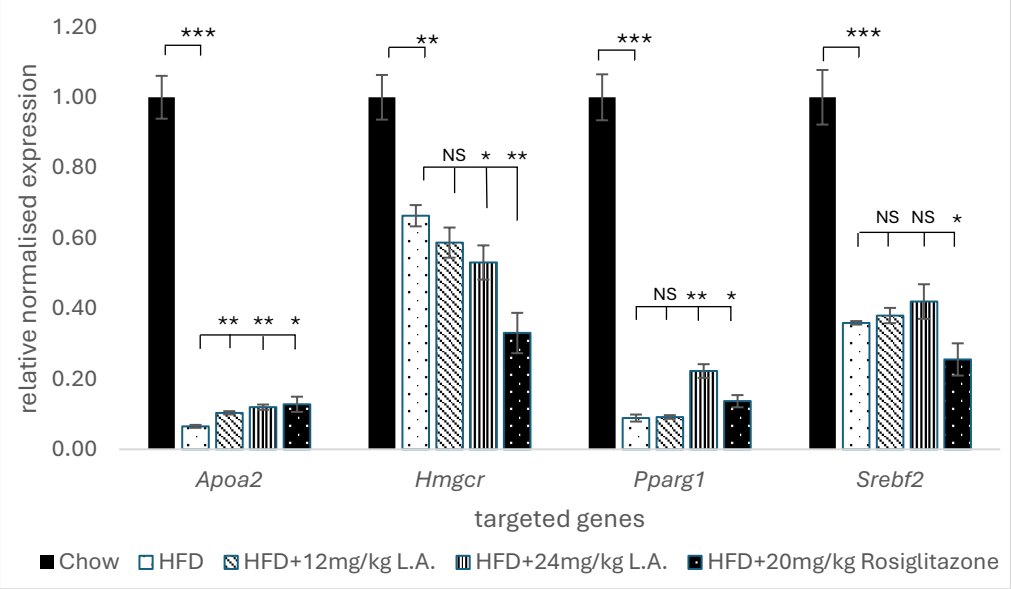

Figure 4.9: **The relative normalised expression of lipid regulation genes across experimental groups**. Each bar represents the mean ± SEM profile (n = 3). The pairwise comparisons shown in the figure represent the post hoc test results (NS, not significant; *$p \leqslant 0.05$; **$p \leq 0.01$; ***$p \leq 0.001$).

4.10 Lauric acid regulated the protein expression of SREBP1 and SREBP2, and increased AMPK phosphorylation

To further explore the molecular mechanisms of dietary intervention and treatment, the protein expression of the key metabolic regulators was assessed by Western blot (refer to **Section 3.9.6**). The quantification of protein bands was normalised to beta-actin and expressed as a relative expression ratio compared to the chow diet group (normalised to 1).

The SREBP1 is the transcription factor that regulates triglyceride synthesis. A one-way ANOVA test revealed no significant difference among the groups ($F(4,30) = 0.3793$, $p = 0.8216$). As shown in **Figure 4.10 (A)**, the HFD control group showed a slight but non-significant increase in SREBP1 protein (1.052 ± 0.240) compared to the chow diet group. Similarly, treatment with 12 mg/kg lauric acid (0.982 ± 0.244), 24 mg/kg lauric acid (0.929 ± 0.228) and rosiglitazone (0.742 ± 0.139) did not show significant differences in SREBP1 protein levels compared to the chow diet or the HFD control group. These findings suggest that the SREBP1-mediated triglyceride changes were not altered at protein levels under HFD or treatment conditions.

SREBP2, a transcriptional regulator of cholesterol synthesis, showed a reduction in the HFD group (0.747 ± 0.106) compared to the chow diet group. As shown in **Figure 4.10 (B)**, the lauric acid modulated SREBP2 levels in a dose-dependent manner, as the treatment with 24 mg/kg lauric acid showed

restoration of SREBP2 protein levels towards the chow diet group (1.009 ± 0.368), while the 12 mg/kg lauric acid resulted in a moderate level (0.934 ± 0.249). A comparable trend was observed at the mRNA level of *Srebf2*, supporting the consistency of transcription and translation (**Figure 4.9**). In contrast, the rosiglitazone treatment showed a similar trend to the HFD control group, with a lower protein expression of SREBP2 (0.700 ± 0.147). However, the one-way ANOVA test revealed no significant difference among the groups ($F(4,30) = 0.4568$, $p = 0.7667$). The observed changes suggest the potential modulation effect of lauric acid on hepatic cholesterol synthesis.

AMPK functions as a central energy sensor and metabolic regulator and was analysed in phosphorylated form. The HFD group showed a reduced phosphorylation of AMPK (0.812 ± 0.198) compared to the chow diet group, indicating suppressed energy signalling under high-fat conditions (**Figure 4.10 (C)**). The 12 mg/kg lauric acid treatment (0.917 ± 0.211) showed a modest restoration of AMPK phosphorylation compared to the chow diet. Notably, the treatment of 24 mg/kg lauric acid resulted in the highest AMPK phosphorylation level (1.441 ± 0.373), while rosiglitazone also increased the AMPK phosphorylation (1.109 ± 0.323). Although the one-way ANOVA test revealed no significant difference among the groups ($F(4,30) = 0.8878$, $p = 0.4832$), these changes suggest the potential activation of energy metabolism pathways in response to the treatments.

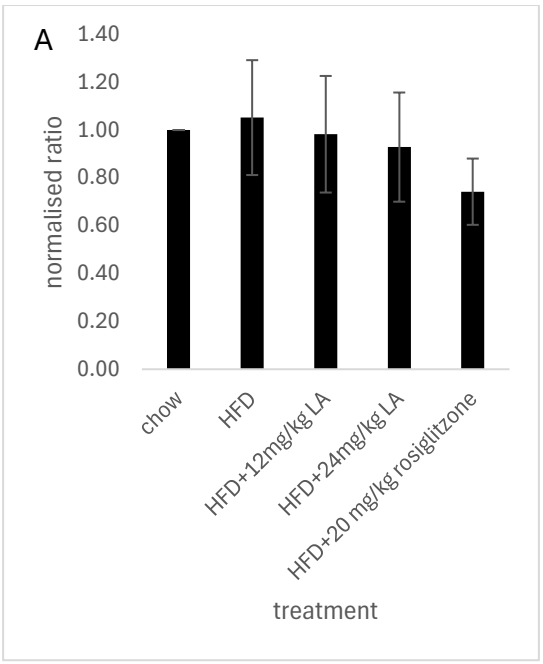
A
normalised ratio
1.40
1.20
1.00
0.80
0.60
0.40
0.20
0.00
chow
HFD
HFD+12mg/kg LA
HFD+24mg/kg LA
HFD+20 mg/kg rosiglitzone
treatment

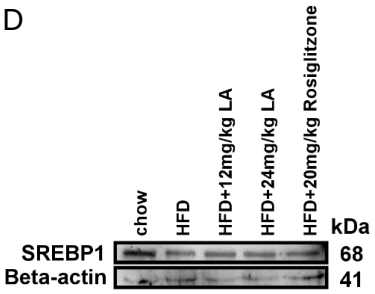
D
chow
HFD
HFD+12mg/kg LA
HFD+24mg/kg LA
HFD+20mg/kg Rosiglitzone
kDa
SREBP1
68
Beta-actin
41

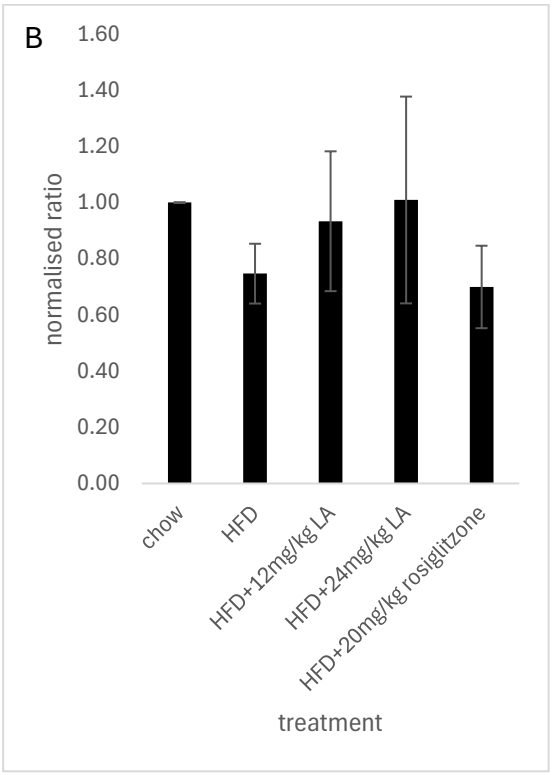
B
normalised ratio
1.60
1.40
1.20
1.00
0.80
0.60
0.40
0.20
0.00
chow
HFD
HFD+12mg/kg LA
HFD+24mg/kg LA
HFD+20mg/kg rosiglitzone
treatment

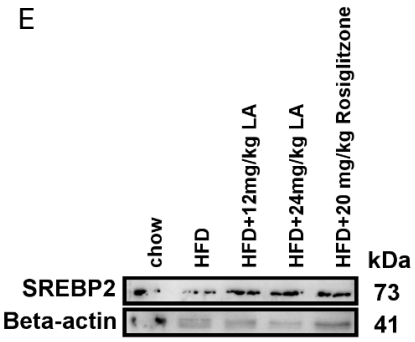
E
chow
HFD
HFD+12mg/kg LA
HFD+24mg/kg LA
HFD+20 mg/kg Rosiglitzone
kDa
SREBP2
73
Beta-actin
41

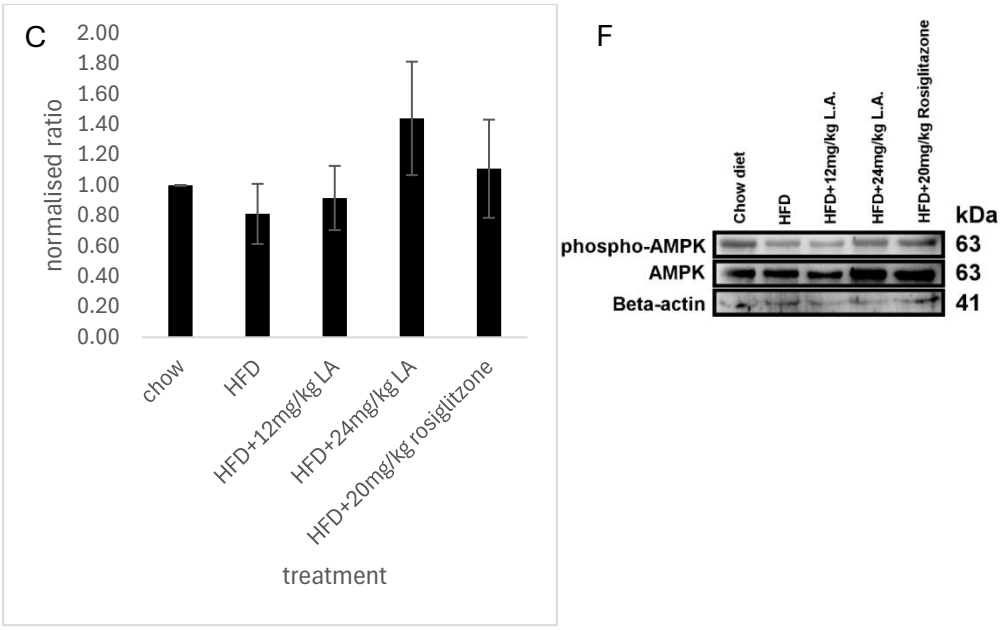

Figure 4.10: **Densitometry analysis and representative images of hepatic proteins**. (A) SREBP1, (B) SREBP2 and (C) phosphorylation of AMPK of different experimental groups. Each bar represents the mean ± SEM profile (n = 7). No statistically significant differences were observed among the groups across the evaluated proteins. (D-F) Representative blot image corresponding to SREBP1, SREBP2 and phosphorylated AMPK, respectively.

CHAPTER 5

DISCUSSION

5.1 Overview

This study evaluated the potential therapeutic effects of lauric acid on the metabolic dysregulation in HFD-induced obese C57BL/6J mice, with the insulin-sensitising drug rosiglitazone serving as a positive control. The results showed that lauric acid, particularly at a dosage of 24 mg/kg, attenuates HFD-induced obesity, dyslipidaemia, impaired glucose tolerance, insulin resistance and enhances hepatic AMPK phosphorylation. Although the effects were not as pronounced as rosiglitazone, lauric acid demonstrates beneficial effects on the hepatic lipogenic pathways, suggesting its potential as a nutritional intervention against metabolic syndrome, particularly in improving insulin resistance.

5.2 The effect of lauric acid on obesity and insulin resistance

The initial phase of the study (week 6 to week 14) served as an induction period to establish diet-induced obesity in the mouse model. Compared with the chow diet group, all HFD-fed groups showed elevated body weight, demonstrating the efficacy of the HFD model (**Section 4.1**). During the pre-treatment period, the body weights among the HFD groups were nearly identical, with no significant differences among them, ensuring a uniform baseline before

the treatments. Although the chow diet group consumed a greater volume of food, the lower calorie density of the chow diet (3.250 kcal/kg vs 5.228 kcal/kg in HFD) resulted in lower overall calorie intake. In contrast, HFD groups consumed more calories, in which the overconsumption of calories directly contributed to weight gain and adiposity. Upon supplementation, both lauric acid and rosiglitazone attenuated the HFD-induced weight gain. Following the initiation of the supplementation at week 14, both the lauric acid and rosiglitazone-treated groups showed a reduction in calorie consumption as compared to the HFD control group (**Section 4.3**). This suggests that lauric acid might improve appetite regulation or induce satiety, thereby attenuating the calorie overconsumption that leads to obesity in HFD feeding. The reduction of calorie consumption may be associated with the beneficial effects of lauric acid on body weight modulation. This finding is consistent with a previous animal study by Guo *et al*. (2023), who demonstrated that dietary lauric acid supplementation significantly enhanced physical performance in sedentary mice. The mice demonstrated enhanced exercise recovery and improved aerobic endurance and muscle strength. Mechanistically, lauric acid altered tissue fatty acid composition, facilitated adipose lipid mobilisation and increased circulating free fatty acids. These fatty acids were efficiently oxidised in the liver, partly mediated by activation of the AMPK–ACC signalling pathway. In addition, lauric acid promoted hepatic gluconeogenesis while sparing muscle glycogen and increased mitochondrial DNA copy number and boosted Krebs cycle activity in skeletal muscle, suggesting enhanced mitochondrial biogenesis and oxidative metabolism. These mechanisms align with the observations of increased AMPK phosphorylation (**Section 4.10**, **Figure 4.10(C)**), reduced lipid

profiles (**Section 4.6**) and reduced insulin resistance, suggesting the mediator effects of AMPK. Recent work by Zhang *et al.* (2020) demonstrated that lauric acid supplementation in HFD-fed female mice restored impaired brown adipose tissue (BAT) thermogenesis and improved overall energy metabolism, including enhanced glucose handling and normalisation of oestrous cycle irregularities. These results suggest that lauric acid may increase energy expenditure through thermogenic activation, providing a possible mechanistic basis for the observed attenuation of weight gain in the current study, in addition to its appetite-modulating effects. Human evidence also suggests a potential appetite-suppressing effect. Feltrin *et al*. (2014) reported that the acute oral administration of lauric acid can suppress the energy intake in lean, healthy humans without adverse effects. Although limited to short-term effects in healthy individuals, this complements the current findings and supports the hypothesis that lauric acid contributes to weight modulation through appetite regulation. In the population study, the dietary surveys indicated that intake of lauric acid and total polyunsaturated fatty acids was not associated with increased BMI in the USA population. These results showed the opposite effect of long-chain saturated fatty acids, which is positively correlated with adiposity (Raatz *et al*., 2017).

In this study, the HFD control group exhibited elevated blood glucose levels compared to the chow diet group, indicating the impairment of glucose regulation. Treatments with 24 mg/kg lauric acid and rosiglitazone have successfully normalised glucose levels, rendering values statistically indistinguishable from the chow diet group. This improvement was further

supported by the OGTT (**Section 4.4**), in which 24 mg/kg lauric acid-treated mice exhibited improved glucose clearance compared to the HFD control, suggesting enhanced peripheral glucose utilisation. Consistent with these outcomes, fasting insulin levels and HOMA-IR values were reduced, indicative of improved insulin sensitivity (**Section 4.5**). The amelioration of glucose dysregulation may be partly attributed to the activation of hepatic AMPK, which promotes glucose uptake and fatty acid oxidation while inhibiting gluconeogenic and lipogenic pathways. Complementary evidence highlights the protective role of lauric acid. In an HFD/streptozotocin-induced type 2 diabetes Wistar rat model, the administration of lauric acid has possessed strong antihyperglycemic potential by significantly reducing the fasting blood glucose levels. Importantly, lauric acid also attenuated pancreatic β-cell necrosis and vacuolization, suggesting its capacity to preserve or possibly regenerate β-cell mass (Alex *et al*., 2020). Similarly, Saraswathi *et al*. (2020) have compared the effect of lauric acid and palmitic acid in high-fat diet-induced obese mice, showing that both fatty acids promoted fat accumulation; only palmitic acid exerted more adverse effects, developing pronounced insulin resistance, as indicated by impaired insulin tolerance, along with higher adipose inflammation and elevated hepatic injury markers.

In contrast, the lauric acid maintained insulin responsiveness despite increased adiposity, reduced inflammatory markers and no evidence of insulin resistance, supporting its protective effects against HFD-induced metabolic dysfunction. Supporting the findings on HFD-fed mice, Anuar *et al*. (2023) have shown that oral administration of lauric acid (25-100 mg/kg for 8 weeks)

significantly improved fasting blood glucose, glucose tolerance and insulin resistance in streptozotocin-induced obese rats, accompanied by normalised insulin levels, restored antioxidant enzyme activity and improved testosterone levels. These results indicate that lauric acid can mitigate hyperglycaemia and restore glucose–insulin homeostasis in pathological models marked by β-cell injury and oxidative stress, suggesting systemic antihyperglycemic properties beyond hepatic AMPK activation.

Human data also support the insulin-sensitising potential of medium-chain fatty acids. In a randomised crossover trial, Lundsgaard *et al.* (2020) showed that 30 g/day of MCFAs preserved insulin sensitivity, as measured by hyperinsulinemic–euglycemic clamp, whereas an equivalent intake of long-chain saturated fats induced insulin resistance. More recently, Xia *et al*. (2024) reported that medium-chain triglycerides (MCTs) supplementation, specifically caprylic (C8), capric (C10), and lauric (C12) triglycerides, in HFD-induced obese rats for 12 weeks significantly improved fasting glycaemia, OGTT, HOMA-IR, and inflammatory markers, via PI3K/AKT pathway and PPARγ activation, with reduced PPARγ Ser237 phosphorylation. This aligns with the current study's observation that high-dose lauric acid upregulates hepatic *Pparg*, implicating PPARγ-dependent transcription control of its metabolic benefits. Additional mechanisms may involve insulin-independent pathways. Tham *et al*. (2020) reported that lauric acid restored glucose uptake in insulin-resistant THP-1 macrophages by upregulating GLUT1 and GLUT3 expression and promoting mitochondrial biogenesis. Pujol *et al*. (2018) further demonstrated that other MCFAs (caprylic acid (C8), capric acid (C10), and their mixtures)

enhanced β-cell function through G Protein Coupled Receptor 40 (GPR40) activation, promoting ketogenesis, and improved mitochondrial health, with β-hydroxybutyrate (BHB) supporting expression of key β-cell genes such as glucose transporter 2 (GLUT2), MAF bZIP Transcription Factor A (MafA), and neuronal differentiation 1(NeuroD1), thereby enhancing insulin secretion and glycaemic regulation. Although lauric acid was not included, these findings suggest that it may similarly preserve β-cell function and enhance secretory capacity. Together, these findings indicate that lauric acid improves glycaemic control, likely through enhanced glucose utilisation and improved insulin sensitivity. At the molecular level, high-dose lauric acid significantly increased *Pparg* expression compared with the HFD control (**Section 4.9**), suggesting partial activation of PPARγ-mediated pathways. However, the expression level remained distinct from the chow diet group, indicating that lauric acid did not fully normalise PPARγ activity. In contrast, hepatic AMPK phosphorylation did not differ significantly among groups, although high-dose lauric acid showed a modest ~1.4-fold increase relative to the chow diet group (**Section 4.10**). These results suggest that the improvements in glucose metabolism are partly mediated through PPARγ upregulation, while AMPK activation is unlikely to represent the main mechanism. Further studies are warranted to clarify whether lauric acid directly modulates glucose transporters or β-cell function, as these pathways were not directly validated in this study.

5.3 Lauric acid altered HFD-induced dyslipidaemia

In addition to the improvement of glucose metabolism, lauric acid was found to modulate lipid homeostasis disrupted by the HFD-induced dyslipidaemia. The high dose lauric acid significantly reduced the serum triglyceride and LDL levels compared to the HFD control group, while total cholesterol levels were moderately lower than the HFD control group but slightly higher relative to low dose lauric acid and rosiglitazone (**Section 4.6**). Importantly, high-dose lauric acid elevated HDL levels, indicating an overall improvement in the lipid profile. These serum changes were paralleled by transcriptional alteration. *Apoa2* and *Pparg1* expression were upregulated, supporting the enhanced lipid transport and storage capacity, whereas *Srebf2* expression was increased, but its downstream target *Hmgcr*, the rate-limiting enzyme for cholesterol synthesis, was downregulated (**Section 4.9**). At the protein level, no significant changes in SREBP1, SREBP2, or phosphorylated AMPK across groups; however, directional effects were consistent with metabolic modulation. High-dose lauric acid showed lower SREBP1, which aligns with reduced lipogenic drive and the observed decreases in circulating serum triglyceride. SREBP2 protein was restored toward chow levels by high-dose lauric acid despite an increase in *Srebf2* mRNA, suggesting post-transcriptional regulation of cholesterol synthesis. A modest elevation of phospho-AMPK further supported a role for AMPK-mediated reprogramming of hepatic lipid metabolism, although the effect did not reach statistical significance (**Section 4.10**).

These findings are consistent with the previous human and animal studies. Mensink *et al*. (2003) reported that lauric acid significantly elevates total cholesterol in a meta-analysis of 60 controlled trials, but largely via an increase in HDL cholesterol, leading to a decrease in the total-to-HDL cholesterol ratio. Similarly, Sedik *et al*. (2014) demonstrated that lauric acid supplementation reduced serum triglycerides, total cholesterol, fasting glucose, and insulin in HFD-induced MAFLD rats. Importantly, they observed upregulation of hepatic genes including IRS1, AMPK, PI3K, and SIRT1, alongside improved antioxidant enzyme levels and reduced hepatic apoptosis, which aligned with ameliorated liver histology. Given the established role of AMPK in inhibiting SREBP1c-driven lipogenesis and promoting fatty acid oxidation, this trend may partly contribute to the observed lipid-related genes. A study by Chen *et al*. (2021) revealed that AMPK phosphorylated and stabilised Krüppel-like factor 10 (KLF10), a transcriptional repressor that binds and downregulates SREBP-1C and reduces the key lipogenic enzymes, including ATP citrate lyase (ACLY), acetyl-CoA carboxylase 1 (ACC1), and fatty acid synthase (FASN).

Mechanistically, activation of AMPK is known to suppress lipogenesis by inhibiting SREBP-1 activation, as demonstrated by Jung *et al*. (2011). In models of orotic acid–induced fatty liver, suppression of AMPK signalling led to increased SREBP1 maturation and lipogenic gene expression. Conversely, pharmacological or genetic activation of AMPK reversed these effects and mitigated lipid accumulation. Jang *et al*. (2017) demonstrated in 3T3-L1 adipocytes that berberine activated AMPK, which phosphorylated the precursor

SREBP-1c, preventing its maturation, nuclear translocation, and DNA binding, and reducing the lipogenic gene expression and lipid accumulation. Consequently, the lipogenic gene expressions such as ACC1 and FAS were suppressed and reduced intracellular fat accumulation. Although the current study's data showed only a modest (~1.4-fold) increase in hepatic AMPK phosphorylation with high-dose lauric acid, without statistical significance, the result is nevertheless consistent with a partial mechanistic role for AMPK in downregulating SREBP-1-driven lipogenesis.

Additional evidence from a multi-omics study in HFD-fed mice showed that lauric acid, glycerol monolaurate (GML), and lauric triglyceride ameliorated hyperlipidaemia, improved glucose intolerance and reduced visceral fat deposition, while significantly modulating gut microbiota composition, characterised by increased *Bifidobacterium* and reduced *Desulfovibrio*, and altering host phospholipid metabolism and bile acid profiles (Zhao *et al*., 2022). Notably, GML had especially pronounced effects on glucose metabolism and inflammation, reinforcing the idea that lauric acid may exert part of its metabolic benefit through the gut-liver axis. These outcomes complement observations of improved glucose metabolism, serum triglycerides, LDL and HDL levels, suggesting that the systemic metabolic effect of lauric acid is contributed to by hepatic and gut-mediated mechanisms. The possible explanation for the cholesterol homeostasis observed in this study might also contribute to the AMPK activation. AMPK suppresses cholesterol synthesis downstream of transcription through inhibition or phosphorylation of HMGCR and reduced SREBP2 processing or activation, thereby lowering intracellular

cholesterol flux. In response to the reduced cholesterol flux, hepatocytes increase the *Srebf2* mRNA levels as homeostatic feedback to low cholesterol. However, the continued suppression of *Hmgcr* limited the regulatory function of *Srebf2*, consistent with the lower triglyceride and LDL levels with high dose lauric acid, while total cholesterol falls only modestly, which might be partly explained by increased HDL levels. This finding is consistent with the controlled crossover study in humans by De Roos, Schouten and Katan (2001), who showed that consumption of solid fat rich in lauric acid produced more favourable lipid profiles compared to trans-fat–rich alternatives. Lauric acid–rich dietary fat significantly increased HDL cholesterol vs trans-fat, with stable LDL and triglycerides.

Other studies have presented the role of AMPK activation on hepatic steatosis and hypercholesterolemia. Liu *et al.* (2015) demonstrated that activation of AMPK via 5-aminoimidazole-4-carboxyamide ribonucleoside (AICAR) in HepG2 cells and mouse liver directly inhibited SREBP-2 maturation through phosphorylation. This action subsequently reduced expression of downstream cholesterol synthesis enzymes, such as HMGCR and 3-hydroxy-3-methylglutaryl-CoA synthase (HMGCS). In the current study, high-dose lauric acid significantly downregulated *Hmgcr* despite an upregulation of *Srebf2* mRNA, suggesting that post-translational regulation of SREBP-2 by even modest AMPK activation may underlie decreased cholesterol synthesis. This mechanism likely contributes to the lower LDL and near-normal total cholesterol levels observed with lauric acid supplementation. In a study with chlorogenic acid, it was shown to activate hepatic AMPK, which

subsequently bond to SREBP2, disrupting its interaction with heat shock protein 90 (HSP90) and preventing both SREBP2 and pregnane X receptor (PXR) from translocating to the nucleus. This suppressed downstream targets like Niemann-Pick C1-like 1 (NPC1L1) and HMGCR and reduced cholesterol accumulation in hepatocytes (Meng *et al*., 2023). This mechanism could further explain the observation in the current study, where high-dose lauric acid downregulated *Hmgcr* despite upregulated *Srebf2*, supporting the possibility of AMPK-mediated post-translational inhibition of SREBP2 activity. Beyond AMPK, lauric acid might act directly through the nuclear receptor pathway. Arunima and Rajamohan (2018) demonstrated that lauric acid is a natural ligand for PPARα, enhancing the secretion of ApoA1 and reducing ApoB output in cultured rat hepatocytes through activation of PPARα-dependent pathways, alongside upregulation of fatty acid β-oxidation genes such as Acyl-CoA oxidase (ACOX) and carnitine palmitoyl transferase I (CPT1).

Lauric acid and related MCFAs also stimulate ω-oxidation. Ding *et al.* (2013) demonstrated that MCFAs from coconut oil, particularly lauric acid, stimulated hepatic ω-oxidation genes, including cytochrome P450 family 4 subfamily a polypeptide 10 and 14 (Cyp4a10, Cyp4a14), which lead to the generation of dicarboxylic fatty acids. These intermediates activated both ω- and β-oxidation pathways through PPARα and PPARγ. The L-peroxisomal bifunctional enzyme (L-PBE) is required to degrade the dicarboxylic acids and prevent their toxic accumulation and consequent liver damage. A study by Jarrar, Nasser and Lee (2025) also showed that lauric acid participated in the fatty acid ω-oxidation by inducing a dose-dependent upregulation of COX-2 expression.

In the present study, high-dose lauric acid supplementation enhanced the lipid profile and upregulated *Pparg1* (**Section 4.6**, **Section 4.9**), without inducing histological liver injury (**Section 4.8**), indicating effective peroxisomal clearance of MCFA intermediates and beneficial PPARγ-mediated lipid handling. This supports the notion that lauric acid, under normal metabolic processing, is safe and metabolically favourable. PPARγ in the liver plays complex yet protective roles in steatosis and lipid metabolism. While hepatic PPARγ overexpression has been linked to steatosis and fibrosis (Lee *et al*., 2023), PPARγ also acts as a lipid buffer, protecting peripheral tissues from lipotoxicity. Gavrilova *et al.* (2003) demonstrated that in lipoatrophic A-ZIP/F-1 (AZIP) mice, deletion of hepatic PPARγ reduced liver fat accumulation but unexpectedly worsened hyperlipidaemia, impaired triglyceride clearance, and exacerbated muscle insulin resistance. This result showed that hepatic PPARγ protects other tissues from lipid overload by reducing the circulating fatty acids and even causes hepatic steatosis. In addition, the lipid buffering effect of PPARγ2 also contributes to the protective effect against insulin resistance and lipid metabolism. Medina-Gómez *et al*. (2007) showed that PPARγ2 enables adipose expansion and safe lipid deposition in liver, muscle, and β-cells, preventing accumulation of lipotoxic species and preserving metabolic function. Thus, the lauric acid-induced upregulation of *Pparg1* observed here may represent a compensatory mechanism that promotes safe lipid deposition in adipose tissue rather than ectopic accumulation in the liver. Together, these data suggest that lauric acid improves lipid homeostasis through multiple mechanisms: AMPK-mediated suppression of lipogenic and cholesterol synthesis, PPARγ-driven promotion of fatty acid oxidation and lipid storage.

This integrated metabolic reprogramming likely underlies the improved lipid profiles and reduced steatotic burden observed with high-dose lauric acid supplementation.

5.4 The effect of lauric acid on MAFLD

In this study, all HFD and treated groups displayed predominantly microvesicular steatosis without evidence of inflammation, fibrosis, or necrosis, whereas the chow diet group demonstrated normal hepatic morphology. These findings are consistent with Eccleston *et al.* (2011), who reported that chronic HFD feeding in C57BL/6 mice leads to hepatic steatosis, hepatocyte ballooning, and mitochondrial dysfunction. They further demonstrated that prolonged fat intake exacerbates oxidative stress and impairs nitric oxide signalling, processes that contribute to liver injury and metabolic dysfunction. Together, these data confirmed that the HFD model employed here reliably recapitulates key pathogenic features of MAFLD and provided a valid platform to examine the modulatory effects of lauric acid on glucose and lipid metabolism. The HFD control group exhibited the highest absolute liver weight among the groups, suggesting hepatic enlargement under chronic lipid overload. However, when normalised to body weight, no significant differences were observed in relative liver weight among the groups (**Section 4.7**), indicating that the liver enlargement was proportional to the overall weight gain rather than reflecting specific organ targeting. Importantly, neither lauric acid nor rosiglitazone improved the degree of microvesicular steatosis in HFD-fed mice (**Section 4.8**).

Notably, the high-dose lauric acid-treated group even showed a trend towards increased absolute liver weight, suggesting a potential shift of lipid flux into the liver despite improvements in systemic metabolic markers. However, it remains debatable that the steatosis observed in this study might represent an early stage of macrovesicular steatosis, rather than microvesicular steatosis. While the histology most closely resembled microvesicular steatosis, the absence of a foamy cytoplasmic appearance and the presence of smaller vacuoles without nuclear displacement suggest the possibility of mediovesicular changes, representing an early transition toward macrovesicular steatosis (Bedossa, 2017). Macrovesicular steatosis is characterised by a single large lipid droplet displacing the nucleus and is the predominant histological pattern in MAFLD (Leow *et al*., 2022). Microvesicular steatosis is marked by multiple small lipid droplets with centrally located nuclei and is rarer and more often associated with mitochondrial dysfunction, Reye syndrome, and severe forms of liver injury (Patel and Sanyal, 2013).

Experimental evidence by other researchers further supports this interpretation. Both high-fat (HF) and high-sucrose (HS) diets individually lead to severe steatosis (grade 3) without progression to inflammatory or fibrotic stages, whereas the combined HFHS diet intensified fat accumulation and promoted early fibrosis, particularly when fructose was present in high amounts (Simoes *et al.*, 2020). Clinically, steatosis in MAFLD patients most often presents as macrovesicular; however, microvesicular changes, though less common, are associated with worsened metabolic status, hepatocellular injury, and higher fibrosis risk (Tandra *et al*., 2010; Germano *et al*., 2023). Consistent

with these findings, Magee *et al*. (2022) showed that mice fed a high-fat, high-cholesterol and high fructose (HFHC) diet developed obesity, insulin resistance, dyslipidaemia, and early-stage hepatic steatosis, without inflammatory or fibrotic changes. Their hepatic transcriptomic profiling revealed altered gene expression regulating lipid metabolism and cellular stress, reflecting a pathophysiological progression toward MAFLD. Specifically, both macro- and microvesicular steatosis were observed after one month of the diet administration, with macrovesicular steatosis becoming more dominant after three months of diet administration. Upregulation of *Pparg* and its downstream targets, including the fatty acid translocase (Cd36) and the lipid droplet membrane protein gene, Cell death-inducing DFFA-like effector C (*Cidec*), highlighted the role of enhanced fatty acid uptake and lipid droplet formation in steatosis development, alongside de novo lipogenesis, impaired lipid oxidation and reduced VLDL secretion. Together, these parallels reinforce that the current high-fat diet model captures the early mechanisms of steatosis development. This provides a relevant context for assessing how lauric acid modulates systemic metabolic parameters, even if direct histological improvements in hepatic lipid accumulation were not observed.

5.5 The use of rosiglitazone in this study

Rosiglitazone is a thiazolidinedione class drug and PPARγ agonist, serving as a positive control in this study. In the HFD-fed mice model, the rosiglitazone produced outcomes broadly comparable to lauric acid on body

weight, calorie intake, fasting blood glucose and OGTT (**Section 4.1-4.4**). Rosiglitazone exhibited a stronger effect on insulin homeostasis as it significantly reduced insulin levels and HOMA-IR values in HFD-fed mice, showing normalisation towards the chow diet group, indicating robust improvement in insulin sensitivity (**Section 4.5**). Rosiglitazone also improved the blood lipid profile, with reductions in triglycerides and LDL levels and an increase in HDL levels (**Section 4.6**). These biochemical changes were consistent with transcriptional adaptations, including reduced *Hmgcr* and *Srebf2* expression, together with increased *Apoa2* and *Pparg1* expression. At the protein level, rosiglitazone decreased the abundance of SREBP1 and SREBP2 and normalised phosphorylated AMPK, further supporting its role in lipid regulation (**Sections 4.9** and **4.10**). Notably, *Pparg1* upregulation was less pronounced than in the high-dose lauric acid group, suggesting differential engagement of PPARγ-driven pathways between the two treatments. These changes align with the clinical findings, where rosiglitazone improved insulin sensitivity, enhanced insulin-stimulated glucose disposal, preserved β-cell function and the combination of rosiglitazone with metformin or sulfonylurea in type 2 diabetic patients has significant HDL elevation and improved cardiovascular safety (Mayerson *et al*., 2002; Deeks and Keam, 2007; Home *et al.*, 2009). However, rosiglitazone posed adverse effects such as weight gain, fluid retention and increased heart failure risk (Home *et al*., 2009; Lu *et al*., 2011; Mayer *et al*., 2016). Although rosiglitazone did not reverse steatosis in this study (**Section 4.8**), its consistent insulin-sensitising and lipid-modulating effects validate its use as a comparison to evaluate the efficacy of lauric acid.

5.6 Limitations of the study

Several limitations must be acknowledged, particularly in relation to study duration, mechanistic studies, and translational relevance. First, the duration of interventions may have been insufficient to fully capture the long-term effects of lauric acid and rosiglitazone, particularly on hepatic histology. Some metabolic adaptations, such as AMPK phosphorylation, as well as potential modulations of hepatic steatosis, may require a longer treatment period to become evident. Similarly, the relatively short duration of HFD feeding, while sufficient to induce obesity and insulin resistance, may not allow the development of more advanced hepatic pathophysiology. Second, LDL values were estimated using the Friedewald formula; however, as this equation was originally derived for human physiology, these data were intended to illustrate proportional trends between groups rather than provide absolute quantification. Unlike humans, mice exhibit an HDL-dominant lipoprotein profile with relatively low LDL levels; therefore, VLDL measurements are often considered more appropriate than LDL for evaluating lipid metabolism in murine models (Sun *et al*., 2020). Third, the mechanistic analysis is limited. Although changes in AMPK were assessed, additional protein analysis, such as ACC1 and HMGCR, would have provided a deeper insight into the effects of lauric acid on cholesterol metabolism via the AMPK pathway. Furthermore, complementary histological approaches, such as Oil Red O staining (Levene *et al.*, 2012), could have been included to visualise hepatic lipid accumulation better and to clarify whether PPARγ-mediated influx and fatty acid oxidation are affected in lauric acid-treated mice. Besides, only two doses of lauric acid

were tested, and it remains possible that higher or intermediate doses might produce different or more pronounced metabolic outcomes. It should also be noted that the control groups did not receive vehicle gavage, and no vehicle-only group was included. Thus, potential confounding effects associated with repeated gavage handling or low-dose ethanol exposure cannot be completely excluded. Additionally, this study focused on diet-induced obesity without incorporating streptozotocin, which limits conclusions about lauric acid's potential effects in more severe or mixed models of insulin resistance and diabetes. Finally, while the HFD-fed C57BL/6J mouse is a well-established model, the findings cannot be directly extrapolated to humans with MAFLD or type 2 diabetes mellitus, where genetic, hormonal and lifestyle factors contribute to the disease complexity. Differences in lipid metabolism between rodents and humans, including variations in lipoprotein distribution and APOA2 function (Florea *et al*., 2022), may further restrict translational applicability. Despite these limitations, the study demonstrates that lauric acid has promising effects on insulin resistance and lipid metabolism in a mouse model of HFD-induced obesity.

5.7 Future study

Future studies should aim to expand these findings by comparing lauric acid with glycerol monolaurate (GML) in attenuating dysregulated lipid metabolism and improving insulin resistance. GML has been reported to exert broader health benefits, particularly stronger antimicrobial effects and more

pronounced glucose metabolism (Zhao *et al*., 2022) and could provide additional insights into medium-chain fatty acid biology. Beyond conventional biochemical assays, the potential effects of lauric acid on gut microbiota composition and bile acid metabolism warrant further investigation, as suggested by Wong, Choo and Chew (2020), who demonstrated that coconut milk modestly influenced lipid profiles while exerting a stronger effect on bile acid secretion. To gain mechanistic insights, functional assays should be included in future experiments. For example, the AMPK activity assay (Jang *et al.*, 2017) would clarify the role of AMPK in lauric acid-mediated lipid homeostasis. Hepatic triglyceride content measurement, hepatic VLDL secretion rate (Metz *et al*., 2023), and fatty acid β-oxidation measurement (Moliterni *et al*., 2024) would help test the hypothesis of plasma-liver lipid redistribution. In the case of microvesicular steatosis, serum ALT and AST levels should be evaluated (Mumtaz *et al*., 2024), as these often rise with mitochondrial injury. Complementary mitochondrial function assays, such as hepatic oxygen consumption by high-resolution respirometry (Zhao *et al*., 2020), as well as CPT1 and acyl-CoA dehydrogenases (ACAD) enzyme activity, could provide deeper insights into oxidative metabolism. Transmission electron microscopy (TEM) could be employed to visualise mitochondrial swelling and cristae disruption, which are hallmarks of mitochondrial dysfunction and oxidative stress (Zhao *et al*., 2023; Kido *et al*., 2025). At the molecular level, qPCR analysis of genes involved in β-oxidation (*Pparα, CPT1, Acox1, Pgc1α*) and oxidative stress regulation (*Nrf2, SOD2*) would further elucidate lauric acid's impact on hepatic metabolism. In addition, future studies should explore the role of the PI3K/AKT pathway, given its central involvement in MAFLD

pathophysiology and insulin signalling, to determine whether lauric acid exerts mandatory effects on this axis (Sun *et al.*, 2022; Shao and Xu, 2025). Finally, to better mimic human MAFLD or T2DM, a more severe disease model induced by HFD feeding combined with streptozotocin could be employed, thereby allowing the evaluation of lauric acid's therapeutic potential in advanced metabolic dysfunction and hepatic steatosis. Although this study demonstrates the metabolic benefits of lauric acid in an HFD-induced mouse model, further clinical studies are required to evaluate its efficacy and safety in humans. Previous clinical studies have reported that lauric acid–rich coconut oil may improve lipid profiles by increasing HDL cholesterol levels, suggesting potential cardiometabolic benefits (Khaw *et al.*, 2018).

.

CHAPTER 6

CONCLUSION

This study evaluated the effect of lauric acid on insulin resistance and lipid metabolism in the HFD-induced obese C57BL/6J mouse model. Lauric acid exhibited dose-dependent effects: the low dose was more effective in reducing body weight and calorie intake, whereas the high dose produced greater improvements in fasting blood glucose, fasting insulin levels and HOMA-IR. High-dose lauric acid also improved lipid metabolism, lowered triglyceride and LDL levels while increasing the HDL level, suggesting potential cardiovascular benefits. At the molecular level, high-dose lauric acid upregulated *Apoa2* and *Pparg1* expression, while downregulating *Hmgcr* despite an upregulation of *Srebf2*. Protein analysis showed a trend of reduction in SREBP1 and a normalisation of SREBP2, and modestly elevated AMPK phosphorylation in the high-dose lauric acid-treated group, indicating that the observed metabolic improvements may be partly mediated through AMPK activation. These findings highlight the dose-dependent metabolism of lauric acid in a diet-induced obesity model.

Lauric acid reduced the body weight in HFD-fed mice, which was associated with decreased calorie intake and may suggest a potential satiety-related mechanism. Glucose homeostasis was also improved, which is critical for alleviating insulin resistance. Enhanced glucose clearance in the high-dose

lauric acid-treated group might be attributed to the increased *Pparg* expression and partly to the activation of hepatic AMPK. The lipid-modulating effects of lauric acid might be partly mediated by AMPK activation through suppression of SREBP1 and HMGCR, thereby reducing lipogenesis and cholesterol synthesis, even in the presence of increased SREBP2 levels. However, neither lauric acid nor rosiglitazone could reverse the hepatic steatosis within the study period.

Despite these promising findings, this study was limited by the duration, as a longer period of HFD feeding and lauric acid treatment could reflect chronic metabolic change, and chronic administration of lauric acid may provide further insight into the metabolic effects of lauric acid. Additionally, other regulatory pathways, such as ACC and PI3K, were not investigated and should be included in future work to provide a more comprehensive understanding of lauric acid's effects. Future studies should also compare lauric acid with glycerol monolaurate and investigate their role in β-oxidation and mitochondrial function to clarify their impact on oxidative metabolism.

In conclusion, lauric acid improved insulin resistance and lipid profile in the HFD-C57BL/6J mice model, potentially mediated by AMPK pathway activation. While further mechanistic studies are needed, lauric acid shows promise as a nutraceutical candidate that could complement pharmacological treatment and lifestyle interventions in managing obesity and related metabolic disorders.

Reference

Akiyama, T. *et al.* (2024) 'Serum Apolipoprotein-A2 levels are a strong predictor of future cardiovascular events in patients undergoing percutaneous coronary intervention,' *Circulation Journal*, 88(11), pp. 1770–1777. https://doi.org/10.1253/circj.cj-24-0242.

Al. Rijjal, D. and Wheeler, M.B. (2022) 'A protocol for studying glucose homeostasis and islet function in mice,' *STAR Protocols*, 3(1), p. 101171. https://doi.org/10.1016/j.xpro.2022.101171.

Alex, E.A. *et al.* (2020) 'Evaluation of oral administration of lauric acid supplement on fasting blood glucose level and pancreatic histomorphological studies in High Fat Diet/Streptozotocin-Induced Type 2 Diabetic Male Wistar rats,' *Journal of Diabetes & Metabolism*, 11(7), pp. 1–7. https://doi.org/10.35248/2155-6156.20.11.849.

Al-Lahham, R., Deford, J.H. and Papaconstantinou, J. (2015) 'Mitochondrial-generated ROS down regulates insulin signaling via activation of the p38MAPK stress response pathway,' *Molecular and Cellular Endocrinology*, 419, pp. 1–11. https://doi.org/10.1016/j.mce.2015.09.013.

Alqahtani, S.A. and Schattenberg, J.M. (2021) 'NAFLD in the elderly,' *Clinical Interventions in Aging*, 16, pp. 1633–1649. https://doi.org/10.2147/cia.s295524.

Ameena, A. *et al*. (2024) 'Biomedical applications of lauric acid: A narrative review', *Cureus*, 16. https://doi.org/10.7759/cureus.62770

Amini-Salehi, E. *et al.* (2024) 'Global prevalence of nonalcoholic fatty liver disease: an updated meta-analysis on 78 million population over 38 countries,' *Archives of Medical Research*, 55(6), p. 103043. https://doi.org/10.1016/j.arcmed.2024.103043

Anuar, N.S. *et al.* (2023) 'Lauric acid improves hormonal profiles, antioxidant properties, sperm quality and histomorphometric changes in testis and epididymis of streptozotocin-induced diabetic infertility rats,' *Toxicology and Applied Pharmacology*, 470, p. 116558. https://doi.org/10.1016/j.taap.2023.116558.

Arrese, M. *et al.* (2016) 'Innate immunity and inflammation in NAFLD/NASH,' *Digestive Diseases and Sciences*, 61(5), pp. 1294–1303. https://doi.org/10.1007/s10620-016-4049-x.

Ballard, C.R. and Cazarin, C.B.B. (2022). 'Measures of food intake, body weight gain, and energy efficiency in mice', In: Betim Cazarin, C.B. (eds) *Basic Protocols in Foods and Nutrition. Methods and Protocols in Food Science.* New York: Humana Press. https://doi.org/10.1007/978-1-0716-2345-9_2

Ballestri, S. *et al*. (2016). 'Nonalcoholic fatty liver disease is associated with an almost twofold increased risk of incident type 2 diabetes and metabolic syndrome. Evidence from a systematic review and meta-analysis,' *Journal of Gastroenterology and Hepatology*, 31(5), pp. 936–944. https://doi.org/10.1111/jgh.13264

Battistella, S. *et al.* (2022) 'Liver transplantation for non-alcoholic fatty liver disease: indications and post-transplant management,' *Clinical and Molecular Hepatology*, 29(Suppl), pp. S286–S301. https://doi.org/10.3350/cmh.2022.0392.

Bedossa, P. (2017) 'Pathology of non-alcoholic fatty liver disease,' *Liver International*, 37(S1), pp. 85–89. https://doi.org/10.1111/liv.13301.

Belfort, R. *et al.* (2006) 'A placebo-controlled trial of pioglitazone in subjects with nonalcoholic steatohepatitis,' *New England Journal of Medicine*, 355(22), pp. 2297–2307. https://doi.org/10.1056/nejmoa060326.

Boccatonda, A. *et al*. (2023) 'From NAFLD to MAFLD: Definition, pathophysiological basis and cardiovascular implications', *Biomedicines*, 11(3), 883. https://doi.org/10.3390/biomedicines11030883

Boden, G. *et al.* (2015) 'Excessive caloric intake acutely causes oxidative stress, GLUT4 carbonylation, and insulin resistance in healthy men,' *Science Translational Medicine*, 7(304). https://doi.org/10.1126/scitranslmed.aac4765.

Boivin, G. P.*et al*. (2014) 'Biomechanical properties and histology of db/db diabetic mouse Achilles tendon,' *Muscles, Ligaments and Tendons Journal*, 4(3), 280–284.https://pubmed.ncbi.nlm.nih.gov/25489543/

Boudaba, N. *et al*. (2018). 'AMPK re-activation suppresses hepatic steatosis but its downregulation does not promote fatty liver development,' *EBioMedicine*, 28, pp. 194–209. https://doi.org/10.1016/j.ebiom.2018.01.008

Boughanem, H. *et al.* (2020) 'Association between the APOA2 rs3813627 Single Nucleotide Polymorphism and HDL and APOA1 Levels Through BMI,' *Biomedicines*, 8(3), p. 44. https://doi.org/10.3390/biomedicines8030044.

Brown, T., Mackey, K., and Du, T. (2004). 'Analysis of RNA by northern and slot blot hybridization', *Current Protocols in Molecular Biology*. https://doi.org/10.1002/0471142727.mb0409s67

Buchynskyi, M. *et al.* (2025) 'Unlocking the gut-liver axis: microbial contributions to the pathogenesis of metabolic-associated fatty liver disease,' *Frontiers in Microbiology*, 16. https://doi.org/10.3389/fmicb.2025.1577724.

Buettner, R., Schölmerich, J. and Bollheimer, L.C. (2007) 'High-fat diets: Modeling the metabolic disorders of human obesity in rodents,' *Obesity*, 15(4), pp. 798–808. https://doi.org/10.1038/oby.2007.608.

Burke, S.J. *et al*. (2017) 'db/db Mice exhibit features of human type 2 diabetes that are not present in weight-matched C57BL/6J mice fed a western diet,' *Journal of Diabetes Research*, pp. 1–17. https://doi.org/10.1155/2017/8503754.

Buzzetti, E., Pinzani, M. and Tsochatzis, E.A. (2016) 'The multiple-hit pathogenesis of non-alcoholic fatty liver disease (NAFLD),' *Metabolism*, 65(8), pp. 1038–1048. https://doi.org/10.1016/j.metabol.2015.12.012.

Caballero, F. *et al.* (2009) 'Enhanced free cholesterol, SREBP-2 and StAR expression in human NASH,' *Journal of Hepatology*, 50(4), pp. 789–796. https://doi.org/10.1016/j.jhep.2008.12.016.

Cacho, J., *et al.* (2008). 'Validation of simple indexes to assess insulin sensitivity during pregnancy in Wistar and Sprague-Dawley rats', *American Journal of Physiology. Endocrinology and Metabolism*, 295(5), pp. E1269–E1276. Available at: https://doi.org/10.1152/ajpendo.90207.2008

Cao, L. *et al.* (2024) 'Global epidemiology of type 2 diabetes in patients with NAFLD or MAFLD: a systematic review and meta-analysis,' *BMC Medicine*, 22(1). https://doi.org/10.1186/s12916-024-03315-0.

Cassiday, L. (2016) 'Coconut oil boom,' *INFORM International News on Fats Oils and Related Materials*, 27(5), pp. 6–16. https://doi.org/10.21748/inform.05.2016.06.

Cazac, G.-D. *et al.* (2022) 'New insights into non-alcoholic fatty liver disease and coronary artery disease: the liver-heart axis,' *Life*, 12(8), p. 1189. https://doi.org/10.3390/life12081189.

Chakraborty, S. *et al.* (2023) 'Cardiometabolic risk factors associated with Type 2 diabetes mellitus: a mechanistic insight,' *Clinical Medicine Insights Endocrinology and Diabetes*, 16. https://doi.org/10.1177/11795514231220780.

Chan, K.E. *et al.* (2022) 'Global prevalence and clinical characteristics of metabolic-associated fatty liver Disease: A Meta-Analysis and Systematic Review of 10,739,607 individuals,' *The Journal of Clinical Endocrinology & Metabolism*, 107(9), pp. 2691–2700. https://doi.org/10.1210/clinem/dgac321.

Chan, W.K. *et al.* (2022) 'Malaysian Society of Gastroenterology and Hepatology consensus statement on metabolic dysfunction-associated fatty liver disease,' *Journal of Gastroenterology and Hepatology*, 37(5), pp. 795–811. https://doi.org/10.1111/jgh.15787

Chen, H. *et al.* (2022) 'Regulated degradation of HMG CoA reductase requires conformational changes in sterol-sensing domain,' *Nature Communications*, 13(1). https://doi.org/10.1038/s41467-022-32025-5.

Chen, H. *et al.* (2023) 'Sex- and age-specific associations between abdominal fat and non-alcoholic fatty liver disease: a prospective cohort study,' *Journal of Molecular Cell Biology*, 15(11). https://doi.org/10.1093/jmcb/mjad069.

Chen, Y.-C. *et al.* (2021) 'Therapeutic targeting of nonalcoholic fatty liver disease by downregulating SREBP-1C expression via AMPK-KLF10 axis,' *Frontiers in Molecular Biosciences*, 8. https://doi.org/10.3389/fmolb.2021.751938.

Choi, S.-S., Park, J. and Choi, J.H. (2014) 'Revisiting PPARγ as a target for the treatment of metabolic disorders,' *BMB Reports*, 47(11), pp. 599–608. https://doi.org/10.5483/bmbrep.2014.47.11.174.

Corella, D. *et al.* (2007) 'The −256T>C polymorphism in the apolipoprotein A-II gene promoter is associated with body mass index and food intake in the genetics of lipid lowering drugs and diet network study,' *Clinical Chemistry*, 53(6), pp. 1144–1152. https://doi.org/10.1373/clinchem.2006.084863.

Dang, S.-W. *et al*. (2023) 'Metabolic characteristics of non-obese and obese metabolic dysfunction-associated fatty liver disease in type 2 diabetes mellitus and its association with diabetic peripheral neuropathy and diabetic retinopathy,' *Frontiers in Medicine*, 10. https://doi.org/10.3389/fmed.2023.1216412.

Davidson, M.B. and Pan, D. (2017) 'An updated meta-analysis of pioglitazone exposure and bladder cancer and comparison to the drug's effect on cardiovascular disease and non-alcoholic steatohepatitis,' *Diabetes Research and Clinical Practice*, 135, pp. 102–110. https://doi.org/10.1016/j.diabres.2017.11.002.

Dayrit, F.M. (2014) 'The properties of lauric acid and their significance in coconut oil,' *Journal of the American Oil Chemists Society*, 92(1), pp. 1–15. https://doi.org/10.1007/s11746-014-2562-7.

De Roos, N.M., Schouten, E.G. and Katan, M.B. (2001) 'Consumption of a solid fat rich in lauric acid results in a more favorable serum lipid profile in healthy men and women than consumption of a solid fat rich in trans-fatty acids,' *Journal of Nutrition*, 131(2), pp. 242–245. https://doi.org/10.1093/jn/131.2.242.

Deeks, E.D. and Keam, S.J. (2007) 'Rosiglitazone: a review of its use in type 2 diabetes mellitus,' *Drugs*, 67(18), pp.2747-2779.

Della Vedova, M.C. *et al*. (2016) 'A mouse model of diet-induced obesity resembling most features of human metabolic syndrome,' *Nutrition and Metabolic Insights*, 9, pp. 93–102. https://doi.org/10.4137/nmi.s32907.

Ding, J. *et al.* (2013) 'The peroxisomal enzyme L-PBE is required to prevent the dietary toxicity of medium-chain fatty acids,' *Cell Reports*, 5(1), pp. 248–258. https://doi.org/10.1016/j.celrep.2013.08.032.

Ding, Y. *et al.* (2023) 'Clinical classification of obesity and implications for Metabolic Dysfunction-Associated Fatty Liver Disease and treatment,' *Diabetes Metabolic Syndrome and Obesity*, 16, pp. 3303–3329. https://doi.org/10.2147/dmso.s431251.

Donnelly, K.L. *et al.* (2005) 'Sources of fatty acids stored in liver and secreted via lipoproteins in patients with nonalcoholic fatty liver disease,' *Journal of Clinical Investigation*, 115(5), pp. 1343–1351. https://doi.org/10.1172/jci23621.

Duan, S. *et al.* (2025) 'Application of insulin resistance score in type 2 diabetes mellitus complicated with fatty liver and liver fibrosis,' *European Journal of Gastroenterology & Hepatology*, 37(10), pp. 1155-1165. https://doi.org/10.1097/meg.0000000000002998

Eccleston, H.B. *et al.* (2010) 'Chronic exposure to a high-fat diet induces hepatic steatosis, impairs nitric oxide bioavailability, and modifies the mitochondrial proteome in mice,' *Antioxidants and Redox Signaling*, 15(2), pp. 447–459. https://doi.org/10.1089/ars.2010.3395.

Enooku, K. *et al.* (2019) 'Altered serum acylcarnitine profile is associated with the status of nonalcoholic fatty liver disease (NAFLD) and NAFLD-related hepatocellular carcinoma,' *Scientific Reports*, 9(1), p.10663. https://doi.org/10.1038/s41598-019-47216-2.

Eslam, M. *et al*. (2020a) 'A new definition for metabolic dysfunction-associated fatty liver disease: An international expert consensus statement', *Journal of Hepatology*, 73(1), pp. 202–209. https://doi.org/10.1016/j.jhep.2020.03.039

Eslam, M. *et al*. (2020b) 'The Asian Pacific Association for the study of the liver clinical practice guidelines for the diagnosis and management of metabolic associated fatty liver disease', *Hepatology International*, 14(6), pp.889–919. https://doi.org/10.1007/s12072-020-10094-2

Fang, C. *et al.* (2022) 'The AMPK pathway in fatty liver disease,' *Frontiers in Physiology*, 13. https://doi.org/10.3389/fphys.2022.970292.

Fang, Y.-L. *et al.* (2018) 'Pathogenesis of non-alcoholic fatty liver disease in children and adolescence: From "two hit theory" to "multiple hit model",' *World Journal of Gastroenterology*, 24(27), pp. 2974–2983. https://doi.org/10.3748/wjg.v24.i27.2974.

Faulkner, R. and Jo, Y. (2022) 'Synthesis, function, and regulation of sterol and nonsterol isoprenoids,' *Frontiers in Molecular Biosciences*, 9. https://doi.org/10.3389/fmolb.2022.1006822.

Feltrin, K.L. *et al.* (2014) 'Acute oral administration of lauric acid reduces energy intake in healthy males,' *e-SPEN Journal*, 9(2), pp. e69–e75. https://doi.org/10.1016/j.clnme.2014.01.004.

Florea, G. *et al.* (2022) 'Apolipoprotein A-II, a player in multiple processes and diseases,' *Biomedicines*, 10(7), p. 1578. https://doi.org/10.3390/biomedicines10071578.

Fraulob, J.C. *et al*. (2010) 'A mouse model of metabolic syndrome: insulin resistance, fatty liver and Non-Alcoholic Fatty pancreas Disease (NAFPD) in

C57BL/6 mice fed a high fat diet,' *Journal of Clinical Biochemistry and Nutrition*, 46(3), pp. 212–223. https://doi.org/10.3164/jcbn.09-83.

Fujiwara-Tani, R. *et al.* (2025) 'Energy metabolism and stemness and the role of lauric acid in reversing 5-Fluorouracil resistance in colorectal cancer cells,' *International Journal of Molecular Sciences*, 26(2), p. 664. https://doi.org/10.3390/ijms26020664.

Fullerton, M.D. *et al.* (2013) 'Single phosphorylation sites in Acc1 and Acc2 regulate lipid homeostasis and the insulin-sensitizing effects of metformin,' *Nature Medicine*, 19(12), pp. 1649–1654. https://doi.org/10.1038/nm.3372.

Furuta, Y. *et al.* (2023) 'Postprandial fatty acid metabolism with coconut oil in young females: a randomized, single-blind, crossover trial,' *American Journal of Clinical Nutrition*, 117(6), pp. 1240–1247. https://doi.org/10.1016/j.ajcnut.2023.03.015.

Gallou-Kabani, C. *et al.* (2007) 'C57BL/6J and A/J mice fed a high-fat diet delineate components of metabolic syndrome,' *Obesity*, 15(8), pp. 1996–2005. https://doi.org/10.1038/oby.2007.238.

Gan, Z. *et al.* (2024) 'Mitochondrial nicotinamide nucleotide transhydrogenase: role in energy metabolism, redox homeostasis, and cancer,' *Antioxidants and Redox Signaling*, 41(13–15), pp. 927–956. https://doi.org/10.1089/ars.2024.0694.

Gao, Y. *et al.* (2022) 'Coconut oil and medium-chain fatty acids attenuate high-fat diet-induced obesity in mice through increased thermogenesis by activating brown adipose tissue,' *Frontiers in Nutrition*, 9. https://doi.org/10.3389/fnut.2022.896021

Garcia, D. and Shaw, R.J. (2017) 'AMPK: Mechanisms of cellular energy sensing and restoration of metabolic balance,' *Molecular Cell*, 66(6), pp. 789–800. https://doi.org/10.1016/j.molcel.2017.05.032.

Gargiulo, S. *et al.* (2024) 'Integrated ultrasound characterization of the diet-induced obesity (DIO) model in young adult c57bl/6j mice: Assessment of cardiovascular, renal and hepatic changes,' *Journal of Imaging*, 10(9), p. 217. https://doi.org/10.3390/jimaging10090217.

Gavrilova, O. *et al.* (2003) 'Liver peroxisome proliferator-activated receptor γ contributes to hepatic steatosis, triglyceride clearance, and regulation of body fat mass,' *Journal of Biological Chemistry*, 278(36), pp. 34268–34276. https://doi.org/10.1074/jbc.m300043200.

Germano, C.W. *et al.* (2023) 'Microvesicular steatosis in individuals with obesity: a histological marker of non-alcoholic fatty liver disease severity,' *Obesity Surgery*, 33(3), pp. 813–820. https://doi.org/10.1007/s11695-023-06467-9.

Gofton, C. *et al*. (2022) ‘MAFLD: How is it different from NAFLD?’, *Clinical and Molecular Hepatology*, 29(Suppl), S17–S31. https://doi.org/10.3350/cmh.2022.0367

Grenier, A. *et al.* (2016) 'Rosiglitazone influences adipose tissue distribution without deleterious impact on heart rate variability in coronary heart disease patients with type 2 diabetes,' *Clinical Autonomic Research*, 26(6), pp. 407–414. https://doi.org/10.1007/s10286-016-0373-7.

Grobe, J.L. (2017) 'Comprehensive assessments of energy balance in mice,' *Methods in Molecular Biology*, pp. 123–146. https://doi.org/10.1007/978-1-4939-7030-8_10.

Guo, J. *et al*. (2023) 'Dietary supplementation with lauric acid improves aerobic endurance in sedentary mice via enhancing fat mobilization and glyconeogenesis,' *Journal of Nutrition*, 153(11), pp. 3207–3219. https://doi.org/10.1016/j.tjnut.2023.09.006.

Guo, Z. *et al.* (2025) 'Global burden of MAFLD, MAFLD related cirrhosis and MASH related liver cancer from 1990 to 2021,' *Scientific Reports*, 15(1). https://doi.org/10.1038/s41598-025-91312-5.

Gusdon, A.M., Song, K.-X. and Qu, S. (2014) 'Nonalcoholic fatty liver disease: pathogenesis and therapeutics from a mitochondria-centric perspective,' *Oxidative Medicine and Cellular Longevity*, 2014, pp. 1–20. https://doi.org/10.1155/2014/637027.

Gutiérrez-Cuevas, J., Santos, A. and Armendariz-Borunda, J. (2021) 'Pathophysiological molecular mechanisms of obesity: A link between MAFLD and NASH with cardiovascular diseases,' *International Journal of Molecular Sciences*, 22(21), p. 11629. https://doi.org/10.3390/ijms222111629.

Ha, J. *et al.* (2024) 'Metabolic dysfunction-associated fatty liver disease increases the risk of type 2 diabetes mellitus in young Korean adults,' *Diabetes Research and Clinical Practice*, 212, p. 111584. https://doi.org/10.1016/j.diabres.2024.111584.

Haluzik, M. *et al*. (2004) 'Genetic background (C57BL/6J Versus FVB/N) strongly influences the severity of diabetes and insulin resistance in ob/ob mice,' *Endocrinology*, 145(7), pp. 3258–3264. https://doi.org/10.1210/en.2004-0219.

Herdiyati, Y. *et al.* (2020) 'Potential fatty acid as antibacterial agent against oral bacteria of Streptococcus mutans and Streptococcus sanguinis from Basil (Ocimum americanum): In vitro and in silico studies,' *Current Drug Discovery Technologies*, 18(4), pp. 532–541. https://doi.org/10.2174/1570163817666200712171652.

Herzig, S. and Shaw, R.J. (2017) 'AMPK: guardian of metabolism and mitochondrial homeostasis,' *Nature Reviews Molecular Cell Biology*, 19(2), pp. 121–135. https://doi.org/10.1038/nrm.2017.95.

Higuchi, N. *et al.* (2008) 'Liver X receptor in cooperation with SREBP-1c is a major lipid synthesis regulator in nonalcoholic fatty liver disease,' *Hepatology Research*, 38(11), pp. 1122–1129. https://doi.org/10.1111/j.1872-034x.2008.00382.x.

Home, P.D. *et al.* (2009) 'Rosiglitazone evaluated for cardiovascular outcomes in oral agent combination therapy for type 2 diabetes (RECORD): a multicentre, randomised, open-label trial,' *The Lancet*, 373(9681), pp. 2125–2135. https://doi.org/10.1016/s0140-6736(09)60953-3.

Huang, L., Gao, L. and Chen, C. (2021) 'Role of medium-chain fatty acids in healthy Metabolism: A clinical perspective,' *Trends in Endocrinology and Metabolism*, 32(6), pp. 351–366. https://doi.org/10.1016/j.tem.2021.03.002.

Huang, T.-S. *et al.* (2023) 'Long-term statins administration exacerbates diabetic nephropathy via ectopic fat deposition in diabetic mice,' *Nature Communications*, 14(1), p. 390. https://doi.org/10.1038/s41467-023-35944-z.

Huang, W.-C. *et al.* (2013) 'Anti-bacterial and anti-inflammatory properties of capric acid against Propionibacterium acnes: A comparative study with lauric acid,' *Journal of Dermatological Science*, 73(3), pp. 232–240. https://doi.org/10.1016/j.jdermsci.2013.10.010.

Hurrle, S. and Hsu, W.H. (2017) 'The etiology of oxidative stress in insulin resistance,' *Biomedical Journal*, 40(5), pp. 257–262. https://doi.org/10.1016/j.bj.2017.06.007.

Imai, T. *et al.* (2004) 'Peroxisome proliferator-activated receptor γ is required in mature white and brown adipocytes for their survival in the mouse,' *Proceedings of the National Academy of Sciences*, 101(13), pp. 4543–4547. https://doi.org/10.1073/pnas.0400356101.

Institute for Public Health (IKU) (2024) *National Health and Morbidity Survey (NHMS) 2023: Non-Communicable Diseases and Healthcare Demand: Technical Report.* Available at: https://iku.gov.my/index.php (Assessed: 28 July 2025).

Ito, M. *et al*. (2007) 'Longitudinal analysis of murine steatohepatitis model induced by chronic exposure to high‐fat diet,' *Hepatology Research*, 37(1), pp. 50–57. https://doi.org/10.1111/j.1872-034x.2007.00008.x.

Iturbe-Rey, S. *et al.* (2025) 'Lipotoxicity-driven metabolic dysfunction-associated steatotic liver disease (MASLD),' *Atherosclerosis*, 400, p. 119053. https://doi.org/10.1016/j.atherosclerosis.2024.119053.

Jackson Laboratory, 2014. *Jaxpheno5 project protocol: Growth curve analysis of 10 strains of mice*. Available at: https://phenome.jax.org/projects/Jaxpheno5/protocol (Assessed 1 September 2025).

Jafari Azad, B. *et al.* (2022). 'Interaction between Apo A-II -265T > C polymorphism and dietary total antioxidant capacity on some oxidative stress and inflammatory markers in patients with type 2 diabetes mellitus,' *The British journal of nutrition*, 128(1), pp. 13–29. https://doi.org/10.1017/S0007114521002993

Jang, J. *et al.* (2017) 'Berberine activates AMPK to suppress proteolytic processing, nuclear translocation and target DNA binding of SREBP-1c in 3T3-L1 adipocytes,' *Molecular Medicine Reports*, 15(6), pp. 4139–4147. https://doi.org/10.3892/mmr.2017.6513.

Jarrar, Y.B., Nasser, W. and Lee, S.-J. (2025) 'Lauric acid modulates cytochrome 4V2 expression in the human THP1 macrophages,' *Drug Metabolism and Personalized Therapy* [Preprint]. https://doi.org/10.1515/dmpt-2025-0008.

Jeeyavudeen, M.S. *et al.* (2023) 'Management of metabolic-associated fatty liver disease: The diabetology perspective,' *World Journal of Gastroenterology*, 29(1), pp. 126–143. https://doi.org/10.3748/wjg.v29.i1.126.

Jung, E.-J. *et al.* (2011) 'Role of the AMPK/SREBP-1 pathway in the development of orotic acid-induced fatty liver,' *Journal of Lipid Research*, 52(9), pp. 1617–1625. https://doi.org/10.1194/jlr.m015263.

Kao, A.C.-C. *et al.* (2018) 'Prebiotic attenuation of olanzapine-induced weight gain in rats: analysis of central and peripheral biomarkers and gut microbiota,' *Translational Psychiatry*, 8, p.66. https://doi.org/10.1038/s41398-018-0116-8.

Karim, G. and Bansal, M.B. (2023) 'Resmetirom: An Orally Administered, Small-molecule, Liver-directed, β-selective THR Agonist for the Treatment of Non-alcoholic Fatty Liver Disease and Non-alcoholic Steatohepatitis,' *touch REVIEWS in Endocrinology*, 19(1), p. 60. https://doi.org/10.17925/ee.2023.19.1.60.

Khan, H.U. *et al.* (2020) 'Lauric acid ameliorates lipopolysaccharide (LPS)-induced liver inflammation by mediating TLR4/MyD88 pathway in Sprague Dawley (SD) rats,' *Life Sciences*, 265, p. 118750. https://doi.org/10.1016/j.lfs.2020.118750.

Khan, R.S. *et al*. (2019) 'Modulation of insulin resistance in nonalcoholic fatty liver disease,' *Hepatology*, 70(2), pp.711-724. https://doi.org/10.1002/hep.30429

Khaw, K.-T. *et al.* (2018) 'Randomised trial of coconut oil, olive oil or butter on blood lipids and other cardiovascular risk factors in healthy men and women,' *BMJ Open*, 8(3), p. e020167. https://doi.org/10.1136/bmjopen-2017-020167.

Kido, H. *et al.* (2025) 'Abnormalities of intracellular organelles in metabolic dysfunction-associated steatotic disease,' *Journal of Gastroenterology*, 60(8), pp. 990–999. https://doi.org/10.1007/s00535-025-02257-5.

Kim, B. *et al*. (2016) 'Astaxanthin inhibits inflammation and fibrosis in the liver and adipose tissue of mouse models of diet-induced obesity and nonalcoholic steatohepatitis,' *The Journal of Nutritional Biochemistry*, 43, pp. 27–35. https://doi.org/10.1016/j.jnutbio.2016.01.006.

Knebel, B. *et al.* (2012) 'Liver-specific expression of transcriptionally active SREBP-1c is associated with fatty liver and increased visceral fat mass,' *PLoS ONE*, 7(2), p. e31812. https://doi.org/10.1371/journal.pone.0031812.

Koppen, A. and Kalkhoven, E. (2010) 'Brown vs white adipocytes: The PPARγ coregulator story,' *FEBS Letters*, 584(15), pp. 3250–3259. https://doi.org/10.1016/j.febslet.2010.06.035.

Kroker, A.J. and Bruning, J.B. (2015) 'Review of the structural and dynamic mechanisms of PPARγ partial agonism,' *PPAR Research*, 2015, p.816856. https://doi.org/10.1155/2015/816856.

Lai, C.-Q. *et al.* (2018) 'Epigenomics and metabolomics reveal the mechanism of the APOA2-saturated fat intake interaction affecting obesity,' *American Journal of Clinical Nutrition*, 108(1), pp. 188–200. https://doi.org/10.1093/ajcn/nqy081.

Lappano, R. *et al.* (2017) 'The lauric acid-activated signaling prompts apoptosis in cancer cells,' *Cell Death Discovery*, 3(1). https://doi.org/10.1038/cddiscovery.2017.63.

Lara-Castro, C. *et al.* (2005) 'Apolipoprotein A-II polymorphism and visceral adiposity in African-American and white women,' *Obesity Research*, 13(3), pp. 507–512. https://doi.org/10.1038/oby.2005.53.

Latorre, J. *et al.* (2017) 'Decreased lipid metabolism but increased FA biosynthesis are coupled with changes in liver microRNAs in obese subjects with NAFLD,' *International Journal of Obesity*, 41(4), pp. 620–630. https://doi.org/10.1038/ijo.2017.21.

Le, Y., Wang, B. and Xue, M. (2022) 'Nutraceuticals use and type 2 diabetes mellitus,' *Current Opinion in Pharmacology*, 62, pp. 168–176. https://doi.org/10.1016/j.coph.2021.12.004.

Lee, J.-H. and Lee, J. (2022) 'Endoplasmic reticulum (ER) stress and its role in pancreatic B-Cell dysfunction and senescence in type 2 diabetes,' *International Journal of Molecular Sciences*, 23(9), p. 4843. https://doi.org/10.3390/ijms23094843.

Lee, S.M. *et al.* (2023) 'Hepatocyte PPARγ contributes to the progression of non-alcoholic steatohepatitis in male and female obese mice,' *Cellular and Molecular Life Sciences*, 80(2). https://doi.org/10.1007/s00018-022-04629-z.

Leow, W.-Q. *et al.* (2022) 'Non-alcoholic fatty liver disease: the pathologist's perspective,' *Clinical and Molecular Hepatology*, 29(Suppl), pp. S302–S318. https://doi.org/10.3350/cmh.2022.0329.

Levene, A.P. *et al.* (2012) 'Quantifying hepatic steatosis – more than meets the eye,' *Histopathology*, 60(6), pp. 971–981. https://doi.org/10.1111/j.1365-2559.2012.04193.x.

Li, J. *et al.* (2023) 'HMGCR gene polymorphism is associated with residual cholesterol risk in premature triple-vessel disease patients treated with moderate-intensity statins,' *BMC Cardiovascular Disorders*, 23(1). https://doi.org/10.1186/s12872-023-03285-w.

Li, Y. *et al.* (2011) 'AMPK phosphorylates and inhibits SREBP activity to attenuate hepatic steatosis and atherosclerosis in diet-induced insulin-resistant mice,' *Cell Metabolism*, 13(4), pp. 376–388. https://doi.org/10.1016/j.cmet.2011.03.009.

Lim, W.-S. *et al.* (2015) 'Lauric acid abolishes interferon-gamma (IFN-γ)-induction of intercellular adhesion molecule-1 (ICAM-1) and vascular cell adhesion molecule-1 (VCAM-1) expression in human macrophages,' *Asian Pacific Journal of Reproduction*, 4(3), pp. 217–221. https://doi.org/10.1016/j.apjr.2015.06.005.

Liu, H. *et al.* (2025) 'Bariatric surgery for metabolic dysfunction-associated steatotic liver disease (MASLD): Current knowledge of mechanisms,' *Hepatology*. https://doi.org/10.1097/hep.0000000000001417.

Liu, J. *et al*. (2021) 'Estimating global prevalence of Metabolic Dysfunction-Associated Fatty liver disease in overweight or obese adults,' *Clinical Gastroenterology and Hepatology*, 20(3), pp. e573–e582. https://doi.org/10.1016/j.cgh.2021.02.030.

Liu, J. *et al.* (2022) 'Estimating global prevalence, incidence, and outcomes of non-alcoholic fatty liver disease from 2000 to 2021: systematic review and meta-analysis,' *Chinese Medical Journal*, 135(14), pp.1682–1691 https://doi.org/10.1097/cm9.0000000000002277.

Liu, S. *et al.* (2015) 'AICAR-induced activation of AMPK inhibits TSH/SREBP-2/HMGCR pathway in liver,' *PLoS ONE*, 10(5), p. e0124951. https://doi.org/10.1371/journal.pone.0124951.

Liu, X. and Green, R.M. (2019) 'Endoplasmic reticulum stress and liver diseases,' *Liver Research*, 3(1), pp. 55–64. https://doi.org/10.1016/j.livres.2019.01.002.

Loh, K. *et al*. (2018) 'Inhibition of Adenosine Monophosphate–Activated Protein Kinase–3-Hydroxy-3-Methylglutaryl Coenzyme A Reductase signaling leads to hypercholesterolemia and promotes hepatic steatosis and

insulin resistance,' *Hepatology Communications*, 3(1), pp.84-98.https://doi.org/10.1002/hep4.1279

Lu, F. *et al.* (2024) 'Global trends and inequalities of liver complications related to Metabolic Dysfunction-Associated Steatotic Liver Disease: an analysis from 1990 to 2021,' *Liver International*, 45: e16120. https://doi.org/10.1111/liv.16120.

Lu, M. *et al*. (2011) 'Brain PPAR-γ promotes obesity and is required for the insulin–sensitizing effect of thiazolidinediones,' *Nature Medicine*, 17(5), pp. 618–622. https://doi.org/10.1038/nm.2332.

Lund-Katz, S. and Phillips, M.C. (2010) 'High density lipoprotein structure–function and role in reverse cholesterol transport,' *Sub-cellular Biochemistry*, 51, pp. 183–227. https://doi.org/10.1007/978-90-481-8622-8_7.

M, A. *et al*. (2024) 'Biomedical applications of lauric acid: A narrative review,' *Cureus*, 16(6). https://doi.org/10.7759/cureus.62770.

Magee, N. *et al.* (2022) 'Hepatic transcriptome profiling reveals early signatures associated with disease transition from non-alcoholic steatosis to steatohepatitis,' *Liver Research*, 6(4), pp. 238–250. https://doi.org/10.1016/j.livres.2022.11.001.

Mancini, A. *et al.* (2015) 'Biological and nutritional properties of palm oil and palmitic acid: Effects on health,' *Molecules*, 20(9), pp. 17339–17361. https://doi.org/10.3390/molecules200917339.

Matthews, D.R. *et al*. (1985) 'Homeostasis model assessment: insulin resistance and beta-cell function from fasting plasma glucose and insulin concentrations in man', *Diabetologia*, 28(7), pp.412-419. Available at: https://doi.org/10.1007/bf00280883

Mayerson, A.B. *et al.* (2002) 'The effects of rosiglitazone on insulin sensitivity, lipolysis, and hepatic and skeletal muscle triglyceride content in patients with type 2 diabetes,' *Diabetes*, 51(3), pp. 797–802. https://doi.org/10.2337/diabetes.51.3.797.

Maznan, M.A.F. et al. (2025) 'Lauric acid improves kidney structure and function of streptozotocin-induced diabetic nephropathy rats,' *Malaysia Journal of Medicine and Health Sciences*, 21(3), pp. 337-345. https://doi.org/10.47836/mjmhs.21.3.39

McVeay, C. *et al.* (2019) 'Effects of duodenal infusion of lauric acid and L-Tryptophan, alone and combined, on fasting glucose, insulin and glucagon in healthy men,' *Nutrients*, 11(11), p. 2697. https://doi.org/10.3390/nu11112697.

Medina-Gomez, G. *et al.* (2007) 'PPAR gamma 2 prevents lipotoxicity by controlling adipose tissue expandability and peripheral lipid metabolism,' *PLoS Genetics*, 3(4), p. e64. https://doi.org/10.1371/journal.pgen.0030064.

Meng, C. *et al.* (2023) 'Chlorogenic acid regulates the expression of NPC1L1 and HMGCR through PXR and SREBP2 signaling pathways and their interactions with HSP90 to maintain cholesterol homeostasis,' *Phytomedicine*, 123, p. 155271. https://doi.org/10.1016/j.phymed.2023.155271.

Mensink, R.P. *et al.* (2003) 'Effects of dietary fatty acids and carbohydrates on the ratio of serum total to HDL cholesterol and on serum lipids and apolipoproteins: a meta-analysis of 60 controlled trials,' *American Journal of Clinical Nutrition*, 77(5), pp. 1146–1155. https://doi.org/10.1093/ajcn/77.5.1146.

Metz, M. *et al.* (2023) 'Measuring VLDL1 secretion in humans with an intravenous fat emulsion test,' *STAR Protocols*, 4(1), p. 102089. https://doi.org/10.1016/j.xpro.2023.102089.

Min, H.-K. *et al.* (2012) 'Increased hepatic synthesis and dysregulation of cholesterol metabolism is associated with the severity of nonalcoholic fatty liver disease,' *Cell Metabolism*, 15(5), pp. 665–674. https://doi.org/10.1016/j.cmet.2012.04.004.

Ministry of Health Malaysia (2020). *Clinical Practice Guideline: Management of Type 2 Diabetes Mellitus (6th edition).* Available at: https://www.moh.gov.my/moh/resources/Penerbitan/CPG/Endocrine/CPG_T2DM_6th_Edition_2020_13042021.pdf (Accessed 27 July 2025)

Moliterni, C. *et al.* (2024) 'Lipotoxicity of palmitic acid is associated with DGAT1 downregulation and abolished by PPARα activation in liver cells,' *Journal of Lipid Research*, 65(12), p. 100692. https://doi.org/10.1016/j.jlr.2024.100692.

Mori, S. *et al.* (2025) 'Anti-cancer and pro-immune effects of lauric acid on colorectal cancer cells,' *International Journal of Molecular Sciences*, 26(5), p. 1953. https://doi.org/10.3390/ijms26051953.

Moslehi, A. and Hamidi-Zad, Z. (2018) 'Role of SREBPs in liver diseases: A mini-review,' *Journal of Clinical and Translational Hepatology*, 6(3), pp. 332-338. https://doi.org/10.14218/jcth.2017.00061.

Mumtaz, T. *et al.* (2024) 'A case-control regression analysis of liver enzymes in obesity-induced metabolic disorders in South Asian females,' *PLoS ONE*, 19(7), p. e0303835. https://doi.org/10.1371/journal.pone.0303835.

Nagaya, T. *et al.* (2010) 'Down-regulation of SREBP-1c is associated with the development of burned-out NASH,' *Journal of Hepatology*, 53(4), pp. 724–731. https://doi.org/10.1016/j.jhep.2010.04.033.

Nakatsuji, T. *et al.* (2009) 'Antimicrobial property of lauric acid against propionibacterium acnes: Its therapeutic potential for inflammatory acne vulgaris,' *Journal of Investigative Dermatology*, 129(10), pp. 2480–2488. https://doi.org/10.1038/jid.2009.93.

Narayanankutty, A. *et al.* (2018) 'Virgin coconut oil reverses hepatic steatosis by restoring redox homeostasis and lipid metabolism in male Wistar rats,' *Journal of the Science of Food and Agriculture*, 98(5), pp. 1757–1764. https://doi.org/10.1002/jsfa.8650.

Nassir, F. (2022) 'NAFLD: Mechanisms, treatments, and biomarkers,' *Biomolecules*, 12(6), p. 824. https://doi.org/10.3390/biom12060824.

Nitbani, F.O. *et al.* (2022) 'Antimicrobial properties of lauric acid and monolaurin in virgin coconut oil: a review,' *ChemBioEng Reviews*, 9(5), pp. 442–461. https://doi.org/10.1002/cben.202100050.

Office of the Commissioner (2024) *FDA Approves First Treatment for Patients with Liver Scarring Due to Fatty Liver Disease*. https://www.fda.gov/news-events/press-announcements/fda-approves-first-treatment-patients-liver-scarring-due-fatty-liver-disease (Accessed: June 24, 2025).

Okuno, A. *et al.* (1998) 'Troglitazone increases the number of small adipocytes without the change of white adipose tissue mass in obese Zucker rats.,' *Journal of Clinical Investigation*, 101(6), pp. 1354–1361. https://doi.org/10.1172/jci1235.

Omachi, D.O., Aryee, A.N.A. and Onuh, J.O. (2024) 'Functional lipids and cardiovascular disease reduction: A concise review,' *Nutrients*, 16(15), p. 2453. https://doi.org/10.3390/nu16152453

Ong, M.-H.-L. *et al.* (2019) 'Pro-atherogenic proteoglycanase ADAMTS-1 is down-regulated by lauric acid through PI3K and JNK signaling pathways in THP-1 derived macrophages,' *Molecular Biology Reports*, 46(3), pp. 2631–2641. https://doi.org/10.1007/s11033-019-04661-6.

Ota, T., Gayet, C. and Ginsberg, H.N. (2008) 'Inhibition of apolipoprotein B100 secretion by lipid-induced hepatic endoplasmic reticulum stress in rodents,' *Journal of Clinical Investigation*, 118(1), pp. 316–332. https://doi.org/10.1172/jci32752.

Patel, V. and Sanyal, A.J. (2013) 'Drug-Induced steatohepatitis,' *Clinics in Liver Disease*, 17(4), pp. 533–546. https://doi.org/10.1016/j.cld.2013.07.012.

Petersen, M.C. and Shulman, G.I. (2017) 'Roles of diacylglycerols and ceramides in hepatic insulin resistance,' *Trends in Pharmacological Sciences*, 38(7), pp. 649–665. https://doi.org/10.1016/j.tips.2017.04.004.

Quek, J. *et al.* (2022) 'Global prevalence of non-alcoholic fatty liver disease and non-alcoholic steatohepatitis in the overweight and obese population: a systematic review and meta-analysis,' T*he Lancet. Gastroenterology & Hepatology*, 8(1), pp. 20–30. https://doi.org/10.1016/s2468-1253(22)00317-x.

Raatz, S. *et al.* (2017) 'Relationship of the reported intakes of fat and fatty acids to body weight in US adults,' *Nutrients*, 9(5), p. 438. https://doi.org/10.3390/nu9050438.

Rahman, M.S. *et al.* (2021) 'Role of insulin in health and disease: An update,' *International Journal of Molecular Sciences*, 22(12), p. 6403. https://doi.org/10.3390/ijms22126403.

Ramya, V. *et al.* (2022) 'Dual roles of coconut oil and its major component lauric acid on Redox Nexus: Focus on cytoprotection and cancer cell death,' *Frontiers in Neuroscience*, 16, p.833630. https://doi.org/10.3389/fnins.2022.833630.

Repa, J.J. *et al.* (2000) 'Regulation of mouse sterol regulatory element-binding protein-1c gene (SREBP-1c) by oxysterol receptors, LXRα and LXRβ,' *Genes & Development*, 14(22), pp. 2819–2830. https://doi.org/10.1101/gad.844900.

Riazi, K. *et al.* (2022) 'The prevalence and incidence of NAFLD worldwide: a systematic review and meta-analysis,' *The Lancet. Gastroenterology & Hepatology*, 7(9), pp. 851–861. https://doi.org/10.1016/s2468-1253(22)00165-0.

Sakurai, Y. *et al.* (2021) 'Role of insulin resistance in MAFLD,' *International Journal of Molecular Sciences*, 22(8), p. 4156. https://doi.org/10.3390/ijms22084156.

Salgado, A.L.F.de.A. *et al.* (2010) 'Insulin resistance index (HOMA-IR) in the differentiation of patients with non-alcoholic fatty liver disease and healthy individuals,' *Arquivos De Gastroenterologia*, 47(2), pp. 165–169. Available at: https://doi.org/10.1590/s0004-28032010000200009

Samuel, V.T. and Shulman, G.I. (2016) 'The pathogenesis of insulin resistance: integrating signaling pathways and substrate flux,' *Journal of Clinical Investigation*, 126(1), pp. 12–22. https://doi.org/10.1172/jci77812.

Sandhya, S., Talukdar, J. and Bhaishya, D. (2016) 'Chemical and biological properties of lauric acid: a review,' *International Journal of Advanced Research*, 4, pp. 1123–1128. https://doi.org/10.21474/ijar01/952.

Sanyal, A.J. *et al.* (2010) 'Pioglitazone, vitamin E, or placebo for nonalcoholic steatohepatitis,' *New England Journal of Medicine*, 362(18), pp. 1675–1685. https://doi.org/10.1056/nejmoa0907929.

Sarkar, S. *et al.* (2024) 'APOA2 increases cholesterol efflux capacity to plasma HDL by displacing the C-terminus of resident APOA1,' *Journal of Lipid Research*, 65(12), p. 100686. https://doi.org/10.1016/j.jlr.2024.100686.

Sedik, A.A. *et al.* (2024) 'Lauric acid attenuates hepato-metabolic complications and molecular alterations in high-fat diet-induced nonalcoholic fatty liver disease in rats,' *Toxicology Mechanisms and Methods*, 34(4), pp. 454–467. https://doi.org/10.1080/15376516.2023.2301344.

Sekarsari, Y. *et al.* (2023) 'Prevalence of metabolic associated fatty liver disease with controlled attenuation parameter and liver stiffness measurements in patients with type 2 diabetes mellitus,' *Journal of the ASEAN Federation of Endocrine Societies*, 38(S3), p. 13. https://doi.org/10.15605/jafes.038.afes.13.

Shaheryar, Z.A. *et al.* (2023) 'Lauric acid provides neuroprotection against oxidative stress in mouse model of hyperglycaemic stroke,' *European Journal of Pharmacology*, 956, p. 175990. https://doi.org/10.1016/j.ejphar.2023.175990.

Shao, C. and Xu, Y. (2025). 'PI3K/AKT signaling pathway plays an important role in the pathogenesis of metabolic dysfunction-associated steatotic liver disease,' *Scientific Reports*, 15(1), p. 20593. https://doi.org/10.1038/s41598-025-07612-3

Sharma, R.B. *et al.* (2015) 'Insulin demand regulates β cell number via the unfolded protein response,' *Journal of Clinical Investigation*, 125(10), pp. 3831–3846. https://doi.org/10.1172/jci79264.

Sheela, D.L. *et al.* (2016) 'In silico and wet lab studies reveal the cholesterol lowering efficacy of lauric acid, a medium chain fat of coconut oil,' *Plant Foods for Human Nutrition*, 71(4), pp. 410–415. https://doi.org/10.1007/s11130-016-0577-y

Sheela, D.L. *et al.* (2017) 'Coconut phytocompounds inhibits polyol pathway enzymes: Implication in prevention of microvascular diabetic complications,' *Prostaglandins Leukotrienes and Essential Fatty Acids*, 127, pp. 20–24. https://doi.org/10.1016/j.plefa.2017.10.004.

Shionoya, K. *et al.* (2025) 'Evaluating the usefulness of the blood apolipoprotein A2 isoform index for pancreatic cancer diagnosis,' *Cancers*, 17(7), p. 1071. https://doi.org/10.3390/cancers17071071.

Siersbæk, M.S. *et al*. (2020) 'C57BL/6J substrain differences in response to high-fat diet intervention,' *Scientific Reports*, 10(1), p. 14052. https://doi.org/10.1038/s41598-020-70765-w.

Silalahi, J. *et al*. (2018) 'Composition of fatty acid and identification of lauric acid position in coconut oil and palm kernel oils,' *Indonesian Journal of Pharmaceutical and Clinical Research*, 1(2), pp.1-8.

Simões, A.E. *et al.* (2013) 'Efficient recovery of proteins from multiple source samples after Trizol® or Trizol®LS RNA extraction and long-term storage,' *BMC Genomics*, 14(1). https://doi.org/10.1186/1471-2164-14-181.

Simoes, I.C.M. *et al.* (2020) 'Western diet causes obesity-induced nonalcoholic fatty liver disease development by differentially compromising the autophagic response,' *Antioxidants*, 9(10), p. 995. https://doi.org/10.3390/antiox9100995.

Skat-Rørdam, J. *et al.* (2018) 'A role of peroxisome proliferator-activated receptor γ in non-alcoholic fatty liver disease,' *Basic & Clinical Pharmacology & Toxicology*, 124(5), pp. 528–537. https://doi.org/10.1111/bcpt.13190.

Smith, G.I. *et al.* (2020) 'Insulin resistance drives hepatic de novo lipogenesis in nonalcoholic fatty liver disease,' *Journal of Clinical Investigation*, 130(3), pp. 1453–1460. https://doi.org/10.1172/jci134165.

Son, N.-H. *et al.* (2007) 'Cardiomyocyte expression of PPARγ leads to cardiac dysfunction in mice,' *Journal of Clinical Investigation*, 117(10), pp. 2791–2801. https://doi.org/10.1172/jci30335.

Staels, B. and Fruchart, J.-C. (2005) 'Therapeutic roles of peroxisome proliferator–activated receptor agonists,' *Diabetes*, 54(8), pp. 2460–2470. https://doi.org/10.2337/diabetes.54.8.2460.

Standaert, M.L. *et al.* (2002) 'CBL, IRS-1, and IRS-2 mediate effects of rosiglitazone on PI3K, PKC-lambda, and glucose transport in 3T3/L1 adipocytes,' *Endocrinology*, 143(5), pp. 1705–1716. https://doi.org/10.1210/endo.143.5.8812.

Steinberg, G.R. and Hardie, D.G. (2022) 'New insights into activation and function of the AMPK,' *Nature Reviews Molecular Cell Biology*, 24(4), pp. 255–272. https://doi.org/10.1038/s41580-022-00547-x.

Ströher, D.J. *et al*. (2020) 'Virgin coconut oil associated with high-fat diet induces metabolic dysfunctions, adipose inflammation, and hepatic lipid accumulation', *Journal of Medicinal Food*, 23(7), pp.689–698. https://doi.org/10.1089/jmf.2019.0172

Sucharski, H.C. and Koenig, S.N. (2022) 'Mechanisms of lipoproteins and reverse cholesterol transport in atherosclerotic cardiovascular disease', In: Parinandi, N.L., Hund, T.J. (eds). *Cardiovascular Signaling in Health and Disease*. Cham (CH): Springer, pp.343-365. https://doi.org/10.1007/978-3-031-08309-9_12 (Assessed: 27 July 2025).

Sun, C. *et al.* (2022) 'Induction of autophagy via the PI3K/Akt/mTOR signaling pathway by Pueraria flavonoids improves non-alcoholic fatty liver disease in obese mice,' *Biomedicine & Pharmacotherapy*, 157, p. 114005. https://doi.org/10.1016/j.biopha.2022.114005.

Sun, S.-M. *et al.* (2020) 'AMPK activator C24 inhibits hepatic lipogenesis and ameliorates dyslipidemia in HFHC diet-induced animal models,' *Acta Pharmacologica Sinica*, 42(4), pp. 585–592. https://doi.org/10.1038/s41401-020-0472-9.

Swerdlow, D.I. *et al.* (2014) 'HMG-coenzyme A reductase inhibition, type 2 diabetes, and bodyweight: evidence from genetic analysis and randomised trials,' *The Lancet*, 385(9965), pp. 351–361. https://doi.org/10.1016/s0140-6736(14)61183-1.

Takagi, M. *et al.* (2005) 'Sterol Regulatory Element-Binding Protein-2 modulates human brain acyl-CoA hydrolase gene transcription,' *Molecular and Cellular Biochemistry*, 275(1–2), pp. 199–206. https://doi.org/10.1007/s11010-005-1990-y.

Tandra, S. *et al.* (2010) 'Presence and significance of microvesicular steatosis in nonalcoholic fatty liver disease,' *Journal of Hepatology*, 55(3), pp. 654–659. https://doi.org/10.1016/j.jhep.2010.11.021.

Tang, H. *et al.* (2018) 'Pioglitazone and bladder cancer risk: a systematic review and meta-analysis,' *Cancer Medicine*, 7(4), pp. 1070–1080. https://doi.org/10.1002/cam4.1354.

Tham, Y.Y. *et al.* (2020) 'Lauric acid alleviates insulin resistance by improving mitochondrial biogenesis in THP-1 macrophages,' *Molecular Biology Reports*, 47(12), pp. 9595–9607. https://doi.org/10.1007/s11033-020-06019-9.

Thoolen, B., *et al*. (2010). 'Proliferative and nonproliferative lesions of the rat and mouse hepatobiliary system,' *Toxicologic Pathology*, 38(7 Suppl), pp. 5S–81S. https://doi.org/10.1177/0192623310386499

Tirosh, A. *et al.* (1999) 'Oxidative stress disrupts insulin-induced cellular redistribution of insulin receptor substrate-1 and phosphatidylinositol 3-Kinase in 3T3-L1 adipocytes,' *Journal of Biological Chemistry*, 274(15), pp. 10595–10602. https://doi.org/10.1074/jbc.274.15.10595.

Tsai, K. *et al.* (2011) 'NADPH oxidase-derived superoxide Anion-induced apoptosis is mediated via the JNK-dependent activation of NF-κB in cardiomyocytes exposed to high glucose,' *Journal of Cellular Physiology*, 227(4), pp. 1347–1357. https://doi.org/10.1002/jcp.22847.

U.S. Food and Drug Administration (2024) *FDA approves first treatment for patients with liver scarring due to fatty liver disease*. Available at: https://www.fda.gov/news-events/press-announcements/fda-approves-first-treatment-patients-liver-scarring-due-fatty-liver-disease (Accessed: 24 June 2025).

UQ Biological Resources, 2020. *LAB_007 Cervical dislocation in mice and rats.* Available at: https://www.uq.edu.au/research/files/52517/LAB_007%20Cervical%20Dislocatio (Accessed: 1 September 2025).

Vesković, M. *et al.* (2023) 'The interconnection between hepatic insulin resistance and metabolic dysfunction-associated steatotic liver disease—The transition from an adipocentric to liver-centric approach,' *Current Issues in Molecular Biology*, 45(11), pp. 9084–9102. https://doi.org/10.3390/cimb45110570.

Wallace, T.C. (2018) 'Health effects of coconut oil—A narrative review of current evidence,' *Journal of the American College of Nutrition*, 38(2), pp. 97–107. https://doi.org/10.1080/07315724.2018.1497562.

Wan, K.S. *et al*. (2024) *Research highlight. Liver matters: the high burden of metabolic dysfunction-associated fatty liver disease (MAFLD) in Malaysia. The prevalence of metabolic syndrome and metabolic dysfunction-associated fatty liver disease in Malaysia 2023*. Institute for Public Health (IKU). Available at: https://iku.gov.my/mets (Assessed: 28 July 2025).

Wang, D. *et al.* (2023) 'S100A16 deficiency prevents alcohol-induced fatty liver injury via inducing MANF expression in mice,' *International Journal of Biological Sciences*, 19(16), pp. 5074–5088. https://doi.org/10.7150/ijbs.84472.

Wang, Y. *et al.* (2011) 'ApoA-I deficiency in mice is associated with redistribution of apoA-II and aggravated AApoAII amyloidosis,' *Journal of Lipid Research*, 52(8), pp. 1461–1470. https://doi.org/10.1194/jlr.m013235.

Wendel lab. (2003) *RNA gels with formaldehyde electrophoresis*. Available at: https://faculty.sites.iastate.edu/jfw/rna-gels-formaldehyde-electrophoresis. (Accessed: 7 May 2025)

Wong, H.K., Choo, Q.C. and Chew, C.H. (2020) 'Coconut milk gavage enhanced fecal bile excretion by modulating hepatic Fxr expression but failed to improve fasting serum cholesterol profile in C57BL/6 mice', *Oilseeds and Fat, Crops and Lipids*, 27(50). Available at: https://doi.org/10.1051/ocl/2020037

Wu, Z. *et al.* (1995) 'Conditional ectopic expression of C/EBP beta in NIH-3T3 cells induces PPAR gamma and stimulates adipogenesis.,' *Genes & Development*, 9(19), pp. 2350–2363. https://doi.org/10.1101/gad.9.19.2350.

Xia, J. *et al.* (2024) 'Effect of different medium-chain triglycerides on glucose metabolism in high-fat-diet induced obese rats,' *Foods*, 13(2), p. 241. https://doi.org/10.3390/foods13020241.

Yang, H.-T. *et al.* (2018) 'Lauric acid is an inhibitor of Clostridium difficile growth in vitro and reduces inflammation in a mouse infection model,' *Frontiers in Microbiology*, 8. https://doi.org/10.3389/fmicb.2017.02635.

Yang, K. and Song, M. (2023) 'New insights into the pathogenesis of metabolic-associated fatty liver disease (MAFLD): gut–liver–heart crosstalk,' *Nutrients*, 15(18), p. 3970. https://doi.org/10.3390/nu15183970.

Yao, Z. *et al.* (2023) 'Upregulation of WDR6 drives hepatic de novo lipogenesis in insulin resistance in mice,' *Nature Metabolism*, 5(10), pp. 1706–1725. https://doi.org/10.1038/s42255-023-00896-7.

Younossi, Z.M. *et al.* (2023) 'The global epidemiology of nonalcoholic fatty liver disease (NAFLD) and nonalcoholic steatohepatitis (NASH): a systematic

review,' *Hepatology*, 77(4), pp. 1335–1347. https://doi.org/10.1097/hep.0000000000000004.

Zeng, Q. *et al.* (2024) 'Association between dietary vitamin E intake and incident cardiovascular disease, cardiovascular, and all-cause mortality: A prospective cohort study using NHANES 2003-2018 data,' *International Journal of Cardiology Cardiovascular Risk and Prevention*, 24, p. 200340. https://doi.org/10.1016/j.ijcrp.2024.200340.

Zhan, W. *et al.* (2024) 'Dietary lauric acid promoted antioxidant and immune capacity by improving intestinal structure and microbial population of swimming crab (Portunus trituberculatus),' *Fish & Shellfish Immunology*, 151, p. 109739. https://doi.org/10.1016/j.fsi.2024.109739.

Zhang, F. *et al.* (2020) 'Dietary supplementation of lauric acid alleviates the irregular estrous cycle and the impaired metabolism and thermogenesis in female mice fed with high-fat diet (HFD),' *Journal of Agricultural and Food Chemistry*, 68(45), pp. 12631–12640. https://doi.org/10.1021/acs.jafc.0c05235.

Zhang, Q. *et al*. (2023) 'A high-trans fat, high-carbohydrate, high-cholesterol, high-cholate diet-induced nonalcoholic steatohepatitis mouse model and its hepatic immune response,' *Nutrition & Metabolism*, 20(1), p. 28. https://doi.org/10.1186/s12986-023-00749-w.

Zhao, M. *et al*. (2022) 'Differential modulations of lauric acid and its glycerides on high fat diet-induced metabolic disorders and gut microbiota dysbiosis,' *Food Research International*, 157, p. 111437. https://doi.org/10.1016/j.foodres.2022.111437.

Zhao, Q. Y. *et al*. (2020). 'Assessment of mitochondrial function in metabolic dysfunction-associated fatty liver disease using obese mouse models,' *Zoological Research*, 41(5), pp. 539–551. https://doi.org/10.24272/j.issn.2095-8137.2020.051

Zhao, Y. *et al.* (2023) 'Mitochondrial dysfunction in metabolic dysfunction fatty liver disease (MAFLD),' *International Journal of Molecular Sciences*, 24(24), p. 17514. https://doi.org/10.3390/ijms242417514.

Zhou, L. *et al.* (2022) 'Endoplasmic reticulum stress in innate immune cells - a significant contribution to non-alcoholic fatty liver disease,' *Frontiers in Immunology*, 13. https://doi.org/10.3389/fimmu.2022.951406.

Appendixes

Appendix A

Ethical approval from SERC, UTAR

UNIVERSITI TUNKU ABDUL RAHMAN
Wholly Owned by UTAR Education Foundation (Company No. 578227-M)

Re: U/SERC/241/2021

21 October 2021

Dr Chew Choy Hoong
Department of Allied Health Sciences
Faculty of Science
Universiti Tunku Abdul Rahman
Jalan Universiti
Bandar Baru Barat
31900 Kampar, Perak

Dear Dr Chew,

Ethical Approval For Research Project/Protocol

We refer to your application which was circulated for consideration of the UTAR Scientific and Ethical Review Committee (SERC). We are pleased to inform that your application for ethical approval of your research project involving the use of animals has been approved by SERC.

The details of the project are as follows:

Research Title	Investigation of the Effect of Lauric Acid in Hepatic Steatosis and Insulin Resistance in Diet-induced Obese Mice
Investigator(s)	Dr Chew Choy Hoong Dr Fong Lai Yen Dr Choo Quok Cheong Prof Dr Tengku Sifzizul Tengku Muhammad (UMT)
Research Area	Science
Research Location	UTAR, Kampar Campus
Animal Type/Number	70 C57BL/6J]
Approval Validity	21 October 2021 - 20 October 2024

We note the following:

(1) The animals will be purchased from relevant supplies in UM or Jackson Laboratories in USA or Taiwan.

(2) All the researchers will be responsible for the day-to-day care of the animals, including after hours and weekends.

Kampar Campus : Jalan Universiti, Bandar Barat, 31900 Kampar, Perak Darul Ridzuan, Malaysia
Tel: (605) 468 8888 **Fax**: (605) 466 1313
Sungai Long Campus : Jalan Sungai Long, Bandar Sungai Long, Cheras, 43000 Kajang, Selangor Darul Ehsan, Malaysia
Tel: (603) 9086 0288 **Fax**: (603) 9019 8868
Website: www.utar.edu.my

Please note that the conduct of this project must be in compliance with procedures set out in related policies of UTAR such as the UTAR Research Ethics and Code of Conduct, Code of Practice for the Care and Use of Animal for Scientific Purposes and other related policies/guidelines.

The University wishes you all the best in your research.

Thank you.

Yours sincerely,

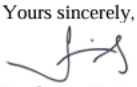

Professor Ts Dr Faidz bin Abd Rahman
Chairman
UTAR Scientific and Ethical Review Committee

c.c Dean, Faculty of Science
Director, Institute of Postgraduate Studies and Research

Kampar Campus : Jalan Universiti, Bandar Barat, 31900 Kampar, Perak Darul Ridzuan, Malaysia
Tel: (605) 468 8888 **Fax**: (605) 466 1313
Sungai Long Campus : Jalan Sungai Long, Bandar Sungai Long, Cheras, 43000 Kajang, Selangor Darul Ehsan, Malaysia
Tel: (603) 9086 0288 **Fax**: (603) 9019 8868
Website: www.utar.edu.my